Dissertation

The role of Adipose TriGlyceride Lipase (ATGL) in lung cancer and regeneration of bronchiolar epithelia

submitted by

Isabelle STRIESSNIG-BINA, MSc

for the Acadamic Degree of

Doctor of Philosophy

(PhD)

at the

Medical University of Graz

Institute of Pathology

under the Supervision of

Prof. Dr. Gerald HOEFLER

2022

Statutory Declaration

I hereby declare that this thesis is my own original work and that I have fully acknowledged by name all of those individuals and organisations that have contributed to the research for this thesis. Due acknowledgement has been made in the text to all other material used. Throughout this thesis and in all related publications I followed the "Standards of Good Scientific Practice and Ombuds Committee at the Medical University of Graz".

February 9th, 2022

Disclosures

After a brief general introduction about (cancer) metabolism the introductory chapter will focus on lipolysis and its implication in cancer as well as lung development and differentiation. The next chapter will cover Material and Methodology. Some of the results of this study have been published in Manu Manjunath Kanti and Isabelle Striessnig-Bina (co-first author), Beatrix Irene Wieser, Silvia Schauer, Gerd Leitinger, Thomas O. Eichmann, Martina Schweiger, Margit Winkler, Elke Winter, Andrea Lana, Iris Kufferath, Leigh Matthew Marsh, Grazyna Kwapiszewska, Rudolf Zechner, Gerald Hoefler, and Paul Willibald Vesely; Adipose triglyceride lipase mediated lipid catabolism is essential for bronchiolar regeneration; JCI Insight (1).

All co-authors have agreed to the use of their data in this thesis.

In addition, I contributed to one other publication as a co-author by helping with cell culture experiments (2).

Acknowledgment/Danksagung

Und nun ist es soweit: Ich bin bei der Danksagung angekommen und befinde mich am Ende einer unglaublich spannenden, lehrreichen und manchmal auch anstrengenden PhD-Zeit.

An erster Stelle möchte ich mich bei meinem Betreuer Gerald Höfler bedanken. Danke, dass ich an diesem spannenden Projekt arbeiten durfte und du trotz deinen vielen Verpflichtungen immer ein offenes Ohr für deine Studenten hast. Besonders danke ich dir für die vielen interessanten Histo-Analysen, die mir die Welt der Pathologie näher gebracht haben.

Als nächstes möchte ich mich bei meinen lieben Laborkollegen bedanken – vor allem ein großes Danke an meinen zweiten „Betreuer" Paul. Danke für die vielen Erklärungen (auf Schmierzetteln, Laborbänken, Tafeln, etc.) und dass du mir immer geholfen hast und mich auch wenn das Experiment mal wieder nicht funktioniert hat, wieder motiviert hast. Dann möchte ich bei der lieben Silvia bedanken, ohne dich würde im Labor wirklich gar nichts gehen! ☺ Danke für deine Hilfe bei den Experimenten aber auch für die Gespräche und deine guten Ratschläge. Auch ein großes Danke an Trixi, mit dir wurde es im Labor nie langweilig – danke für die vielen fachlichen Hilfestellungen und dafür dass ich in dir eine Freundin gefunden habe!

Ebenso danke ich meiner Kollegin und Freundin Tamara. Thank you for always having an open ear, for the many uplifting conversations and for sharing the highs and lows of this journey with me!

Danke an die DK-MCD family: Karin, alle ProfessorINNEN sowie meine Thesis Committee Members Günter Hämmerle, Ruth Birner-Grünberger und Joachim Reidl für den Input und die Unterstützung.

Am Ende möchte ich mich noch bei meinen Freunden und meiner Familie bedanken. Danke liebe Mama und lieber Papa – ich kann nicht in Worte fassen was ich für ein Glück habe, dass ihr meine Eltern seid. Danke an meine Geschwister und meine besten Freundinnen (Jeanette, Larissa, Anja, Jasmine), dass ihr immer für mich da seid/wart.

Und ohne meine kleine Familie wäre das alles nicht möglich gewesen. Danke lieber Andi, dass du immer zu 100% hinter mir stehst, für deine Liebe und deine bedingungslose Unterstützung.

Funding

This work was supported by the Austrian Science Fund (FWF): Projects LipoLUNG: Adipose Triglyceride Lipase in lung cancer (P30968) and the doctoral school “DK Metabolic and Cardiovascular Disease” (W1226).

Table of contents

Abbrevations

AKO - ATGL knockout
APL - acute promyelocytic leukemia
ATGL - adipose triglyceride lipase
ATI - alveolar type I
ATII - alveolar type II
ATP - adenosinetriphosphate
ATRA - all trans retinoic acid
BADJ - broncho-alveolar duct junction
BALF - broncho-alveolar lavage fluid
BASCs - broncho-alveolar stem cells
BSCs - basal stem cells
CC-AKO - club cell specific ATGL knockout
CCSP - club cell secretory protein
CE - cholesterol ester
CGI-58 - comparative gene identification 58
CRC - colorectal cancer
DG - diacylglycerol
DNA - deoxyribonucleic acid
EMT - epithelial mesenchymal transition
FFA - free fatty acids
FFPE formalin fixed paraffin embedded
G0S2 - G0/G1 switch gene
HSCs - hematopoetic stem cells
HSL - hormone sensitive lipase
IHC - immunohistochemistry
k/d - knockdown
LD - lipid droplet
MEFs - murine embryonic fibroblasts
MG – monoacylglycerol
MGL – monoacylglycerol lipase
NA - Naphthalene

NE - neuroendocrine

NEBs - neuroendocrine bodies

NECs - neuroendocrine cells

O/N - over night

PDAC - pancreatic ductal adenocarcinoma

PPAR - peroxisome proliferator activated receptor

RA - retinoic acid

RE - retinylester

RNA - ribonucleic acid

ROH - retinol

STAT3 – signal and activator of transcription 3

TG - triacylglycerol

Zusammenfassung

Die Veränderung des Stoffwechsels von Krebszellen ist eines der Charakteristika der bösartigen Zelltransformation. Schnell wachsende Krebszellen betreiben in hohem Ausmaß *de novo* Lipogense. Die Rolle des Schrittmacher Enzyms der Lipolyse, Adipozyten-Triglycerid-Lipase (ATGL), in der Krebsentstehung und dem Fortschreiten der Erkrankung ist jedoch noch nicht ausreichend bekannt. Unsere Forschungsgruppe hat herausgefunden, dass ATGL Knockout Mäuse (AKO/cTg) Adenokarzinome der Lunge entwickeln. Eine genauere Charakterisierung der Lunge zeigte nun, dass AKO/cTg Mäuse eine verminderte Lungenfunktion sowie eine massive Fettansammlung, vor allem in den Bronchialepithelzellen den sogenannten Club-Zellen, aufweisen. Weiters konnten wir zeigen, dass ATGL nicht nur Triglycerid-Lipase-Funktion besitzt, sondern auch Retinylester-Hydrolase-Aktivität, wodurch der Vitamin A-Stoffwechsel in der Lunge beeinflusst wird. Club-Zellen von AKO/cTg Mäusen sind nicht in der Lage, das am meisten sekretierte Protein der Lunge, auch Club-Zell sekrektorisches Protein (CCSP) genannt, zu produzieren. Weiters besitzen sie nicht nur signifikant weniger sekretorische Vesikel, in welchen CCSP gelagert wird, sondern auch eine geringere Zahl an Mitochondrien. Dies weist auf ein energetisches Ungleichgewicht hin. Zusätzlich zeigte eine RNA Expressionsanalyse, dass der Peroxisom Proliferator Aktivierter-Rezeptor (PPAR) Signalweg dereguliert ist und die mitochondriale Atmung von AKO/cTg Club-Zellen signifikant reduziert ist.

Die Funktionalität von Club-Zellen *in vivo* kann durch eine Behandlung mit dem Toxin Naphthalen (NA) ermittelt werden. Es stellte sich heraus, dass Club-Zellen von AKO/cTg Mäusen sensibler gegenüber der NA-Behandlung sind und auch nicht vollständig regenerieren. Darüber hinaus zeigte sich, dass es zu einer Aktivierung des pro-onkogenen, inflammatorischen STAT-3 Signalweges kommt, welcher möglicherweise zur Entstehung von neoplastischen Läsionen beiträgt. Interessanterweise konnte die Regulierung des Vitamin A-Stoffwechsels durch die Gabe von all-trans-Retinsäure (ATRA), die Regenerationsfähigkeit von AKO/cTg Club-Zellen wieder herstellen.

Zusammenfassend kann gesagt werden, dass die Lipidakkumulation und/oder das energetische Ungleichgewicht die protektive Funktion von Club-Zellen negativ beeinflusst. Dies könnte zu einer Aktivierung von inflammatorischen/regenerativen Prozessen führen, die die Entstehung von bronchialen Neoplasien begünstigt.

Abstract

Metabolic reprogramming represents a hallmark of malignant cell transformation. Rapidly proliferating cancer cells exhibit high rates of *de novo* lipogenesis. The role of the lipolytic cascade and its rate-limiting enzyme adipocyte triglyceride lipase (ATGL) in cancer development and progression, however, has not been sufficiently investigated so far. Our group has previously reported that mice lacking ATGL (AKO/cTg), develop lung adenocarcinoma. Lung characterization revealed that AKO/cTg mice show decreased lung function and massive lipid accumulation, especially in bronchiolar epithelial club cells. Moreover, we found that ATGL is not only an important TG hydrolase in the lung, but has also prominent retinylester hydrolase activity as seen by deregulated Vitamin A signaling. In addition, AKO/cTg club cells are incapable of producing the most abundant secreted protein in the lung, namely the club cell secretory protein (CCSP). Besides having less secretory vesicles, the main sites for CCSP storage, they have also reduced numbers of mitochondria, indicating an energetic imbalance. Moreover, RNA expression analyses pointed to impaired PPAR signaling and oxygen measurements confirmed reduced mitochondrial respiration in AKO/cTg club cells.

Assessment of club cell functionality *in vivo* by using the club cell toxin NA revealed that AKO/cTg club cells have defective regeneration and are not able to fully repair NA induced bronchial epithelial damage. Additionally, we observe increased pro-oncogenic, inflammatory STAT3 signaling, which might promote bronchial epithelial proliferation. Interestingly, ATRA supplementation intended to rescue defective vitamin A signaling, was able to restore bronchial epithelial regeneration after NA challenge.

Taken together these results indicate that lipid accumulation and/or energetic imbalance impair bronchoprotective club cell functions. This could trigger enhanced repair/inflammatory processes in the bronchiolar epithelium leading to neoplasia development.

1. Introduction

Tissue homeostasis is a tightly controlled process ensuring maintenance of cell number, tissue function and organization. Within cells, biochemical reactions are needed to fulfil daily energetic demands. According to the cell's immediate needs and general functions, metabolic pathways have to be operated in a balanced fashion. Up –and downregulations of metabolic pathways by key metabolites enables cells to respond to changing environmental demands and ensure cellular survival.

Proliferation of cells is regulated by the production and release of growth factors, which bind to cell surface receptors and induce a cascade of downstream signaling events. Cancer cells are able to sustain constant proliferative signaling by deregulating these growth signals.

In order to meet the energetic demand of chronic proliferation, cancer cells adapt their metabolism, and deregulated cellular energetics are considered as one of the hallmarks of cancer (3). Identification of the currently best understood metabolic characteristic of cancer cells dates back to the 1920s, when Otto Warburg defined the phenomenon termed “aerobic glycolysis” also known as the “Warburg-effect” (4). It describes an increased glucose uptake and consumption as well as the use of fermentation, even in the presence of ample oxygen. It is believed, that this metabolic feature enables the biosynthesis of essential building blocks (nucleic-acids, amino acids and lipids), which support the rapid proliferation of cancer cells (5). It is known that many cancer cells exhibit increased uptake and/or increased *de novo* lipogenesis. Amongst others, (KRAS) mutated lung cancer was reported to activate a lipogenic gene expression program (6). However, the role of the lipolytic pathway has not been sufficiently investigated so far (7).

The following introductory chapter will provide insight into the lipolysis pathway and its implication in cancer. Furthermore, it will describe the basics of lung tissue development and regeneration as the lung represents an organ affected by lipolytic deregulations.

1.1 Lipolysis

All cells need to generate energy in the form of adenosine triphosphate (ATP) in order to fulfil their biochemical functions. One of the pathways to produce not only ATP but also signaling molecules is the catabolism of fat. This pathway, called lipolysis, is in essence the breakdown of triacylglycerol (TG), into glycerol and free fatty acids (FFA) mediated by TG hydrolyzing enzymes called lipases. Lipolysis can occur at different sites and can therefore be classified as gastrointestinal lipolysis, vascular lipolysis and intracellular lipolysis (8). Different types of intracellular lipolysis include, acidic lipolysis, facilitated by lysosomal acid lipase (LAL) in lysosomes, and neutral lipid lipolysis at lipid droplets (LDs), where access amounts of TGs are stored. Hence, in times of energy demand these TG stores can be used to generate FFA for ATP production, membrane synthesis and signaling molecules. The main lipases responsible for intracellular neutral lipid catabolism are adipose triglyceride lipase (ATGL), hormone sensitive lipase (HSL) and monoacylglycerol lipase (MGL) (Figure 1).

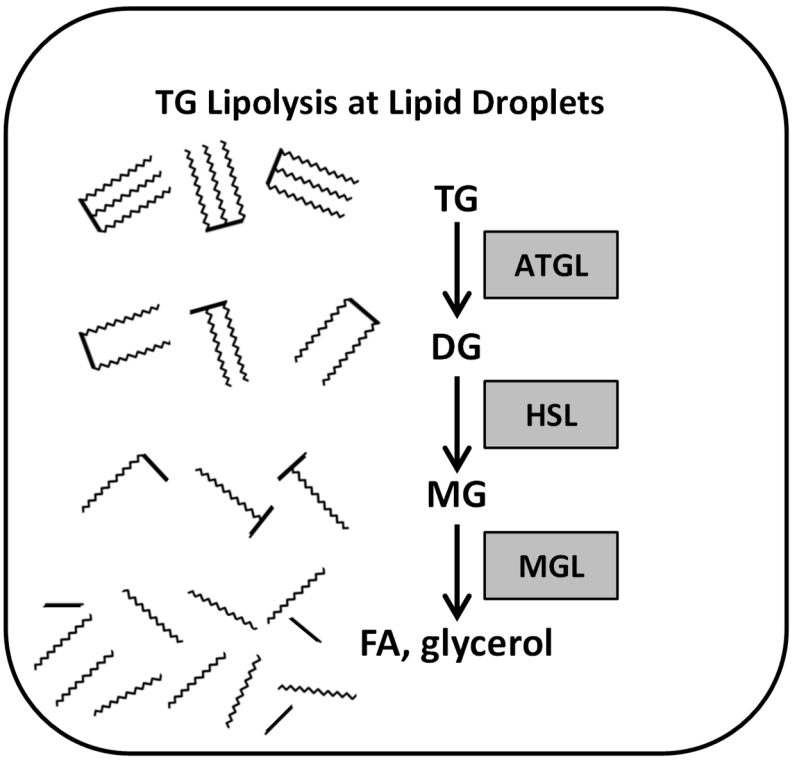

Figure 1: Simplified overview of the intracellular lipolysis pathway. Proteins needed for activation of lipid stores from lipid droplets of adipocytes or muscle-cells and other cell types. ATGL and, to a lesser extent, HSL cleave FA from TG to produce DG. Biochemically, ATGL has a strong preference for the hydrolysis of FA esters at the *sn-2* position of the glycerol backbone but will also act at *sn*-1 when its co-activator, comparative gene identifaction 58 (ABHD5/CGI58), is present (9). HSL's main lipolytic function is hydrolysis of ATGL's hydrolysis products, *sn*-1,3 and *sn*-2,3 DG (10). The third major lipase in this cascade, MGL, does not discriminate between different MGs (11).

ATGL was discovered in 2004 and catalyzes the first and rate-limiting step in the lipolytic cascade, generating diacylglycerol (DG) and FFA (12–14). *Atgl* (mRNA) levels can be increased by glucocorticoids, fasting and peroxisome-proliferator-activated-receptor (PPAR) agonists. Downregulation of *Atgl* is achieved by insulin and food intake. Essentially, ATGL is activated when energy/food supply is limited and downregulated in times of energy/food abundance. Full ATGL activity is obtained by interaction with its co-activator comparative-gene-identification-58 (CGI-58) (15). Interestingly, interaction and stimulation with/of ATGL is achieved by β-andrenergically stimulated protein kinase A (PKA)-mediated phosphorylation of PERILIPIN1. PERILIPIN1 coats the lipid droplet surface and when phosphorylated at S517, releases CGI-58, and enables its binding to ATGL (16). On the contrary, ATGL activity is inhibited by interaction with G0/G1 switch protein 2 (G0S2). This is consistent with the lipolytic activity, which is low in adipose tissue during fasting but increases after refeeding (17).

In humans, ATGL-deficiency leads to the development of neutral lipid storage disease with myopathy. ATGL-deficient mice (AKO) partially mimic the human pathology as they die at the age of 6-10 weeks due to severe cardiac impairment with massive TG accumulation. Interestingly, it was found that ATGL provides ligands for PPAR-α mediated mitochondrial biogenesis and function, and that treatment of AKO mice with PPAR-α agonists could rescue the lethal cardiac phenotype (18). AKO mice accumulate significant amounts of TGs not only in the heart but in virtually all tissues (19). Furthermore, it was recently published that ATGL is not only hydrolysing TGs but also retinylesters (RE) in hepatic stellate cells (20), suggesting that ATGL is also involved in vitamin A metabolism.

The second step of the lipolytic cascade is executed by HSL, that predominantly hydrolyses ATGL derived DGs, but is also able to metabolize REs, TGs, MGs and cholesterol esters (CE) (21). Similar regulatory networks enable ATGL and HSL to work in a coordinated fashion. In contrast to ATGL, HSL is directly phosphorylated and activated by β-adrenergically activated PKA signaling.
MGL is completing the three-step lipolysis pathway by hydrolysing the last fatty acid from the glycerol backbone. MGL is also responsible for the hydrolysis of the endocannabinoid 2-arachidonoylglycerol (2-AG) and, therefore, an interesting drug target for manipulating the endocannabinoid system (22).

1.2 Lipolytic factors and their implication in cancer pathogenesis

It is established that many cancers display a lipogenic phenotype. The importance of liberation of fatty acids and their further use is under current investigation. One of the first insights was given in 2010, when MGL was shown to be highly expressed in various aggressive tumors and responsible for promoting cancer progression by supplying oncogenic signaling lipids (23). On the contrary, recent literature suggested a tumor suppressive role of MGL in human colorectal cancer and lung adenocarcinoma in mice (24, 25). MGL knockout-driven lung tumors were associated with increased pro-inflammatory COX-2/TNFα signaling and activation of EGFR and ERK.
Moreover, HSL deficiency was also leading to increased pancreatic and adipose tissue inflammation and increased development of pancreatic ductal adenocarcinoma (PDAC) in a conditional pancreatic $KRAS^{G12D}$ cancer mouse model (26).
Moreover, double knockout of HSL and ATGL in the adipose tissue led to liposarcoma development in mice (27). Interestingly, single knockouts did not lead to cancer development, which argues for an epistatic interaction of the two lipases. It is of note that the highest downregulated gene in liposarcomas of the double knockout mice, was the co-repressor of ATGL, namely G0S2.
G0S2 has various functions in metabolism and beyond. Originally, it was demonstrated that G0S2 mRNA was upregulated 1-2 hours after a proliferative stimulus in lymphocytes and, therefore, it was considered to be a gene required for cells to commit to the G1 phase of the cell cycle (28). In 2012 however, Yamada *et al.*, reported that one mechanism by which G0S2 can maintain quiescence of hematopoetic stem cells

(HSCs) is via sequestration of nucleolin in the cytosol (29). Intriguingly, G0S2 is also a target of the frontline all-trans-retinoic acid (ATRA) differentiation therapy of acute promyelocytic leukemia (APL) (30). It was reported, that the G0S2 promotor region features ATRA-response elements, but the functional role of G0S2 induction during treatment warrants further investigation. What is known so far, is that RA-mediated growth arrest depends on expression of G0S2 (31). Additionally, several groups proposed further ATGL-independent tumor suppressive functions of G0S2. Welch *et al.* stated that G0S2 is able to interact with the anti-apoptotic protein BCL2, thereby hindering its ability to heterodimerize with BAX, which in turn leads to increased apoptosis (32). Furthermore, G0S2-null murine embryonic fibroblasts (MEFs) are more readily transformed and express MYC target genes (33). Consequently, G0S2 can function as a tumor-suppressor by BCL2 interaction and by opposing MYC induced oncogenesis.

Several studies have also connected epigenetic regulation of G0S2 with cancer. The G0S2 gene was shown to be hyper-methylated in several types of human cancer, suggesting silencing in malignant cells (34–36).

Since G0S2 is involved in many different cellular processes like proliferation, apoptosis, metabolism and carcinogenesis, it is quite tempting to suggest that one of its tumor-suppressive functions is due to regulation of ATGL.

The co-activator of ATGL, CGI-58, has also been reported to function in tumor formation and progression. Ou *et al.* reported in 2014 that CGI-58 promotes colorectal cancer (CRC) development and spreading by inducing epithelial-mesenchymal transition (EMT) through suppression of components from the AMPKα/p53 pathway (37). They report, that CGI-58 acts as a metabolic switch and that its deficiency leads to decreased fat catabolism and, thereby, facilitates the use of aerobic glycolysis. Moreover, CRC samples show an increased amount of LDs accompanied by a decreased abundance of CGI-58 that also correlated with malignant transformation. Interestingly however, the observed phenotype seems to be independent of ATGL, because k/d of *ATGL* in HCT116 colon cancer cells rather suppressed their cancer cell phenotype. In addition, they found no changes in ATGL expression levels between normal colon mucosa and CRC tissue. The authors therefore suggest that CGI-58 facilitates ATGL-independent functions in CRC, which might imply the activation of alternative lipases. Based on one cell culture model and retrospective data from human

samples, this may or may not be the case, but it most definitely does not exclude the possibility that ATGL acts as a tumor suppressor in other tissues than colon.
Recently, it was reported by Zagani *et al.* that G0S2 attenuates tumor growth by inhibition of ATGL (31). The authors reported that G0S2 overexpression as well as genetic and pharmacological ATGL knockdown slows down cell proliferation of human lung cancer cells in a similar manner. They also showed that this genetic interference leads to accumulation of TGs when incubated under fatty acid sufficiency. In accordance, the authors reported that knockdown of G0S2 leads to increased proliferation and invasion. Therefore, it was suggested that ATGL's lipase function is important for energy provision in cancer cells. It has to be noted, however, that the work of Zagani *et al*. is in part questionable due to the incorrect use of pharmacological inhibitor of ATGL, Atglistatin. Specifically, they treated human lung cancer cells with the murine specific inhibitor, which is not effective in human cells. However, they associated reduced cellular growth with the pharmacological ATGL inhibition. Therefore, the conclusions on ATGL's function in lung cancer cells might need reconsideration. Tomin *et al.* addressed this by genetically knocking out *ATGL* in human lung cancer cells and observed that ATGL-deficiency is leading to a more aggressive cancer phenotype (38). Loss of ATGL leads to an increase in p-SRC and pro-oncogenic signaling lipids, which promote an increased migratory potential of ATGL knockout cells. This supports previous findings of our group showing that ATGL-deficient mice spontaneously develop lung pre-neoplasia and adenocarcinoma as they age (39). This is also associated with downregulation of ATGL in human lung cancer, linking ATGL expression with lung homeostasis and disease development.

1.3 Lung development

All organisms in contact with ambient air are dependent on a respiratory system that consists of the trachea, the lungs and the associated vasculature. The main function of the lung is to exchange carbon dioxide with oxygen in order to enable sufficient supply of oxygen to the organism.

During embryonic development, the respiratory system originates from the anterior foregut endoderm, which is responsible for the generation of multiple tissues (40). In the mouse, lung development begins around embryonic day 9 with the expression of the transcription factor Nkx2.1. The essentiality of Nkx2.1 expression is demonstrated by the fact that Nkx2.1-deficient lungs develop only a rudimentary bronchial tree and lack critical lung specific gene expression (41). Embryonic day 9.5 to 12.5 is characterized by the evagination of these Nkx2.1 expressing epithelial cells and the formation of the trachea and two lung buds. These lung buds then undergo a process called branching morphogenesis, which leads to the generation of a tree-like structure of airways with lots of terminal branches. In the course of further development, these terminal branches will narrow and form clusters of epithelial sacs, which will later on advance into the alveoli (places of gas exchange) after birth (42). Besides the expression of Nkx2.1, several other factors are important for the fully functional development of the respiratory system. It was also shown that Wnt signaling is required for Nkx2.1 expression and thereby specification of lung endoderm progenitors. Embryos deficient in Wnt2/2b exhibit complete lung agenesis (43). In addition to Wnt signaling, BMP signaling, especially BMP4 is needed for proper lung development. BMP signaling promotes tracheal development by Sox2 repression and is important for lung bud initiation (44). The branching morphogenesis process is needed for forming both the structural airways as well as the terminal alveolar regions. It is regulated by a network of signaling molecules including Fgf10, BMP4 and Shh (45, 46). In addition, also cell-matrix interactions seem to be of great importance as cell matrix proteins such as fibronectin accumulate at branch point constriction sites (47).

During branching morphogenesis various distinct cell types of the lung appear. The development of the proximal endoderm progenitor lineage is controlled by Sox2 expression, whereas the distal endoderm progenitor lineage is regulated by Sox9 and Id2 expression (Figure 2) (42).

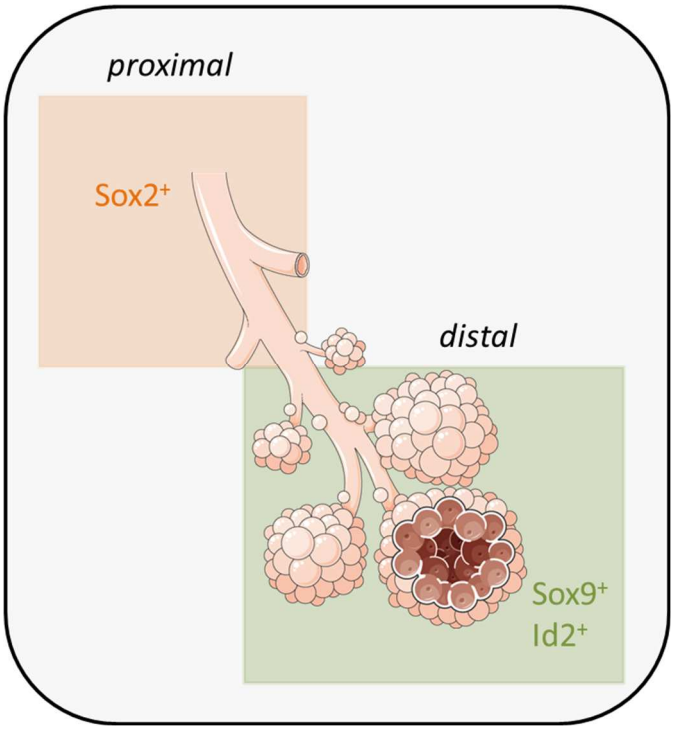

Figure 2: Proximal and distal endoderm progenitors. The Nkx2.1 positive endoderm gives rise to proximal Sox2$^+$ and distal Sox9$^+$/Id2$^+$ progenitor cells. Subsequently, these progenitors will differentiate into specific cell types found in the airways and in the alveoli, respectively. Own graphics with illustrations of SmartServier.

Notably, distal and proximal progenitor lineages give rise to different cell populations (Figure 3). Sox2 regulated proximal progenitors can differentiate into airway secretory cells, ciliated cells, mucosal cells and neuroendocrine cells. Sox9 and Id2 coordinated distal progenitors can differentiate into alveolar type I (ATI) and alveolar type II (ATII) cells.

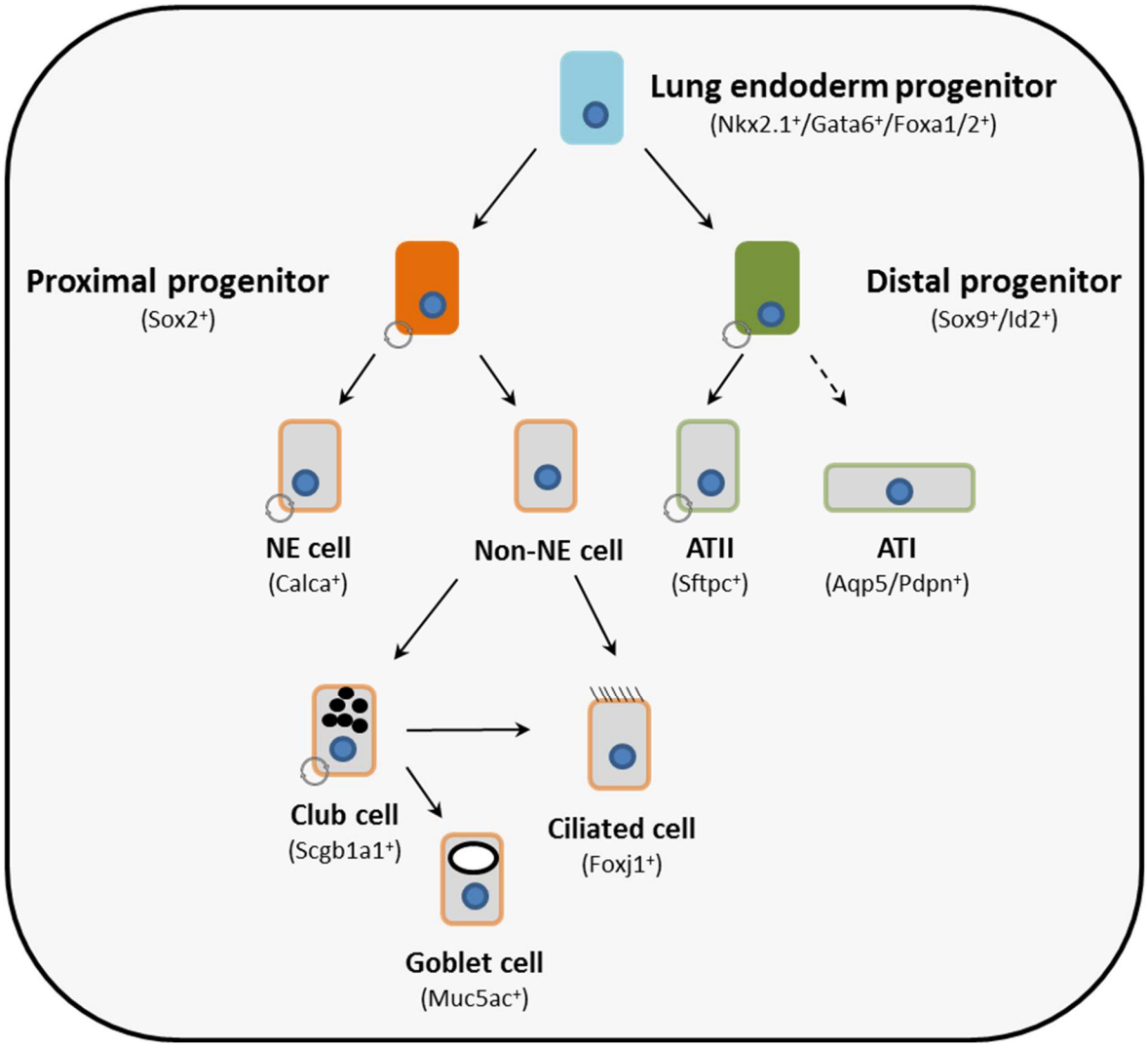

Figure 3: Differentiation of endoderm progenitor cells. The Nkx2.1 positive endoderm progenitor gives rise to proximal Sox2+ and distal Sox9+/Id2+ progenitor cells. Proximal progenitors are differentiating into cell types of the airways. Neuroendocrine cells (NE) and non-NE cells are distinguished. NE cells possess self-renewal capacity, whereas non-NE cells (basal cells) will further differentiate into secretory club cells and ciliated cells. Club cells are able to differentiate into goblet and ciliated cells. Distal progenitors will give rise to alveolar type I (ATI) and alveolar type II (ATII) cells populating the lung alveoli. ATII are able to self-renew and differentiate into ATI cells in the adult lung.

Endoderm progenitor cells display multipotency in early embryonic development, but become more and more restricted towards specific epithelial lineages as time progresses (48).

Tissues like the intestine or liver are characterized by a high turnover rate in contrary to the heart or brain, which respond poorly to insults. The adult lung is fairly quiescent but is able to respond to injury with self-renewal and regenerative signaling.

1.4 Response to injury: repair and regeneration

Although the adult lung does not exhibit a high turnover rate, it has partially defined stem cells, which are able to self-renew after injury. Similar to the developing lung, it has defined populations of stem cells/ progenitors, which give rise to certain cell types in distinct regions like the trachea, bronchi or alveoli (Figure 4). In the trachea, basal stem cells (BSCs) are able to regenerate the pseudostratified epithelium. They are characterized by *Krt-5*, *Trp63* and *Ngfr* expression and located basally of the epithelium consisting of secretory club cells, ciliated cells, neuroendocrine and goblet cells. After injury, BSCs are able to regenerate secretory as well as ciliated cell lineages. Notch signaling partly regulates this differentiation process by inhibiting the ciliated cell fate (49). In addition, HDAC 1/2 are crucial factors for secretory club cell regeneration (50).

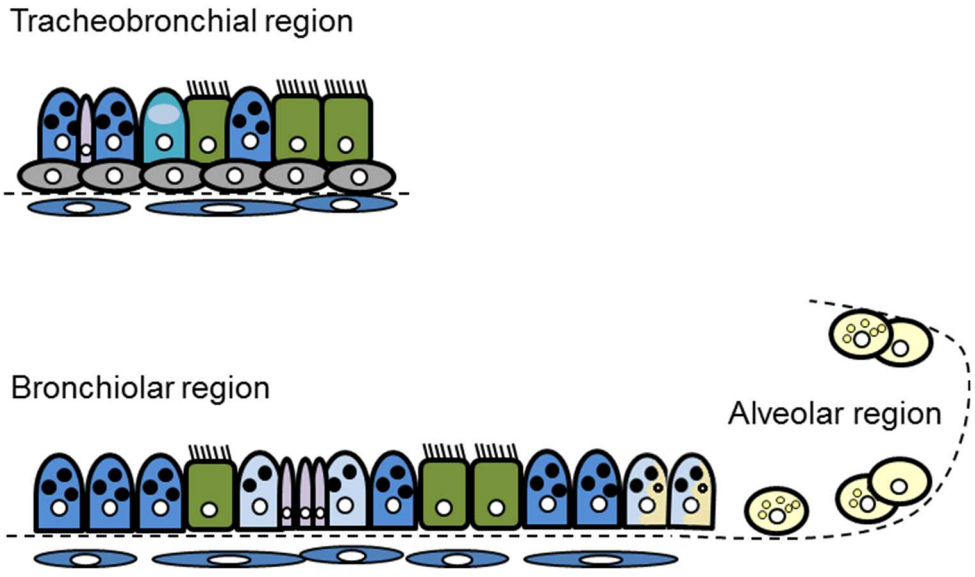

Figure 4: Cell types in the tracheobronchial, bronchiolar and alveolar region. The tracheobronchial region is populated by basal cells (grey), secretory club cells (blue), ciliated cells (green), mucous producing goblet cells (turquoise) and neuroendocrine cells

(lilac). Maintenance of the epithelium is facilitated by basal cells, which function as the stem cell in the tracheobronchial region and can give rise to club and ciliated cells. In addition, club cells can differentiate into goblet and ciliated cells. The bronchiolar region of rodents is devoid of basal cells. The most abundant cell type in this region is the club cell (blue), followed by the ciliated cell (green) and NECs (lilac). Variant club cells (light blue) and BASCs at the BADJ display stem cell function and maintain the bronchiolar epithelium. Variant club cells as well as BASCs can give rise to club, ciliated and ATII cells. In the alveolar region ATI (yellow) and ATII (yellow, granules) are the most abundant cells types. ATII cells can self-renew and give rise to ATI cells. Smooth muscle cells are adjacent to the basal membrane and are able to secrete important signalling molecules for cell differentiation.

The bronchiolar as well as alveolar epithelia are lacking BSCs (in rodents) and have their own defined set of stem cells. In the bronchiolar epithelium, the most abundant cell type is the club cell, which is characterized by *Scgb1a1* and *Cyp2f2* expression. *Scgb1a1* encodes the most abundant secreted protein in the lung, namely the club cell secretory protein (CCSP) (51). Club cells are shown to be important for protection of the bronchiolar epithelium but also for detoxifying processes through the cytochrome P450 enzyme system. Studies with CCSP knockout mice have highlighted the importance of CCSP and/or intact club cell function. CCSP was shown to be anti-inflammatory, cyto-protective and reduced expression associated with smoking and chronic obstructive pulmonary disease (COPD) (52–56).

A tool to study club cell injury is the use of the environmental toxin naphthalene, also found in cigarette smoke. *Cyp2f2* expressing club cells metabolize naphthalene and toxic NA metabolites lead to club cell death. A subset of club cells lack *Cyp2f2* expression. These cells, also called variant club cells are spared from NA induced cell death and are thought to regenerate the bronchiolar epithelium. Another cell type in the bronchiolar epithelium, the neuroendocrine cells (NECs), also possess self-renewal capacity. NECs give rise to club and ciliated cells after NA challenge. Complete ablation of NECs, however, did not impair club cell repopulation, arguing for a minor role of NECs in bronchial epithelial repair (57). NECs accumulate in neuroendocrine bodies (NEBs) and it is thought that theses NEBs indicate regions of enhanced presence of variant/ stem cell Scgb1a1^{+}/Cyp2f2^{-} club cells. Variant club cells are not only characterized by *Scgb1a1* expression and the absence of *Cyp2f2* but are

additionally defined by *Oct-4* and *Upk3a* expression and *Muc5b* deficiency (58, 59). These variant club cells are able to not only self-renew, but also differentiate into ciliated cells upon NA induced injury during normal lung homeostasis (60).
Another cell type of note is the bronchoalveolar stem cell(s) (BASCs) located at bronchiolar and alveolar duct junctions. These cells are characterized by expression of *Scgb1a1* and *Sftpc*, markers for club and ATII cells, respectively. BASCs have been shown to be able to differentiate into club and ATII cells and to initiate lung cancer development. Furthermore, they were shown to proliferate after NA induced club cell ablation and in response to oncogenic KRAS (61).
ATII cells themselves are able to self-renew and differentiate into ATI cells, maintaining alveolar structure and integrity (6, 62).
Interestingly, injury severity also influences which cells and to what extent proliferation occurs. Mild injury is repaired by surviving club cells, which are also able to differentiate into ciliated cells. Severe injury, leading to death of most club cells, stimulates proliferation of variant club cells located at NEBs and BASCs. Therefore, severe injury leads to clonal expansion, resulting in a “patchy” epithelium (63).
Taken together, the two main cell types regenerating the bronchiolar epithelium after injury are variant club cells located near NEBs and BASCs located at the broncho-alveolar duct junction. Due to their regenerative potential, they can be viewed as facultative airway progenitors of the adult lung.

1.4.1 Bronchial epithelial repair signaling

During lung regeneration and injury, many signaling pathways needed during embryonic lung development are reactivated. One of these pathways is the Fgf/β-catenin signaling axis, which is essential for maintenance of epithelial progenitor cells. It was shown that three days after NA induced injury, surviving ciliated cells stimulate, via Wnt7b expression, para-bronchial smooth muscle cells (PSMCs) to express and secrete FGF10 (64). FGF10 expression by PSMCs is needed to induce Snail and Notch signaling in surviving variant club cells and subsequent repopulation of the bronchiolar epithelium. Another signaling pathway activated after NA injury is the Wnt-signaling pathway. However, although activated after injury, club cell specific deletion

of β-catenin does not impair secretory cell regeneration (65). In addition, it was shown that HDAC1/2 deficiency in postnatal club cells impairs their regeneration after NA based injury (50).

Notably, it was shown that NA induces phosphorylation and thereby activation of STAT3 in bronchial epithelial cells. STAT3 deletion in pulmonary epithelial cells resulted in impaired regeneration of the epithelium after injury. Thus, pSTAT3 signaling is an essential pathway for bronchial epithelial cell regeneration (66).

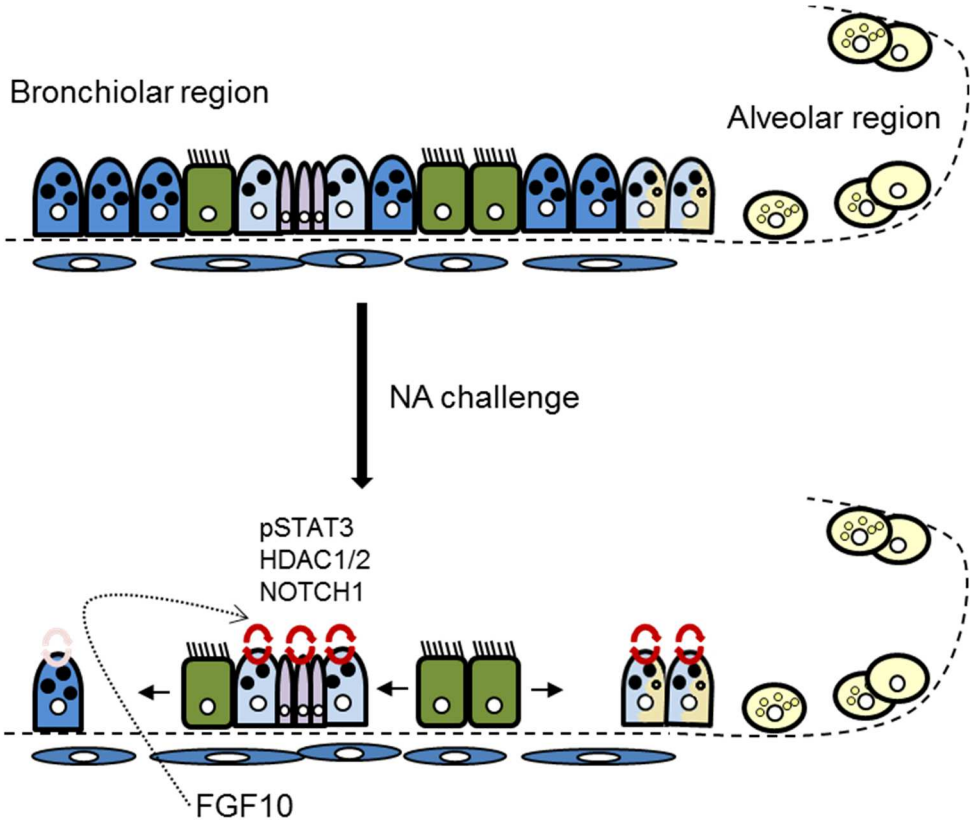

Figure 5: Bronchial epithelial NA injury. NA challenge leads to club cell death due to metabolism of NA in Cyp2f2 expressing club cells. Depending on the dose of NA, a few club cells (Scgb1a1^{+}/Cyp2f2^{+}) will survive and start to proliferate. Severe NA damage will ablate all Scgb1a1^{+}/Cyp2f2^{+} club cells and regeneration of the epithelium will be facilitated by variant club cells (Scgb1a1^{+}/Cyp2f2^{-}) and BASCs (Scgb1a1^{+}/Sftpc^{+}) at the BADJ. Important signaling pathways (STAT3, HDAC1/2 and NOTCH1) are needed for efficient club cell regeneration. Parabronchial smooth muscle cells secrete FGF10, needed for activation of Wnt/β-catenin signalling and subsequent club cell proliferation. Ciliated cells spread and transdifferentiate in order to rescue the bronchiolar epithelium (67).

Another important signaling molecule in bronchiolar but also alveolar repair is retinoic acid (RA). It was shown that vitamin A signaling (*i.e.* RA signaling) is needed for airway and alveolar differentiation and that inhibition of RA signaling leads to increased proliferation (68). RA was also shown to suppress the growth of lung cancer cells (69). Interestingly, many lung developmental/embryonic pathways as well as regenerative signaling cascades are not only active during injury but also in many types of cancer. As they are a feature of stem cells, it also led to the formulation of the cancer stem cell hypothesis implying that cancer is the result of activation of embryonic tissue remnants (70). Therefore, it is conceivable that facultative lung stem cells might be the origin of lung cancer. Indeed, it was shown that lung adenocarcinomas possibly arise from different initiating cells (71).

1.5 Hypothesis and Aims

Literature on the implication of lipolysis, especially the role of ATGL on cancer progression and development is controversial. Intriguingly, we noted that expression of ATGL is frequently diminished in several types of human cancers, including smooth muscle-, pancreas- and lung cancer. Moreover, we observed that lack of both ATGL wt alleles, in a mouse model with normal life span due to ectopic expression of ATGL in cardiac myocytes (AKO/cTg), led to formation of lung pre-neoplasia and adenocarcinoma (39).

Therefore, we hypothesized that ATGL is needed for lung homeostasis, and aimed to decipher molecular mechanisms by which ATGL-deficiency is leading to tumor development. In addition to mouse models, we investigated cancer cell behaviour with and without ATGL expression in *in vitro* models.

Moreover, we examined how ATGL mediated lipid metabolism influences lung tissue function and regeneration. We aimed to understand the functional impact of ATGL loss in lung cells by pharmacological challenge and by analysing different AKO mouse models.

2. Materials and Methods

Most of the text from this section has been slightly adapted or entirely taken from my paper Manu Manjunath Kanti and Isabelle Striessnig-Bina et al. (1).

WT/AKO A549 cells

WT control and AKO A549 cells were established as described by Tomin *et. al.,* 2018 (34, 38). Briefly, cells were transfected with either CRISPR-Cas9 control or ATGL KO plasmids, and site directed repair plasmid, from Santa Cruz Biotechnology, Inc., Santa Cruz, CA. Next, cells were selected for plasmid uptake and single clones were expanded. The modified DNA sequence was verified by Sanger sequencing and ATGL KO was additionally confirmed by western blotting.

Cells were maintained in RPMI 1640 medium (Invitrogen) and seeded at a density of 2 x 10^5 cells per well of a six-well dish for proliferation assays. Doubling time was measured every 24h for at least 5 consecutive days using the CASY cell counter. For xenografts, 2 x 10^6 cells were resuspended in DMEM (Sigma), mixed with matrigel in a 1:1 ratio and injected subcutaneously into 8 weeks old male NSG mice. Tumor growth was monitored and mice sacrificed 39 days post injection.

B16F10 ctrl and Atgl-kd cells

RNAi for sh-ctrl or sh-*Atgl* were purchased from Sigma (MISSON® sh-RNA library) and cells transduced according to the manufacturer's instructions. Briefly, B16F10 cells were transduced with lentiviral particles O/N and bulk populations selected with puromycin. *Atgl*-kd efficiency was confirmed by qRT-PCR analysis and western blotting. Cells were seeded at a density of 2 x 10^5 cells per per well of a six-well dish and proliferation was measured every 24h for at least 5 consecutive days using the CASY cell counter. For analysis of metastatic spread, 2 x 10^5 cells were resuspended in PBS and injected via the tail vein into 8-12 weeks old female C57BL6 wildtype mice. Mice were sacrificed 16 days post injection.

Ethical approval

All animal studies were approved by and performed according to the guidelines of the Ethics committee of the University of Graz and Medical University of Graz, the Austrian Federal Ministry for Science and Research, and are in accordance with the council of Europe Convention (ETS 123). Approved animal applications include BMWFW-66.007/0030-WF/V/3b/2015, BMWFW-66.007/0017-WF/V/3b/2016, BMBWF-66.007/0023-V/3b/2018, BMWFW-66.007/0016-WF/V/3b/2017, BMBWF-66.007/0005-V/3b/2018, BMBWF-66.007/0014-V/3b/2018, BMWFW-66.007/0035-WF/V/3b/2017, BMBWF-66.007/0007-V/3b/2018, BMBWF-66.007/0016-V/3b/2018.

Animals

Atgl-deficient animals with *Atgl* expression in the heart (AKO/cTg) were bred as previously described (72). Club cell specific *Atgl* knockout mice were bred by intercrossing homozygeous CCSP driven CRE expressing B6/D2 mice (MGI:3610310) with homozygeous *Atgl*-flox C57BL6 (B6N.129S-*Pnpla2*^{tm1Eek}/J) mice. Heterozygeous LSL-KRAS^{G12D} (B6.129S4-*Kras*^{tm4Tyj}/J) mice were a kind gift by Emilio Casanova (Medical University of Vienna and LBI for cancer research, Vienna, Austria) and bred with approval from our co-operation partner Tyler Jacks (Massachusetts Institute of Technology, Boston, USA) with homozygeous *Atgl*-flox, *Cgi58*-flox (MGI:5502402) and *G0S2*-flox (73) mice to obtain mice heterozygeous for KRAS^{G12D} and homozygeous for the floxed gene of interest on a C57BL6 background.

Generally, experiments were carried out with male and female mice on a C57BL6J background (for at least 10 generations) or on mixed background (CC-AKO). Animals were kept on a regular light–dark cycle (14 h light–10 h dark) at 22±1 °C in a specific pathogen-free environment and were fed a standard laboratory chow diet ad libitum.

Naphthalene studies

For acute naphthalene (NA, Sigma) treatment, NA was dissolved in corn oil and injected intraperitoneal at a concentration of 200 mg/kg into male, 35 weeks old, AKO/cTg and WT/cTg mice. EdU (Invitrogen) was injected subcutaneously at day two post NA injection at a concentration of 50 mg/kg. Mice were sacrificed on day three post NA injection.

Multiple NA treatment was performed with male and female mice starting when the mice were 24-26 weeks old. Mice received one intraperitoneal NA injection per week

for the first four weeks of the experiment (male: week 1: 200 mg/kg, week 2-4: 80 mg/kg; female: week 1: 130 mg/kg, week 2-4: 50 mg/kg), followed by ten weeks of aging without treatment.

Multiple NA treatment with all-*trans*-retinoic acid (ATRA, Sigma) supplementation was performed with male and female mice starting when the mice were 21-38 weeks old. Mice received one intraperitoneal NA injection per week for the first four weeks of the experiments (male: week 1: 150 mg/kg, week 2-4: 80 mg/kg; female: week 1: 130 mg/kg, week 2-4: 50 mg/kg), followed by one subcutaneous EdU injection on day three post the last NA injection and ten weeks of aging. During the whole experimental time mice received three intraperitoneal ATRA injections per week (Mo/Wed/Fri, 0.5 mg/kg).

Ad-Cre inhalation studies

Adenovirus-Cre mediated activation of $KRAS^{G12D}$ and deletion of either *Atgl*, *Cgi58* or *G0S2* was achieved by intranasal adenovirus instillation and carried out as previously described (74). Briefly, mice were anaesthetised using ketamine/xylazine and inhaled with $2.5*10^7$ PFU of AdCre (purchased from the University of IOWA, VVC-UIowa-5) per mouse. Mice were closely monitored and sacrificed 11 weeks post virus inhalation.

Lung function measurement

Mice were anesthetized deeply using 150 mg/kg ketamine and 20 mg/kg xylazine, followed by intubation and mechanical ventilation (150 breaths/min, tidal volume of 10 ml/kg and a positive end expiratory pressure of two cmH2O). Airway resistance, compliance and total lung capacity was measured using a FlexiVent apparatus (SciReq) as previously described (75).

Bronchoalveolar lavage fluid (BALF)

BALF was obtained after sacrificing the animals by lavage of the lung with 1 ml of cold 1x PBS containing protease and phosphatase inhibitor (Pierce, Thermo Scientific).

FACS

BALF and single cell lung tissue homogenates were analyzed using a LSRII flow cytometer and the FACSDiva software (BD Biosciences). Identification of the cells by the following antibody combinations: neutrophils (CD11b+, CD11c-, Gr-1+), macrophages (CD11b low, CD11c+, Siglec F+), dendritic cells (CD11b+, CD11c+,

MHC-II high), T helper cells (CD3+, CD4+), cytotoxic T cells (CD3+, CD8+), B cells (CD19+), and eosinophils cells (CD11b+, CD11c-, Siglec F+). Antibody details are provided in Table 1.

Table 1: Antibodies used in FACS analysis. Antibodies were used to perfrom immune-profiling of lung homogenates and BALF samples.

Antigen	Label	Company	Clone	Isotype	Dilution
CD3	FITC	eBioscience	145-2C11	Hamster IgG	1:20
CD4	APC	Biolegend	GK1.5	Rat IgG2b, κ	1:100
CD8	PE	Biolegend	53-6.7	Rat IgG2a, κ	1:200
CD11b	V500	BD Bioscience	M1/70	Rat IgG2b, κ	1:50
CD11c	ef450	eBioscience	N418	Hamster IgG	1:50
CD19	AF700	Biolegend	6D5	Rat IgG2a, κ	1:100
CD24	PerCP	BD Bioscience	M1/69	Rat IgG2b, κ	1:500
CD25	APC-Cy7	Biolegend	PC61	Rat IgG1, λ	1:50
CD45	PerCP-Cy5.5	eBioscience	30-F11	Rat IgG2b, κ	1:200
CD45	FITC	Biolegend	30-F11	Rat IgG2b, κ	1:200
CD64	FITC	BD Bioscience	X54-5/7.1	Mouse NOD/Lt IgG1, κ	1:20
gdTCR	AF647	Biolegend	BV421	Hamster IgG	1:50
Gr-1	BV421	Biolegend	RB6-8C5	Rat IgG2b	1:800
MHC-II	PE-Cy7	Biolegend	M5/114.15.2	Rat IgG2b, κ	1:400
Siglec F	PE	BD Bioscience	E50-2440	Rat IgG2a, κ	1:20

FACS analysis was carried out in cooperation with Leigh Marsh from the Ludwig Boltzmann Institute Lung Vascular Research, Graz, Austria.

Tissue preparation and Western blot analysis

Lungs were perfused and excised, washed with 1x PBS and subsequently snap frozen with 2-Methylbutane in liquid nitrogen. Lung tissue pieces were lysed in SDS lysis buffer (100 mM Tris, pH 6.8 and 3% SDS) by using MagNA Lyser Green Beads (Roche, 25 sec, 7000 rpm). Afterwards, the tubes were centrifuged in a table top centrifuge (5 min, 13 000 rpm, 4°C) and the supernatant transferred to a new Eppendorf tube. The lysates were sonicated (Hielscher Ultrasonics, 10 sec, RT), heated (5 min, 70°C) and again centrifuged in a table top centrifuge (5 min, 13 000 rpm, RT). The supernatant was then transferred to a new Eppendorf tube and protein concentration was determined using a Bio-Rad protein assay with BSA as a standard. Proteins of the lysates were separated using 4-20% SDS gels (Bio-Rad) and blotted onto a 0.45 µm nitrocellulose membrane (GE healthcare). Membranes were stained with Ponceau S to check efficient protein transfer and blocked by using 5% skim milk. Proteins were detected using the primary antibodies stated in Table 2 and respective horseradish peroxidase coupled secondary antibodies (Cell Signaling and Dako).

Table 2: Antibodies used for Western blot analysis. Antibodies were diluted in 1% skim milk and proteins detected using secondary antibodies labelled with horseradish peroxidase, accordingly.

Antigen	Company	Number	Host	Dilution
Acetylated tubulin	Sigma	T7451	Mouse	1:10000
AKT	Cell Signaling	9272	Rabbit	1:1000
B-Actin	Sigma	A2228	Mouse	1:30000
CCSP	Abcam	ab40873	Rabbit	1:5000
CGRP	Santa Cruz	sc-57053	Mouse	1:200
Cleaved caspase 3	R&D	AF835	Rabbit	1:200
CYP2F2	Santa Cruz	sc-374540	Mouse	1:1000
MTCOI	Abcam	ab14705	Mouse	1:1000
Mucin5AC	Abcam	ab3649	Mouse	1:1000
NDUFS1	Abcam	ab157221	Rabbit	1:1000
p-AKT	Cell Signaling	4060	Rabbit	1:1000
PCNA	Dako	M0879	Mouse	1:500
Pro-SPC	Abcam	ab90716	Rabbit	1:1000
pS6	Cell Signaling	2111	Rabbit	1:2000
pSTAT3 (Y705)	Cell Signaling	9145	Rabbit	1:1000
S6	Cell Signaling	2217	Rabbit	1:1000
STAT3	Cell Signaling	4904	Rabbit	1:1000
Vinculin	Sigma	hVIN-1	Mouse	1:250000

IL-6 ELISA

Frozen lung tissue pieces were lysed with 1x PBS supplemented with 0.1% Triton X-100 and protein and phosphatase inhibitors by using MagNA Lyser Green Beads (Roche, 25 sec, 7000 rpm). Afterwards, the tubes were centrifuged in a table top centrifuge (5 min, 13 000 rpm, 4°C) and the supernatant transferred to a new Eppendorf tube. The lysates were sonicated (Hielscher Ultrasonics, 10 sec, 4°C) and centrifuged again (5 min, 13 000 rpm, 4°C). The supernatant was then transferred to a new Eppendorf tube and protein concentration was determined using a Bio-Rad protein assay with BSA as a standard. Samples were set to a specific protein concentration and re-measured for subsequent normalization of the obtained IL-6 values to the protein content. IL-6 levels were determined by using the Mouse IL-6 ELISA Ready-SET-Go!^{TM} from eBioscience following the manufacturer's instructions.

Histological analysis and immunohistochemistry

For histological analysis of mouse lung tissue, the left lobe was inflated and fixed with 4% neutral buffered formalin for 24h. Afterwards lungs were embedded in paraffin (Tissue Tek Tec, Sakura), sectioned (2 µm) and stained with haematoxylin–eosin according to standard histopathological techniques (76). Immunohistochemistry (IHC) was performed using primary antibodies mouse CYP2F2 (sc-374540), rabbit CCSP (ab40873) rabbit p-STAT3 (Cell Signaling 9145), mouse acetylated α-tubulin (Sigma, T7401), CK19 (Epitomics, 3863S) and visualized by using an appropriate detection system. IHCs were evaluated by counting the positive cells per bronchiole or per defined length of bronchiolar epithelium. At least 10 bronchioles with similar size per animal were examined.

For immunofluorescence, EdU and cell death analysis, lung tissue was resected, washed in 1x PBS and fixed in 4% PFA for 4h. Thereafter, lungs were transferred to 20% sucrose for 12-24h and subsequently snap frozen with 2-Methylbutane in liquid nitrogen. Lungs were sectioned (4 µm) using Tissue Tek O.C.T. Compound and sections then permeabilized using 0.1% Triton X-100. Proteins were detected using primary antibodies rabbit CCSP antibody (ab40873), rabbit pro-SPC antibody (ab90716) and respective secondary antibodies Alexa Fluor 488 and 594 (Thermo Fisher). EdU positive cells were detected using Click-iT™ EdU Colorimetric IHC Detection Kit (Thermo Fisher) and following the manufacturer's instructions. Apoptotic

cells were visualized by using the In Situ Cell Death Detection Kit (Roche) according to the manufacturer's instructions.
To detect neutral lipid Oil Red-O staining was performed on 4% neutral buffered formalin fixed and stored cryo lung sections.

Atgl *in situ* hydridization

Atgl in situ hybridization was performed using the RNAscope® 2.5 HD Detection Kit according to the manufacturer's instructions using the RNAscope® probe Mm-Pnpla2 with the catalog number 469441 targeting region 1025-2115. Briefly, FFPE tissue sections were deparaffinized and after pre-treatment, RNA specific probes were hybridized to the target RNA. After signal amplification steps, visualization was performed using HRP-labelled probes and a chromogenic substrate. PPIB and the bacterial gene dapB were used as positive and negative control, respectively.

Electron microscopy

For electron microscopy, lung tissue was fixed in 2.5% glutaraldehyde in 0.1 M cacodylate buffer, pH 7.3 for 3-4 hours. After dehydration the tissue was embedded in resin (AGAR-100, Agar Scientific). Ultra thin lung sections (90 nm) were contrasted with uranyl acetate/lead citrate and studied with a Philips CM 100 electron microscope.

Club cell isolation

Club cells were isolated essentially as described by Oreffo *et al.* (77) with several modifications. Briefly, animals were anaesthetized using Narkodorm (60µl per 100g mouse weight, CP Pharma) and sacrificed by cutting through the vena cava. Lungs were perfused with 0.9% NaCl, lavaged 3x with solution I (133 mM NaCl, 5.2 mM KCl, 2.59 mM phosphate buffer pH 7.4, 10.3 mM hepes buffer pH 7.4, 1 mg/ml glucose, 5mM EDTA) and instilled with solution I containing 0.25% trypsin. Then lungs were perfused under constant flow (3 ml per minute) with solution I containing 0.25% trypsin in a 37°C warm water bath for 15 min. Afterwards main bronchi were removed, the rest cut into 1 mm small pieces and transferred to 1x PBS. Bronchial epithelial cells were released by shaking for 1 min. Thereafter, cells were filtered through a 100 µM and 40 µM cell strainer and centrifuged for 10 min, 190 g. The pellet was resuspended in a small volume of 1x PBS and loaded onto a 1.04 and 1.09 iodixanol step gradient. After centrifugation in a Beckmann Coulter Optima^{TM} L-90K (20 min, 3400 rpm, 4°C) the

enriched club cell fraction was recovered. Cells were either subjected to cytospins, RNA isolation, protein analysis by western blot or oxygen consumption measurements.

Oxygen consumption

Oxygen consumption rate of isolated club cells (club cell isolates of 4 mice pooled, 2-4*10^6 cells per measurement) was measured with the Oroboros instrument in a respiration buffer containing 125 mM sucrose, 20 mM K-Tes, 2 mM $MgCl_2$, 1 mM EDTA, 4 mM KH_2PO_4, 3 mM malate and 0.1% BSA, pH 7.2. Cells were permeabilized using 7 µg digitonin and the following substrates and inhibitors added consecutively when the O_2 slope was stable: octanoylcarnitine 0.2 mM, ADP 1 mM, glutamate 10mM, succinate 10 mM, rotenone 0.5 µM, oligomycin 4 µg/ml, antimycin A 2.5 µM. The oxygen consumption rate was normalized to the cell number.

Lipid analysis with mass spectrometry

Total lipids of lung explants (5-30mg) were extracted twice according to Folch *et al.* (78) using chloroform/methanol/water (2/1/0.6, v/v/v) containing 500 nM butylated hydroxytoluene, 1% acetic acid, and 4 nmol internal standard (ISTD) mix (C17-lysophosphatidylcholine, C17-phosphaditylcholine, C17-triacylglycerol) per sample. Extraction was performed under constant shaking for 60 min RT. The organic phase was collected after centrifugation (1000g, 15 min, RT). Combined organic phases of the double-extraction were dried under a stream of nitrogen and dissolved in 200 µl chloroform/methanol/2-propanol (2/1/12, v/v/v) for UPLC-qTOF analysis. Chromatographic separation was performed using an AQUITY-UPLC system (Waters Corporation), equipped with a HSS T3 column (2.1x100 mm, 1.8µm; Waters Corporation) as previously described (79). A SYNAPT™G1 qTOF HD mass spectrometer (Waters Corporation) equipped with an ESI source was used for detection. Data acquisition was done by the MassLynx 4.1 software (Waters Corporation). Lipid classes were analyzed with the “Lipid Data Analyzer 1.6.2” software (80). Extraction efficacy and lipid recovery was normalized using ISTDs. Lipid profiling was performed in cooperation with Thomas Eichmann from the University of Graz, Austria.

TG quantification

Resected lung tissue (5-30mg) was lysed in 1x PBS by using MagNA Lyser Green Beads (Roche, 25 sec, 7000 rpm). Afterwards, the tubes were centrifuged in a table top centrifuge (1 min, 13 000 rpm, 4°C) and the supernatant transferred to a new Eppendorf tube. The lysates were sonicated (Hielscher Ultrasonics, 3x 10 sec, 4°C) and centrifuged again (1 min, 13 000 rpm, 4°C). A small amount of the supernatant was used to determine the protein concentration using a Bio-Rad protein assay and the rest transferred to a glas tube and used for lipid extraction according to Folch *et al.* (78). The lipid fraction was dissolved in 1% Triton X-100 and TAG measured using the Triglycerides Standard FS kit (DiaSys) according to the manufacturer's instructions. TG values were normalized to protein content.

Real time qPCR

Total RNA was isolated using TRIzol (Invitrogen) according to the manufacturer's instructions. Synthesis of cDNA was carried out using the High-Capacity cDNA Reverse Transcription Kit with RNase Inhibitor by Applied Biosystems™ containing random primers. Gene expression analysis was performed with the SYBR Green Luna® Universal qPCR Master Mix (NEB) on the Quantstudio machine (Applied Biosystems™). Relative mRNA levels were obtained by using the ΔΔCt method and normalization to the housekeeping gene *Actb*. Primers were designed using the NCBI primer designing tool and sequences can be found in Table 3.

Table 3: qPCR Primer sequences. Primers were designed using the NCBI Primer-Blast program at https://www.ncbi.nlm.nih.gov/tools/primer-blast/.

Gene name	forward (5'-3')	reverse (5'-3')
Actb	ggctgtattcccctccatcg	ccagttggtaacaatgccatgt
Cpt1a	tgagtggcgtcctctttgg	cagcgagtagcgcatagtca
Mcad	gatgcatcaccctcgtgtaac	aag ccc ttt tcc cct gaa
Acox1	gggagtgctacgggttacatg	cgg ata tcc cca aca gtg atg
Atgl	aacgccactcacatctacgg	gcctccttggacacctcaata
Scgb1a1	ggctgtattcccctccatcg	ccagttggtaacaatgccatgt
Sftpc	tgagtggcgtcctctttgg	cagcgagtagcgcatagtca
Foxj1	gatgcatcaccctcgtgtaac	aag ccc ttt tcc cct gaa
Cyp2f2	gggagtgctacgggttacatg	cgg ata tcc cca aca gtg atg

Microarray

The RNA extraction was done with the miRNeasy Micro Kit (Qiagen) including DNAse treatment on the column.

RNA quality was checked on the BioAnalyzer BA2100 (Agilent) using the RNA 6000 Pico LabChip (Agilent). Linear amplification of the RNA was achieved with the NuGen Ovation Pico WTA System V2 (NuGEN Technologies Inc;) according to the manufacturer's instructions.

Hybridization of all samples to GeneChip Human 2.0 ST arrays as well as washing and staining was performed according to the manufacturer's instructions (Affymetrix).

Arrays were scanned with the Affymetrix GeneChip scanner GCS3000. Labeling controls and hybridization controls were evaluated with Expression Console EC 1.3.1. Amplification, Hybridization and first analysis were carried out at the Division Core Facility for Molecular Biology at the Centre of Medical Research at the Medical University of Graz, Austria. Microarray data were analyzed with Partek Genomic Suite v6.6 software (Partek Inc). The import process of the .CEL files contained RMA normalization (robust multi-chip average) including background correction, quantile normalization across all arrays and median polished summarization based on log transformed expression values.

Retinol determination

Extraction of neutral lipids for HPLC-FD or colorimetric measurement – Lung tissues (10 - 20 mg) were homogenized in 1 ml n-hexane (containing 1 mM butylated hydroxytoluene, BHT), 200 µl H2O, and 200 µl ethanol (containing 1.14 µM all-trans retinyl acetate) by using a ball mill (Retsch GmbH). Phase separation was obtained by centrifugation at 5,000 x g and 4°C for 10 min, and 800 µl upper organic phase was collected. For second extraction, 1 ml n-hexane was added to remaining tissue homogenate, vortexed for 30 sec, and centrifuged as described above. The organic phases were combined, dried in a speed-vac and either stored at -20°C or used for HPLC-FD analysis. Protein determination was performed by dissolving the dried remaining interphase and infranatant in 0.3 N NaOH/0.1% SDS for 4 h. Protein content was determined by Pierce™ BCA Protein Assay Kit (ThermoFisher Scientific Inc.) according to manufacturer's instructions using BSA as standard.

Quantification of retinoids by HPLC-FD – Dried lipids of the n-hexan extraction were dissolved in 100 µl methanol:toluene (1/1, v/v) and separated on a YMC-Pro C18 column (150 x 4.6 mm, S-5 µl, 12 nm, YMC Europe GmbH, Dinslake, Germany) using a gradient solvent system (flow, 1 ml/min; gradient, 1-5 min 100% methanol, 5-14 min 60% / 40% methanol/toluene, and 14- 18 min 100% methanol). Fluorescence was detected at excitation 325nm/emission 450 nm. The HPLC consisted of a Waters e2695 separation module, including a column oven (at 25°C) and a Waters 2475 fluorescence detector (Waters Corp., Milford, MA). Data were analyzed using Empower 3 chromatography data software (Waters Corp.).

Retinol determination was performed in cooperation with Achim Lass and Laura Pajed from the University of Graz, Austria.

Statistical analyses

Each biological replicate was defined as a biological unit, e.g., a cell, or a lung or, a mouse. Biological replicate values were computed as the arithmetic mean value of technical replicate values. All data represent mean values of the biological replicates +/- SD. The number of biological replicates (n) for each experiment, is depicted in each respective figure legend. Statistical analysis between two groups (of biological replicates) were performed by Student's two-tailed t-test, using GraphPadPrism V6.01. Group differences were considered statistically significant for $p < 0.05$ (*), $p < 0.01$ (**), and $p < 0.001$ (***). Outlier analysis was performed using Grubb's test, with alpha = 0.05.

3. Results

Some of the results in this section are published in my paper Manu Manjunath Kanti and Isabelle Striessnig-Bina et al. (1).

3.1 ATGL deficiency does not affect the *in vitro* growth of cancer cells but promotes lung cancer development in mice

Previous findings of our group indicated that ATGL is frequently downregulated in human smooth muscle sarcoma as well as in pancreas and lung adenocarcinoma (39). IHC analysis showed that ATGL is downregulated in tumor cells when compared to the surrounding healthy tissue. Consequently, we hypothesized that loss of ATGL promotes tumor growth. Therefore, we decided to knock out or to knock down ATGL in cancer cells to investigate its effect on cancer cell proliferation.
On the one hand, we analyzed A549 control and ATGL-knockout lung cancer cells, which have been established and kindly provided by the group of Ruth Birner-Grünberger. On the other hand, we lentivirally knocked down ATGL in B16F10 melanoma cells, which are an excellent model to investigate metastatic spread of cancer cells to the lung.

Firstly, ATGL-knockout in A549 cells was confirmed by WB analysis (Figure 6A). When we measured doubling time of ATGL control and knockout cells however, we could not detect any significant differences (Figure 6B). Moreover, when we injected these cells into immuno-compromised NSG mice, we also did not observe any significant changes in tumor weight after 39 weeks (Figure 6C).

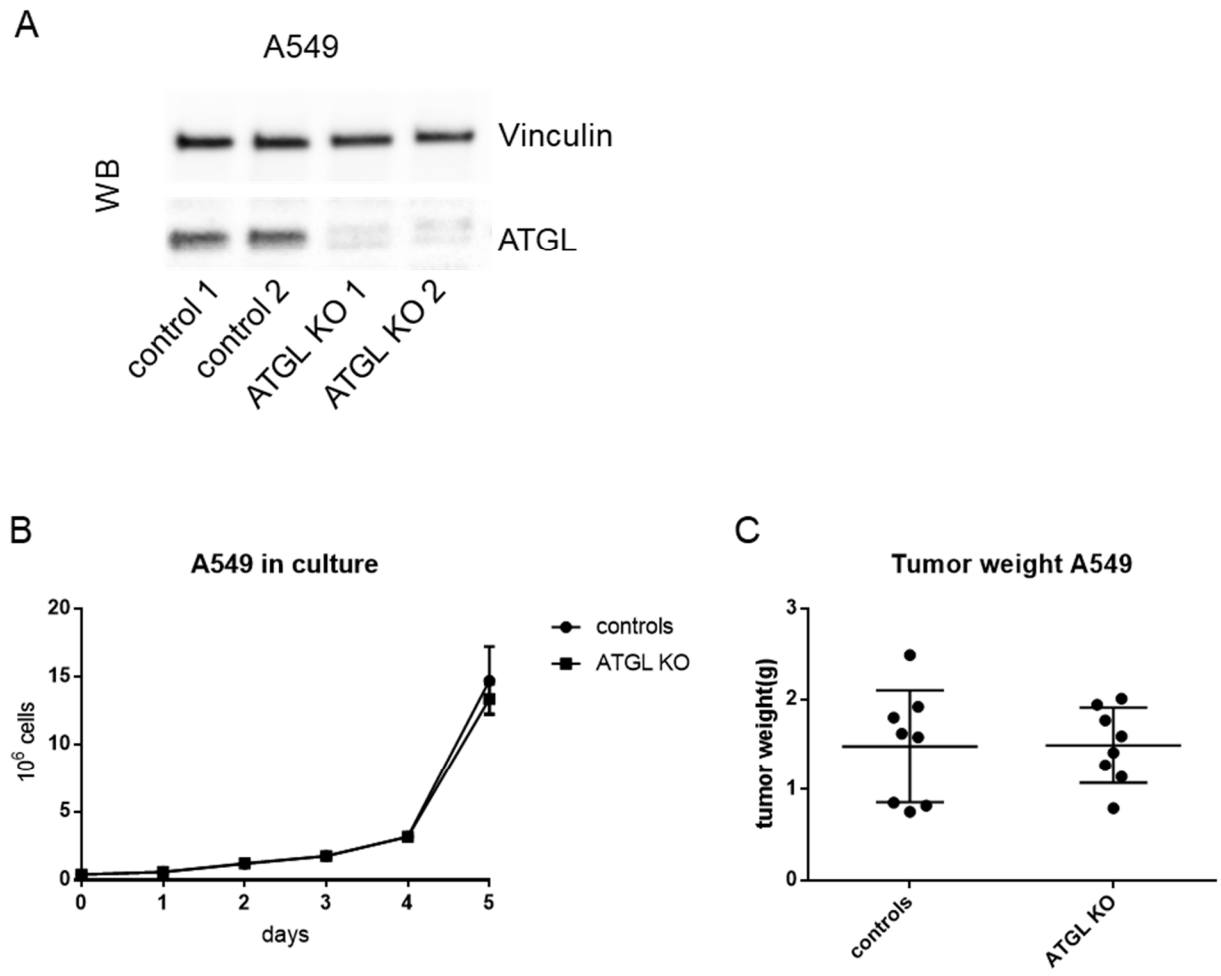

Figure 6: *In vitro* and *in vivo* proliferation of AKO A549 lung cancer cells. (A) WB analysis of ATGL knockout. 2 control and 2 AKO A549 single cell derived clones were analyzed using α-ATGL antibodies. Vinculin was used as a loading control. **(B)** *In vitro* proliferation. Proliferation of A549 single cell derived control and AKO clones was analysed by measuring doubling time with a CASY cell counter. Each data set represents the mean of at least 2 biological replicates. **(C)** *In vivo* tumor growth. At least 2 single cell derived clones were injected into immune-compromised NSG mice and tumor weight was measured after 39 weeks. Each data set represents the mean and SD of at 8 independent biological replicates.

Similar results were obtained when we knocked down ATGL in B16F10 melanoma cells. ATGL knockdown was confirmed by WB -and qRT-PCR analysis and showed about 80% reduction of ATGL expression (Figure 7A). We measured doubling time of control and ATGL knockdown B16F10 cells and did not observe any significant differences in proliferation. When we injected control and knockdown cells into the tail

vein of C57BL/6 mice, we did not see any changes in the metastatic spread and growth of B16F10 cells in the mouse lung (Figure 7BC).

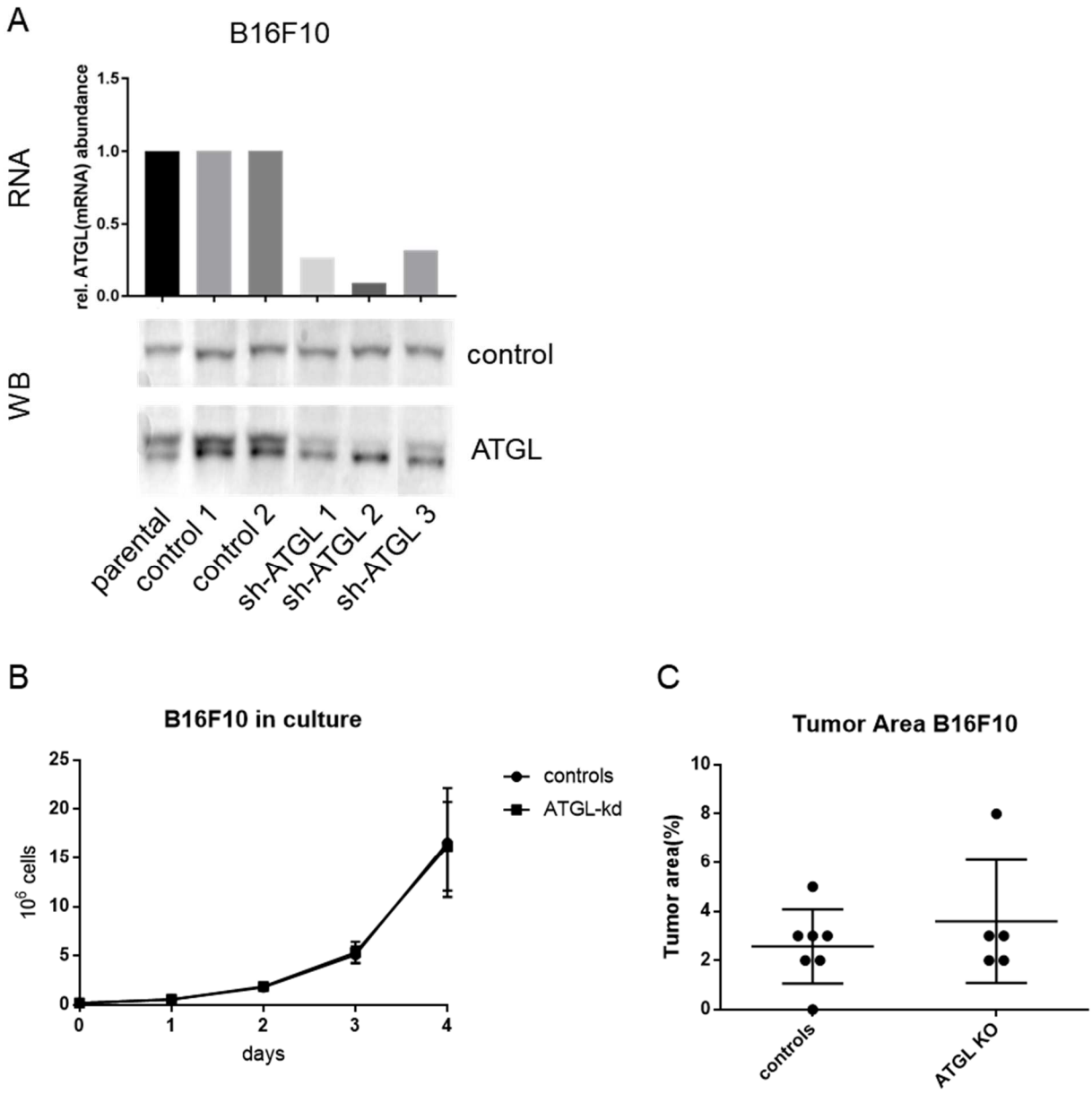

Figure 7: *In vitro* and *in vivo* proliferation of ATGL knockdown B16F10 melanoma cells. (A) WB and qRT-PCR analysis of ATGL knockdown. Parental, 2 control and 3 B16F10 ATGL knockdown cell lines were analysed using α-ATGL antibodies. A non-specific band was used as a loading control. **(B)** *In vitro* proliferation. Proliferation of control and ATGL knockdown B16F10 cell lines was analysed by measuring doubling time with a CASY cell counter. Each data set represents the mean and SD of at least 3

biological replicates. **(C)** *In vivo* tumor growth. Metastatic spread was analysed by injecting control and ATGL knockdown B16F10 cells into the tail vein of C57BL6 mice and histological evaluation of the lung tumor area 16 days post injection. At least 3 control and 3 ATGL knockdown cell lines were injected. Each data set represents the mean and SD of at least 5 biological replicates.

Additionally, we examined other mouse lung cells (C22) and cancer cells (H23, transformed pro B-cells), which yielded similar result (data not shown). Therefore, we concluded that ATGL knockdown or knockout in cancer cells does not influence/promote tumor growth *in vivo* and *in vitro*.

However, in parallel we did note that aged ATGL knockout mice with ATGL expression in the heart (AKO/cTg) developed lung intra-epithelial neoplasia and lung adenocarcinoma, which has been already published by Al-Zoughbi *et al*., 2017 (39). Remarkably, in all (n=49) AKO/cTg animals over 6 months of age, lung bronchiolar intra-epithelial neoplasia occurred spontaneously. When aged over 10 months, invasive adenocarcinoma developed in 5 out of 20 mice. None of the >10 months old littermate control WT/cTg animals developed adenocarcinoma (n=22) and only 2/50 of all age groups showed low grade intra-epithelial neoplasia.
These data pointed to an important role of ATGL in controlling mouse lung tumor development *in vivo*. Therefore, we set out to characterize and examine the lungs of ATGL-deficient mice.

3.2 Metabolic and functional characterization of AKO/cTg lungs

In order to decipher why AKO/cTg mice develop lung neoplasia and adenocarcinoma spontaneously as they age, we analysed the lungs of these animals. We examined H&E stainings of ATGL-deficient lungs and observed that all neoplastic lesions arise in the bronchiolar epithelium, suggesting that bronchial epithelial cells are the origin of the neoplastic development. Figure 8 demonstrates bronchial epithelial hyper-proliferation, leading to spread into the alveolar region. Moreover, IHC analysis could show that bronchial epithelial cells as well as adenocarcinomas of AKO/cTg mice are

CK19 positive, suggesting that adenocarcinomas arise from bronchial epithelial cells (BECs). Taken together these findings argue for an important role of ATGL in BECs, possibly protecting them from neoplastic transformation and development of invasive cancer.

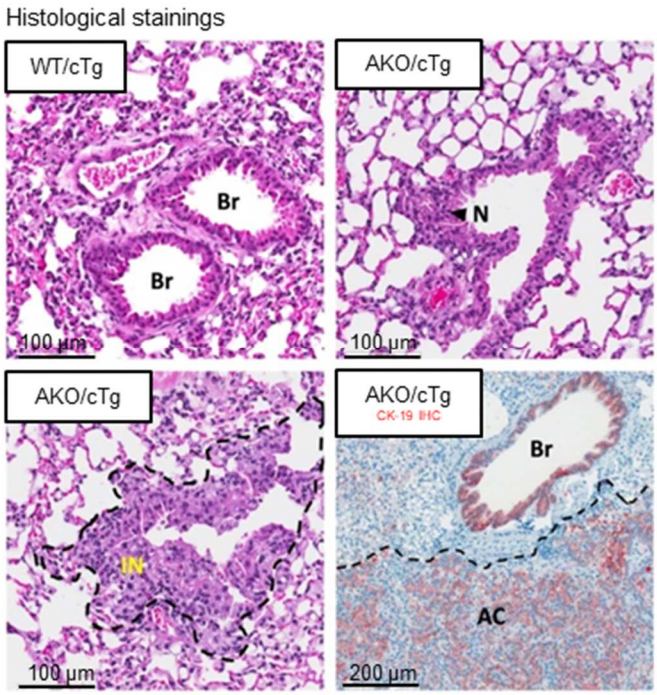

Figure 8: ATGL KO leads to development of bronchial epithelial neoplasia. H&E staining and CK-19 IHC of lung sections from 35-52 weeks old WT/cTg and AKO/cTg mice. Normal bronchiolar epithelium (Br) of WT/cTg mice, bronchoepithelial neoplasia (N) and invading growth into the alveolar space (IN) are indicated. CK-19 IHC shows positive bronchial epithelial cells and adenocarcinomas (AC) of AKO/cTg mice.

In order to determine where *Atgl* is normally expressed in the mouse lung, we performed *Atgl in situ* hybridization. *Atgl* is mainly expressed in the bronchiolar epithelium of WT/cTg mice and absent in AKO/cTg animals (Figure 9), suggesting that lack of ATGL in bronchial epithelial cells triggers cellular proliferation and leads to bronchial epithelial neoplasia.

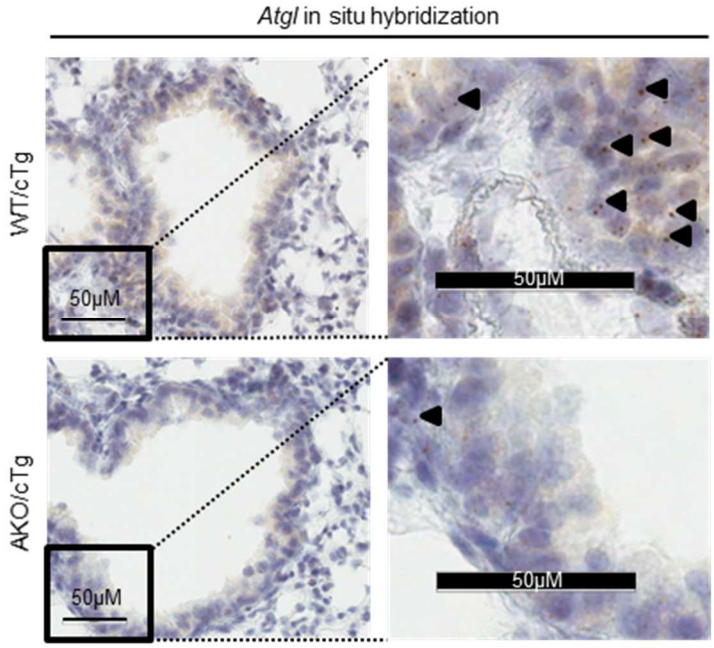

Figure 9: *Atgl* is mainly expressed in bronchial epithelial cells (BECs). *Atgl in situ* hybridization of lung sections from 35 weeks old WT/cTg and AKO/cTg mice.

Consistent with this finding, AKO/cTg mice showed an increased neutral lipid content, as determined by Oil Red O (ORO) staining in bronchial epithelial cells and also in ATII cells. Lipid analysis by mass spectrometry was performed in cooperation with Thomas Eichmann from the University of Graz and showed that only TG species are significantly elevated in AKO/cTg lungs. This observation was confirmed by a targeted biochemical measurement, which showed a 12-fold increase of TG (Figure 10ABC).

A

Lipidomics

Lipid species	Relative LC-MS peak area(AU)/ug protein		Significance
	WT/ctg	Ako/ctg	
Triacylglyceride(TG)	100 +/- 59	239 +/- 11	p = 0,016
Sphingomyelin(SM)	24 +/- 2,3	24,6 +/- 2,1	n.s.
Ceramide(CER)	1,5 +/- 0,18	1,84 +/- 0,48	n.s.
Phosphatidylcholine(PC)	89,9 +/- 1	98,2 +/- 8,4	n.s.
Cholesterol-ester(CE)	0,04 +/- 0,01	0,08 +/- 0,04	n.s.
Free cholesterol(FC)	0,02 +/- 0,01	0,02 +/- 0,002	n.s.
Lysophosphatidylcholine(LPC)	14,1 +/- 1,5	14,4 +/- 2	n.s.

B

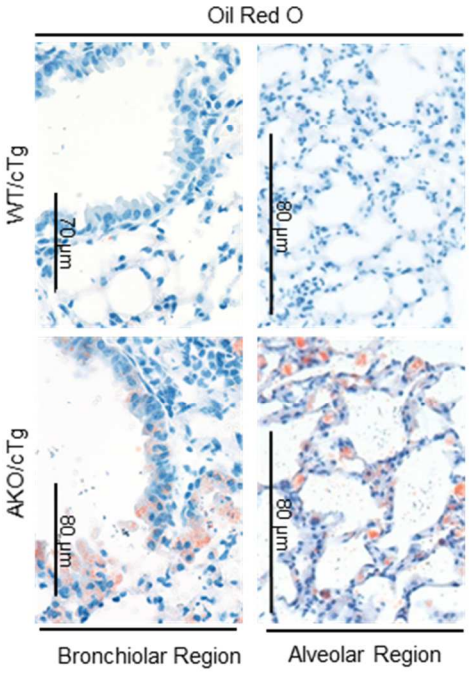

C

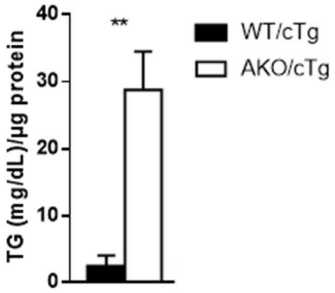

Figure 10: ATGL deficiency leads to massive TG accumulation in the lung. (A) Lipidomics analysis. Lungs of 35 weeks old WT/cTg and AKO/cTg mice were analysed by mass spectrometry. Shown are mean, SD and significance of all identified lipid classes (n=3). **(B)** Lung Oil Red O (ORO) staining of 35 weeks old mice. **(C)** Targeted biochemical measurement of TG from lungs of WT/cTg and AKO/cTg mice. Each data set represents the mean and SD of 3 independent biological replicates. Statistically significant differences were determined by Student's unpaired t-test (two-tailed; **, $p < 0.01$ between genotypes).

Moreover, it was reported that ATGL is not only hydrolyzing neutral lipids but also retinylesters (20). Therefore, we investigated together with Laura Pajed and Achim Lass from the University of Graz, retinylester and free retinol levels in the mouse lung, as vitamin A is an essential metabolite in lung development und function (81, 68, 69).

Interestingly, we observed that retinylesters are increased, whereas retinol is decreased in AKO/cTg lungs (Figure 11D). This implies that ATGL is indeed hydrolyzing retinylesters in the mouse lung and shows that AKO/cTg mice have a perturbed vitamin A metabolism.

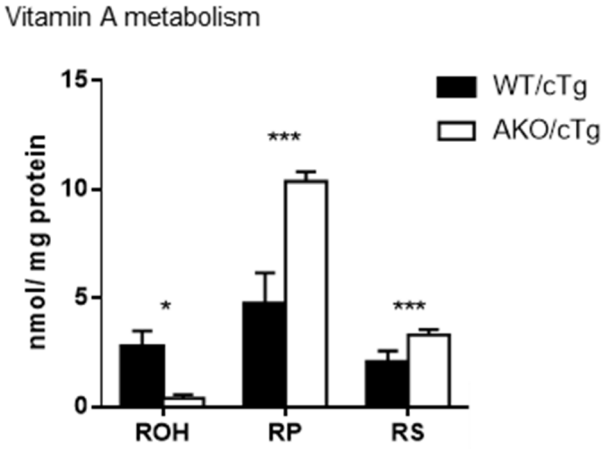

Figure 11: Disturbed vitamin A metabolism. Vitamin A metabolite measurement of 13-15 weeks old WT/cTg and AKO/cTg mice. Each data set represents the mean and SD of 3 independent biological replicates. ROH = retinol, RP = retinylpalmitate, RS = retinylstearate. Statistically significant differences were determined by Student's unpaired t-test (two-tailed; *, $p < 0.05$ and ***, $p < 0.001$ between genotypes).

In order to investigate the functionality of ATGL deficient lungs, we measured lung function in cooperation with Leigh Marsh from the LBI LVR (Graz). Intriguingly, AKO/cTg mice had significantly reduced total lung capacity due to slightly increased airway resistance and decreased airway compliance (Figure 12). In essence, this means that AKO/cTg have stiffer airways, which leads to a reduced amount of air entering the lungs.

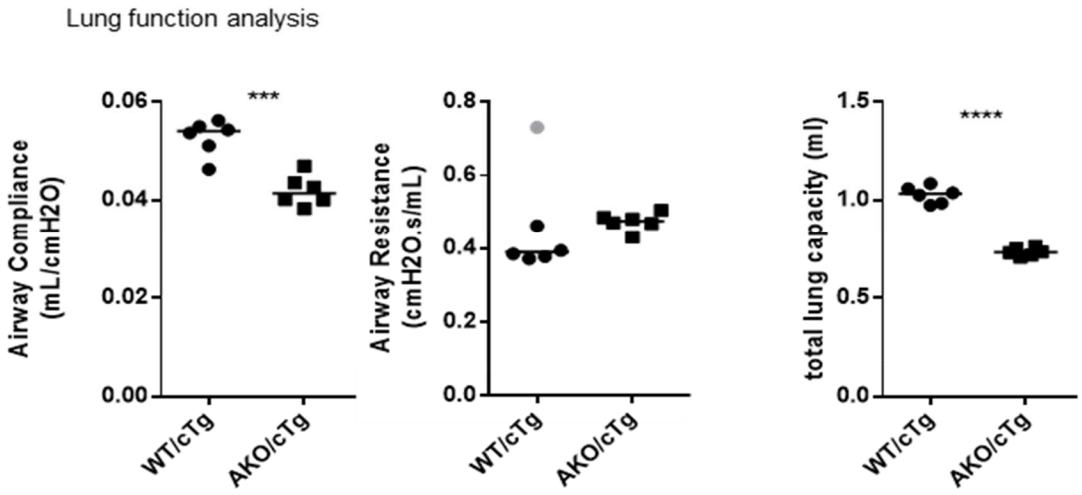

Figure 12: Decreased lung function of AKO/cTg mice. Lung function of 28 weeks old mice was determined by measuring airway compliance, airway resistance and total lung capacity with a FlexiVent apparatus. Each data set represents mean and SD of 6 independent biological replicates. Statistically significant differences were determined by Student's unpaired t-test (two-tailed; ***, $p < 0.001$ and ****, $p < 0.0001$ between genotypes).

Therefore, we conclude from the metabolic and functional characterization of AKO/cTg lungs that ATGL is important for lung lipid metabolism. ATGL-deficiency is leading to severe lipid accumulation in ATII and bronchial epithelial cells, which might lead to increased proliferative capacity and decreased lung function. Moreover, ATGL exerts important retinylester hydrolase activity in the mouse lung, which might affect several developmental and differentiation pathways.

3.3 Impaired club cell function

Our initial experiments indicated that ATGL's function is especially important for BECs, as these cells show severe lipid accumulation and progressive hyperproliferation.
Therefore, we analyzed marker proteins of several main lung cell types, *i.e.* AT-II, ciliated and club cells on protein and RNA level. Strikingly, among all only CCSP was found to be affected. Loss of CCSP pointed to impaired club cells in AKO/cTg mice

(Figure 13A). Most likely, this effect was observed due to decreased CCSP protein stability as *Scgb1a1* mRNA level and CCSP translation remained unchanged (Figure 13BC). In contrast, marker proteins of other lung cells were not affected by ATGL knockout (Figure 13AB).

Due to CCSP's anti-inflammatory and cyto-protective function as well as its involvement in several diseases like COPD and smoking associated cancer, we were wondering if the loss of CCSP is connected to the observed neoplasia phenotype. Therefore, we examined H&E images of 6, 12 and 18 months old CCSP-KO mice in cooperation with Caroline Owen from the Harvard Medical School, Boston, USA. Intriguingly, we could not find any intraepithelial neoplastic lesions in CCSP-KO mice, which suggests that the loss of CCSP alone is not responsible for the neoplasia phenotype in AKO/cTg mice (Figure 13D).

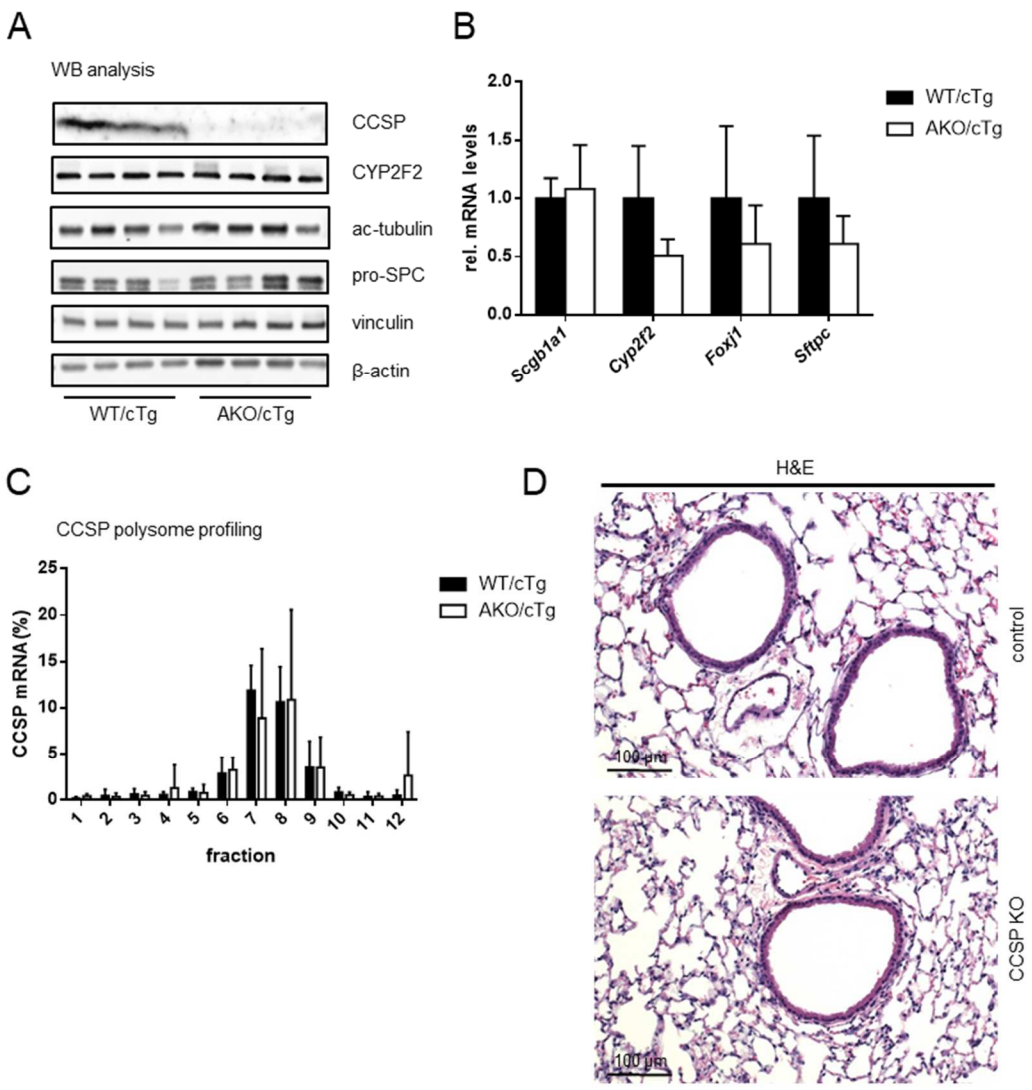

Figure 13: Reduced CCSP protein levels. **(A)** WB analysis of lung tissue samples of 35 weeks old mice. 4 independent biological lung tissue replicates per genotype were analysed using α-CCSP and α-CYP2F2 (club cell markers), α-ac-tubulin (ciliated cell marker) and α-pro-SPC (ATII cell marker) antibodies. Vinculin and β-actin were used as a loading control. **(B)** q-RT PCR analysis. Shown are *Scgb1a1* (club cell marker), *Cyp2f2* (club cell marker), *Foxj1* (ciliated cell marker) and *Sftpc* (ATII cell marker) expression levels of 35 weeks old WT/cTg and AKO/cTg mice normalized to the housekeeping gene *β-actin*. Each data set represents mean and SD of at least 4 independent biological replicates. **(C)** CCSP polysome profiling of 33-38 weeks old mice. CCSP (*Scgb1a1*) mRNA was detected by q-RT PCR analysis in polysome fraction 1-12. Each data set represents mean and SD of at least 5 independent biological replicates. **(D)** H&E of 12 months old control and CCSP KO lung sections. Lung sections of 6, 12 and 18 months old mice have been evaluated by an experienced pathologist.

However, the perturbed CCSP expression indicated that AKO/cTg club cells were affected by ATGL loss and therefore we decided to further analyze bronchial epithelial club cells of WT/cTg and AKO/cTg mice by transmission electron microscopy. Electron microscopy images revealed that the number of club and ciliated cells of WT/cTg and AKO/cTg mice was similar in both genotypes (Figure 14B). However, AKO/cTg club cells displayed a reduced number of mitochondria and secretory vesicles (Figure 14A). In addition, club cell size was enlarged, most likely due to the presence of lipid droplets (Figure 14B). As secretory vesicles in club cells are the main site for CCSP storage it is tempting to suggest that the reduction in CCSP is due to inefficient secretory vesicle biogenesis.

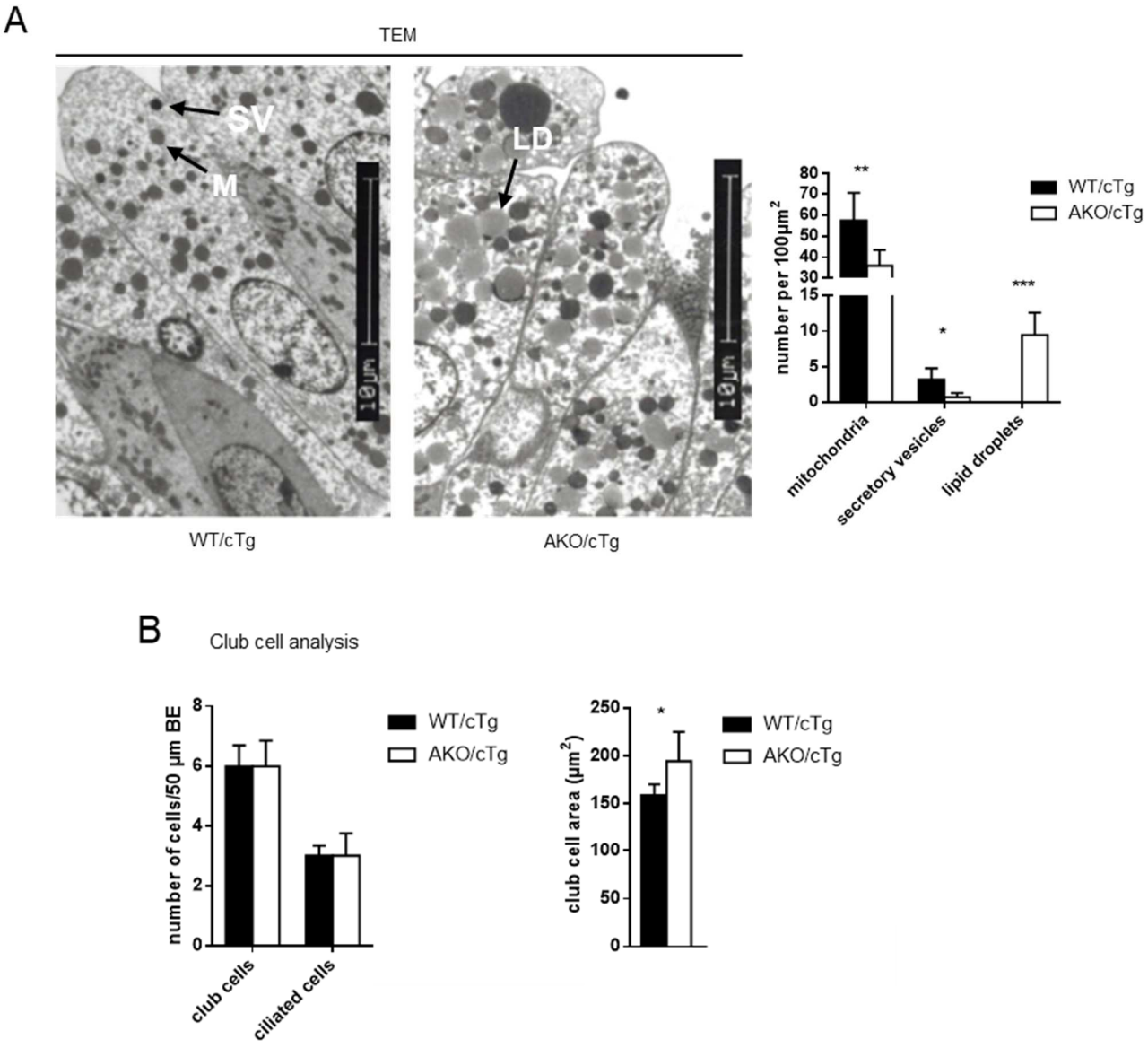

Figure 14: Reduced mitochondrial and secretory vesicle numbers in AKO/cTg club cells. (A) Transmission Electron microscopy (TEM) images showing club cells of 35 weeks old mice. Arrows point to M= mitochondria, SV= secretory vesicles and LD= lipid droplets. Bars represent quantification of TEM images and each data set represents the mean and SD of at least 4 independent biological replicates. (B) Club and ciliated cell number of 35 weeks old mice. Each data set represents the mean and SD of at least 4 independent biological replicates. Statistically significant differences were determined by Student's unpaired t-test (two-tailed; *, $p < 0.05$, **, $p < 0.01$, and ***, $p < 0.001$ between genotypes).

Figure 15 shows high magnification TEM images of WT/cTg and AKO/cTg club cells. Those were used to distinguish between secretory vesicles, mitochondria and lipid

droplets in a cooperation with Gerd Leitinger, Gottfried Schatz Research Center, Molecular Biology and Biochemistry, Graz, Austria.

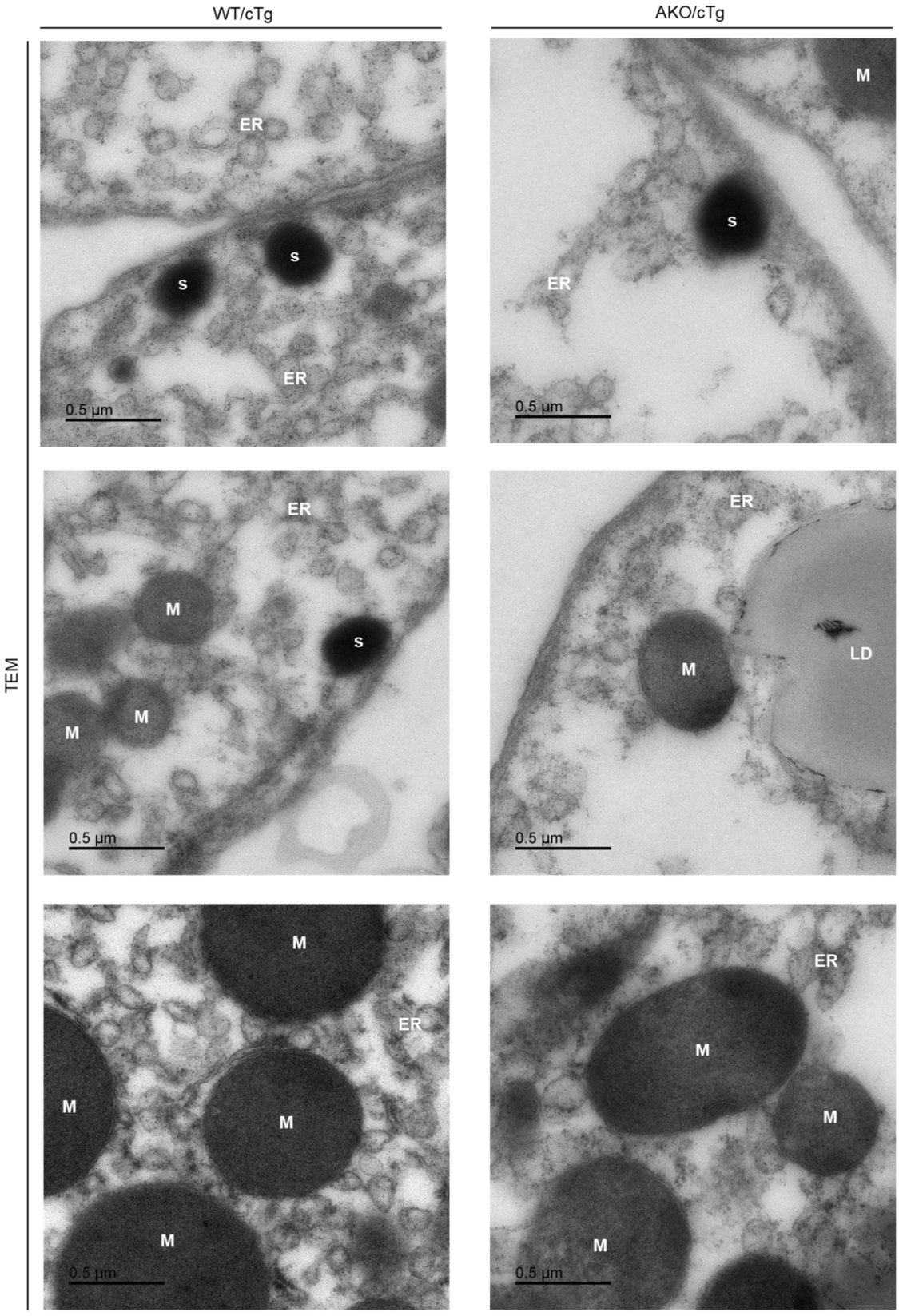

Figure 15: High power TEM images of mitochondria, secretory vesicles and lipid droplets. Club cells from 35 weeks old WT/cTg and AKO/cTg mice were analysed using electron microscopy. Higher power magnification was used to visualize M=Mitochondria, S=Secretory vesicles, ER=endoplasmic reticulum.

The reduced number of mitochondria in AKO/cTg club cells indicated a metabolic impairment. To investigate their metabolic capacity we decided to perform oxygen consumption measurements using the Oroboros instrument.

However, for such an analysis it was needed to enrich the club cell population as they make up only 1% of the whole lung. We established a club cell isolation procedure based on a protocol from Oreffo *et al.* using several modifications as described in the Material and Methods section. By trypsinization and a step gradient, we were able to enrich club cells 20-fold (data not shown). Interestingly, when analyzed in the Oroboros chamber, WT/cTg and AKO/cTg club cells showed similar baseline respiration. However, after permeabilization with digitonin and the addition of FAs (octanoylcarnitine), complex I (glutamate) and complex II (succinate) substrates, the oxygen consumption rate was decreased in AKO/cTg club cells. Using the complex I inhibitor rotenone, it was clearly appreciable that especially complex II was affected by ATGL deficiency. As expected, addition of the ATP-synthase inhibitor oligomycin led to reduced respiration in cells from both genotypes. However, the difference between the genotypes stayed the same. This points to reduced ATP production in mitochondria from AKO/cTg club cells. To understand the contribution of non-mitochondrial respiration, Antimycin A was used to completely disrupt the respiratory electron transport chain (Figure 16).

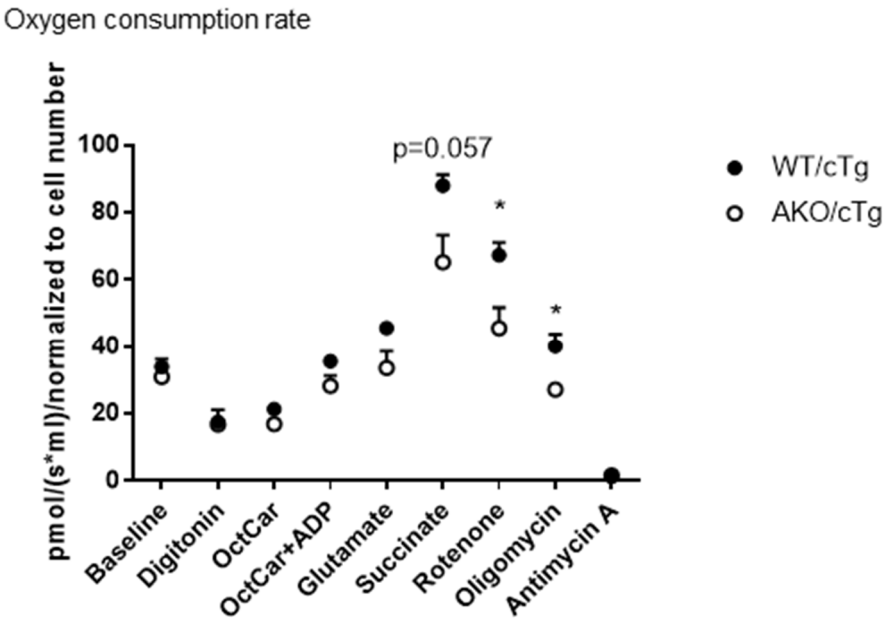

Figure 16: Reduced OCR of AKO/cTg club cells. Club cells were isolated and oxygen consumption rate (OCR) measured using an Oroboros instrument. After baseline OCR was determined, cells were permeabilized with digitonin. Various substrates were added to visualize OCR of mitochondrial complexes, as depicted. Each data set represents the mean and SD of at least 3 independent biological replicates. Per replicate club cell isolations of 4 mice were pooled. Statistically significant differences were determined by Student's unpaired t-test (two-tailed; *, $p < 0.05$ between genotypes).

Moreover, we performed a microarray experiment in cooperation with Karin Wagner from the Core Facility Molecular Biology (Graz) with WT/cTg and AKO/cTg club cell isolations. RNA expression analysis indicated that especially PPAR-γ regulated genes are deregulated in AKO/cTg club cells (Figure 17), supporting the finding of perturbed mitochondrial metabolism. A full list of significant changes can be seen in the Table 4 in the appendix.

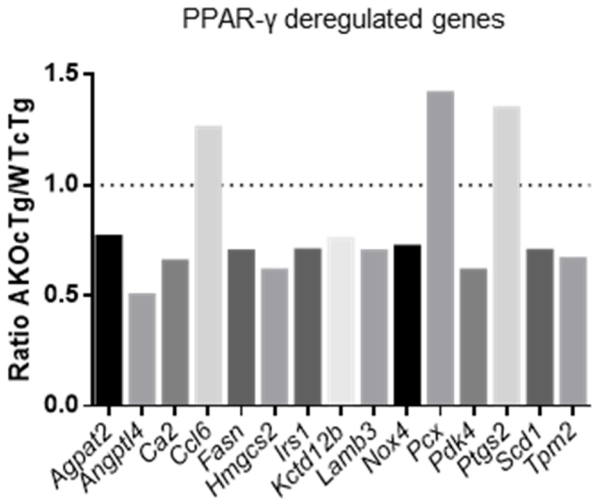

Figure 17: Deregulated PPAR-γ signalling in AKO/cTg club cells. Club cells of 40 weeks old mice were isolated and subjected to RNA expression analysis using a gene expression Microarray as described in the Material and Methods section. Each data set represents the ratio of AKO/cTg (n=4) to WT/cTg (n=4) expression levels of significantly deregulated genes in the PPAR-γ pathway (*Agpat2-Tpm2)*.

Investigation of BECs showed that in particular club cells are impaired in AKO/cTg mice. We could show that under baseline conditions, AKO/cTg club cells have reduced secretory vesicles, CCSP expression and mitochondrial content as well as deregulated PPAR-γ signaling. This resulted in a reduced oxygen consumption rate, which suggests that AKO/cTg club cells face energetic problems.

3.4 Fenofibrate does not reduce lipid levels and neoplasia incidence

Since we observed deregulated lipid metabolism and PPAR signaling in club cells of AKO/ctg mice, we decided to treat mice with the PPAR-α agonist fenofibrate. Thereby, we exploited a similar approach to the one in the work of Haemmerle *et al.* (18). Here, they showed that ATGL produces lipid ligands for PPAR activation, which is an important signaling pathway for normal mitochondrial biogenesis and function. Using PPAR-α agonists, they were able to rescue mitochondrial substrate oxidation and respiration, reduce the lipid accumulation and, thereby, preventing lethal cardiomyopathy and premature death of whole body ATGL KO mice. Hence, we

hypothesized that treatment with fenofibrate might ameliorate lipid accumulation in the lung by increasing mitochondrial β-oxidation of fatty acids generated by other lipases (e.g. HSL).

Consequently, we fed mice a 0.2% fenofibrate diet for 30 weeks, starting after weaning of the animals. Mice were sacrificed at 35-weeks of age and lungs were excised for analysis.
Fenofibrate treatment increased target gene expression in the lungs of WT/cTg as well as AKO/cTg mice as expected (Figure 18A). However, ORO staining and TG analysis showed that fenofibrate supplementation was not able to reduce the lipid amount in the lung of AKO/cTg mice (Figure 18B). Moreover, neoplasia analysis did not show a significant reduction in neoplastic lesions after fenofibrate treatment (data not shown).

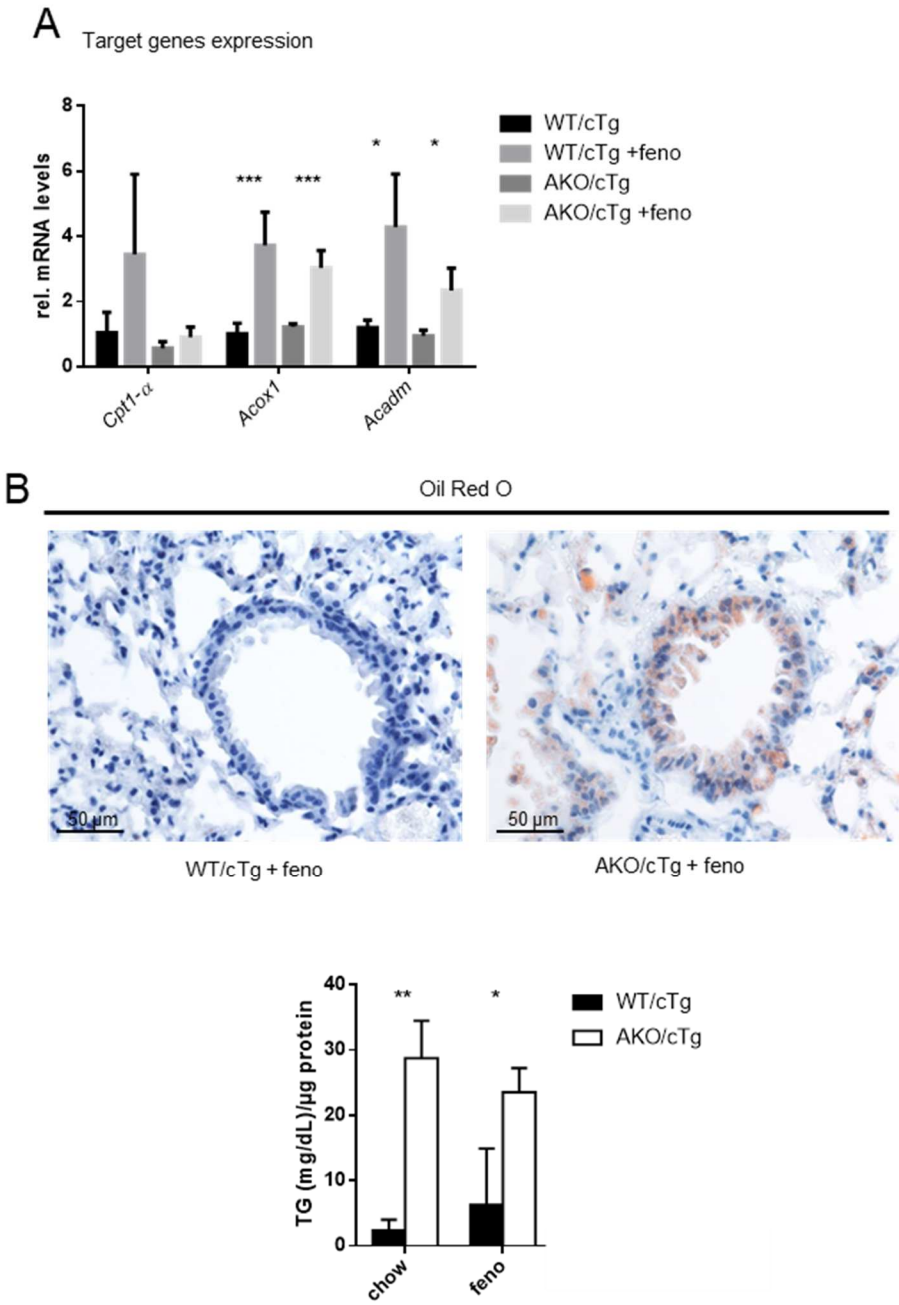

Figure 18: Fenofibrate does not prevent lipid storage. (A) q-RT PCR analysis. Shown are *Cpt-1α*, *Acox1* and *Acadm1* expression levels of chow and 0.2% fenofibrate treated WT/cTg and AKO/cTg mice normalized to the housekeeping gene β-actin. Each data set represents mean and SD of at least 4 independent biological replicates. **(B)** Oli Red O staining of lung sections and targeted biochemical measurement of TG. Mice were either fed a 0.2% fenofibrate or a normal chow diet for 30 weeks. Mice were sacrificed at 35 weeks of age. Mice received either chow or 0.2% fenofibrate diet for 30 weeks Data sets represent the mean and SD of at least 3 independent biological replicates. Statistically significant differences were determined by Student's unpaired t-test (two-tailed; *, $p < 0.05$, **, $p < 0.01$, and ***, $p < 0.001$ between genotypes).

Consequently, treatment with the PPAR-α agonist fenofibrate was not useful to study a link between perturbed lipid metabolism/lipid accumulation and bronchial epithelial neoplasia.

3.5 Reduced regenerative potential after NA challenge

One way to challenge and subsequently analyze club cell regeneration is by using the club cell toxin Naphthalene (NA). NA specifically targets and kills CYP2F2 expressing club cells. Two days after NA injection marks the time point when damage of the bronchiolar epithelium reaches its maximum. Afterwards variant club and double positive (SPC+ and CCSP+) cells start to proliferate and regenerate the bronchiolar epithelium (59, 63).

We hypothesized that the severe lipid accumulation and the subsequent metabolic and energetic impairment due to ATGL-deficiency affects club cell regeneration.
To test our hypothesis *in vivo,* we treated mice with a single dose (acute NA) or multiple doses of NA (mNA). Acute NA treatment consisted of one NA injection (day 0), one EdU injection (day 2 post NA) to trace proliferation and sacrifice of the animals on day 3 post NA injection. This treatment regime allowed us to assess the proliferative capacity of WT/cTg and AKO/cTg variant club cells and the amount of damage that occurred by NA treatment. As variant club cells are spared from NA induced cell death due to their reduced CYP2F2 expression, these cells are able to proliferate after bronchial epithelial cell death. In addition, we were able to assess damage and regeneration by analyzing the cellular composition of the bronchiolar epithelium after NA injection. The multiple NA regime comprised 4 injections of NA in the course of 4 weeks and a subsequent regeneration period of 8-10 weeks. Using this regime, we were able to examine the long-term effects of repeated NA injections on the regeneration of the bronchiolar epithelium.

Acute NA treatment led to expected ablation of CYP2F2 expressing club cells. Interestingly, damage and/or reduced short term regeneration of the bronchiolar epithelium was more pronounced in AKO/cTg mice. AKO/cTg mice displayed significantly less $CYP2F2^{+}$ cells in the bronchiolar epithelium 3 days after NA

treatment. Interestingly, even when the mice had a prolonged regeneration period after multiple NA treatments (mNA), club cell number could not be re-established in AKO/cTg mice to pre-treatment levels. In contrast, NA treated WT/cTg mice were able to restore initial club cell numbers after this prolonged regeneration period (Figure 19).

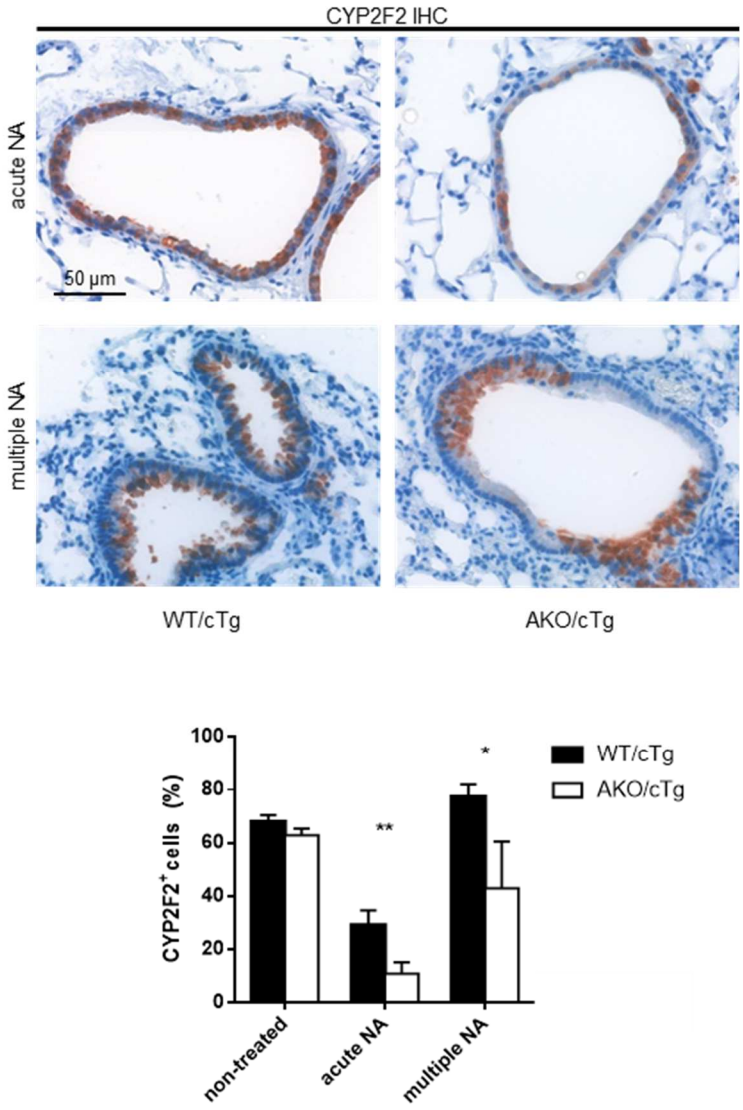

Figure 19: Regeneration after Naphthalene treatment: CYP2F2 IHC of lung sections from NA treated mice. 35 weeks old male mice were treated with one dose of NA and sacrificed 3 days post NA administration (=acute NA). In a separate experiment, 22-25 weeks old male mice were treated 4 times with NA, aged for 8 weeks and sacrificed subsequently (multiple NA, mNA). Bars represent quantification of CYP2F2 cells by immunohistochemistry. Shown are the percentages of $CYP2F2^+$ cells in the bronchiolar epithelium at the respective endpoints. Each data set represents the quantification of at least 3 independent biological replicates. At least 10 bronchioles per replicate were

analyzed. Statistically significant differences were determined by Student's unpaired t-test (two-tailed; *, $p < 0.05$, and **, $p < 0.01$ between genotypes between genotypes).

Western blot analysis confirmed reduced club cell numbers by a decrease in CYP2F2 protein expression, especially after mNA treatment. Moreover, we observed increased pro-inflammatory pSTAT3 signaling that is indicative of still ongoing bronchial epithelial repair after mNA treatment in AKO/cTg mice. Interestingly, we also detected reduced pS6 levels, which argues for a metabolic incapability to carry out the repair process (Figure 20).

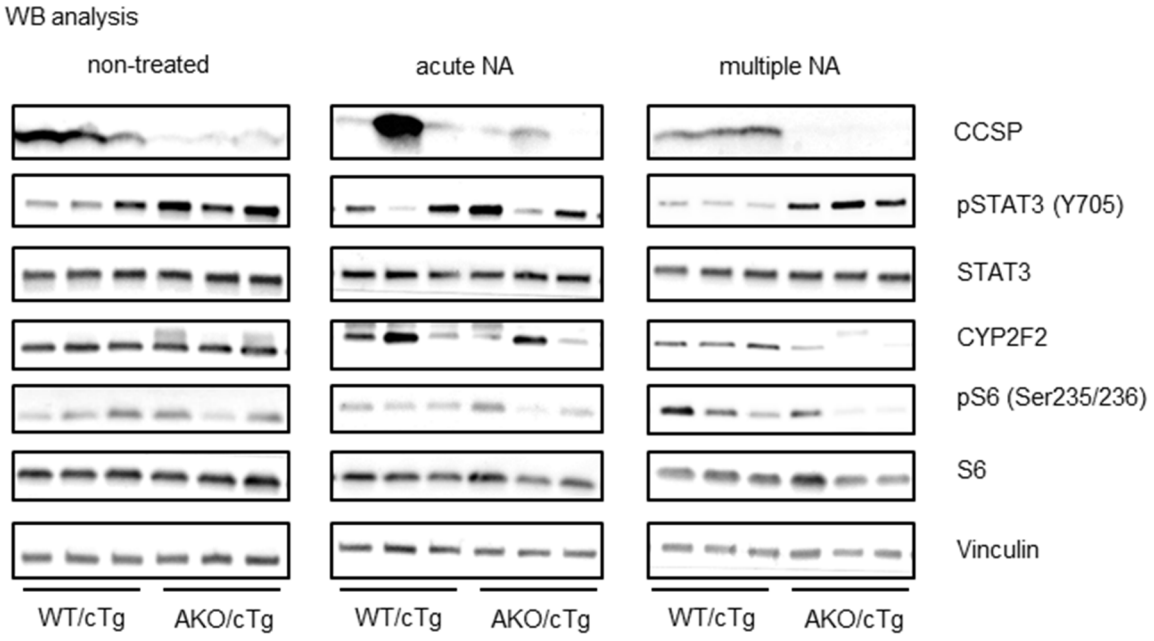

Figure 20: Increased pro-oncogenic, inflammatory STAT3 signaling and reduced metabolic activity. Western blot analysis of lung tissue samples from non-treated, acute NA and multiple NA treated mice. Shown are 3 independent biological samples analysed using the antibodies indicated. Vinculin was used as a loading control.

Differences in the outcome of NA treatment on CYP2F2 expressing club cells between WT/cTg and AKO/cTg animals could not be explained due to decreased proliferation or increased apotosis, as they were similar between the genotypes (Figure 22AB). However, when we examined bronchioles after mNA treatment and long-term regeneration, ciliated cell streches replaced to some extend absent CYP2F2+ cells

(Figure 21). Since NA treatment did not affect proliferation nor apoptosis of WT/cTg and AKO/cTg mice, ciliated cell stretches argue for differentiation of variant club cells and/or double positive cells into the ciliated cell lineage.

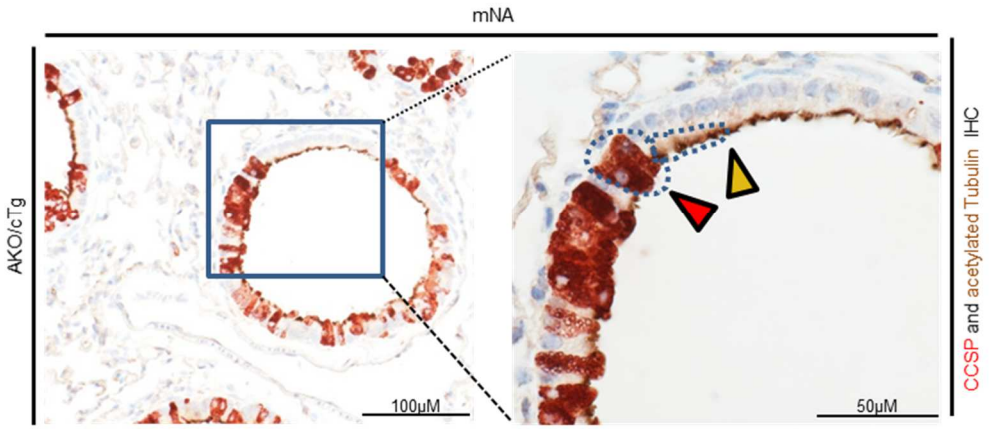

Figure 21: Ciliated cells replace club cells after NA treatment. IHC of CCSP (red) and ac-tubulin (brown) of 35 weeks old male AKO/cTg mice after mNA treatment. Shown is a bronchiole in low and high magnification to visualize ciliated cell stretches.

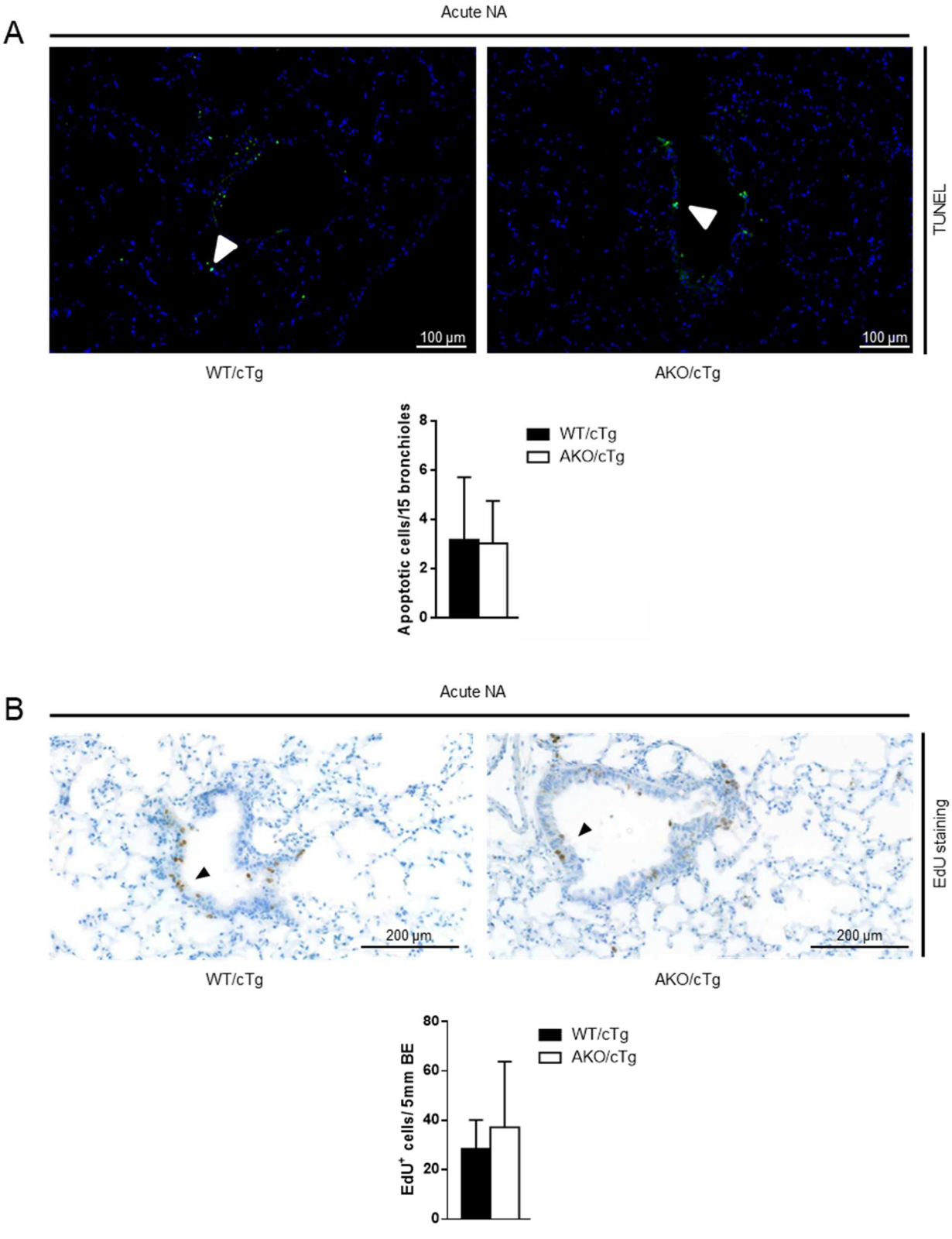

Figure 22: Proliferation and apoptosis in bronchioles of 35 weeks old mice after acute NA treatment. (A) Apoptosis was measured by performing a cell death assay on lung sections. Shown are apoptotic cells (green) per bronchiolar epithelium. Each data set represents mean and SD of at least 3 independent biological replicates. **(B)** Proliferation

was measured by the detection of cells that have incorporated EdU. EdU^+ cells were quantified by counting positively stained cells (brown) on lung sections after detection by the Click-it Edu labeling kit. Shown are EdU^+ cells per length of bronchiolar epithelium. Each data set represents mean and SD of at least 4 independent biological replicates.

Two cell populations, already mentioned in the introduction, which may be important for bronchial epithelial repair after NA challenge are the SPC+ and CCSP+ double positive cells as well as the neuroendocrine cells. Therefore, we investigated these two populations after acute NA and mNA challenge. In line with the literature, the number of SPC and CCSP+ cells did increase after acute NA treatment (Figure 23A). However, there was only a trend towards increased double positive cells in AKO/cTg mice. Intriguingly, the analysis of neuroendocrine cells by CGRP IHC did imply an increased presence of CGRP+ cells (Figure 23B) suggesting, in line with increased pSTAT3 signaling, ongoing bronchial epithelial repair in AKO/cTg animals.

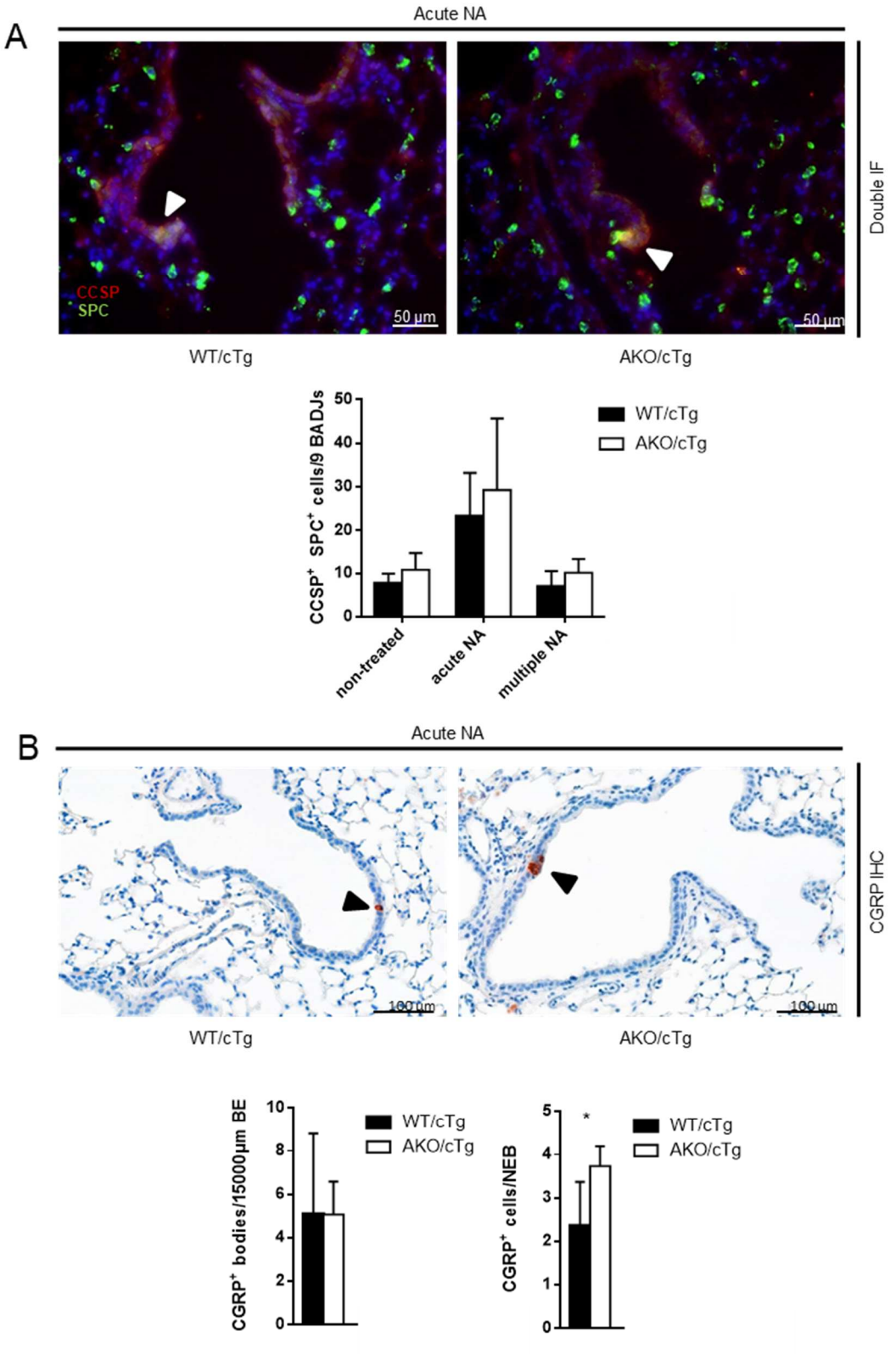

Figure 23: Quantification of double positive and neuroendocrine cells. (A) Double positive cells (yellow) are quantified by analysing double fluorescence images stained for pro-SPC (green) and CCSP (red). Shown are the quantification of $CCSP^+$ and SPC^+ cells per broncho-alveolar duct junction of 35 weeks old non-treated and NA treated mice. Each

data set represents mean and SD of at least 3 independent biological replicates. **(B)** Neuroendocrine cells were counted by analysing $CGRP^+$ cells (red) in a CGRP IHC of 35 weeks old male mice after acute NA treatment. Shown are $CGRP^+$ bodies per bronchiolar epithelium and $CGRP^+$ cells per body. Each data set represents mean and SD of at least 4 independent biological replicates. Statistically significant differences were determined by Student's unpaired t-test (two tailed; *, $p < 0.05$ between genotypes).

3.5.1 Pro-inflammatory signaling in the bronchiolar epithelium of AKO/cTg mice

The experiments using NA to assess club cell functionality implied that AKO/cTg animals are not able to fully regenerate and repair the bronchiolar epithelium. One such indicator was the increased amount of phosphorylated STAT3 in the lungs of mNA treated AKO/cTg animals. Therefore, we used the IL-6/pSTAT3 signaling pathway as a marker to assess the fitness of the bronchiolar epithelium at the steady state level. We investigated IL-6 and pSTAT3 levels in whole lung lysates of 10, 35 and 60 weeks old mice. Moreover, we performed pSTAT3-IHC in cooperation with Lukas Kenner from the Medical University in Vienna, to determine which cells are responsible for the increased p-STAT3 signal.

IHC analysis showed that bronchial epithelial cells are positive for p-STAT3 and that the number of $pSTAT3^+$ cells increases with age. When the mice were around 60 weeks old, one of the upstream activators of STAT3 signaling, namely IL-6, as well as the number of $pSTAT3^+$ bronchial epithelial cells was significantly increased in AKO/cTg mice (Figure 24A and 25). This resulted also in increased pSTAT3 levels in whole lung lysates (Figure 24B). Furthermore, enriched club cell isolations show increased pSTAT3 levels (Figure 24C).

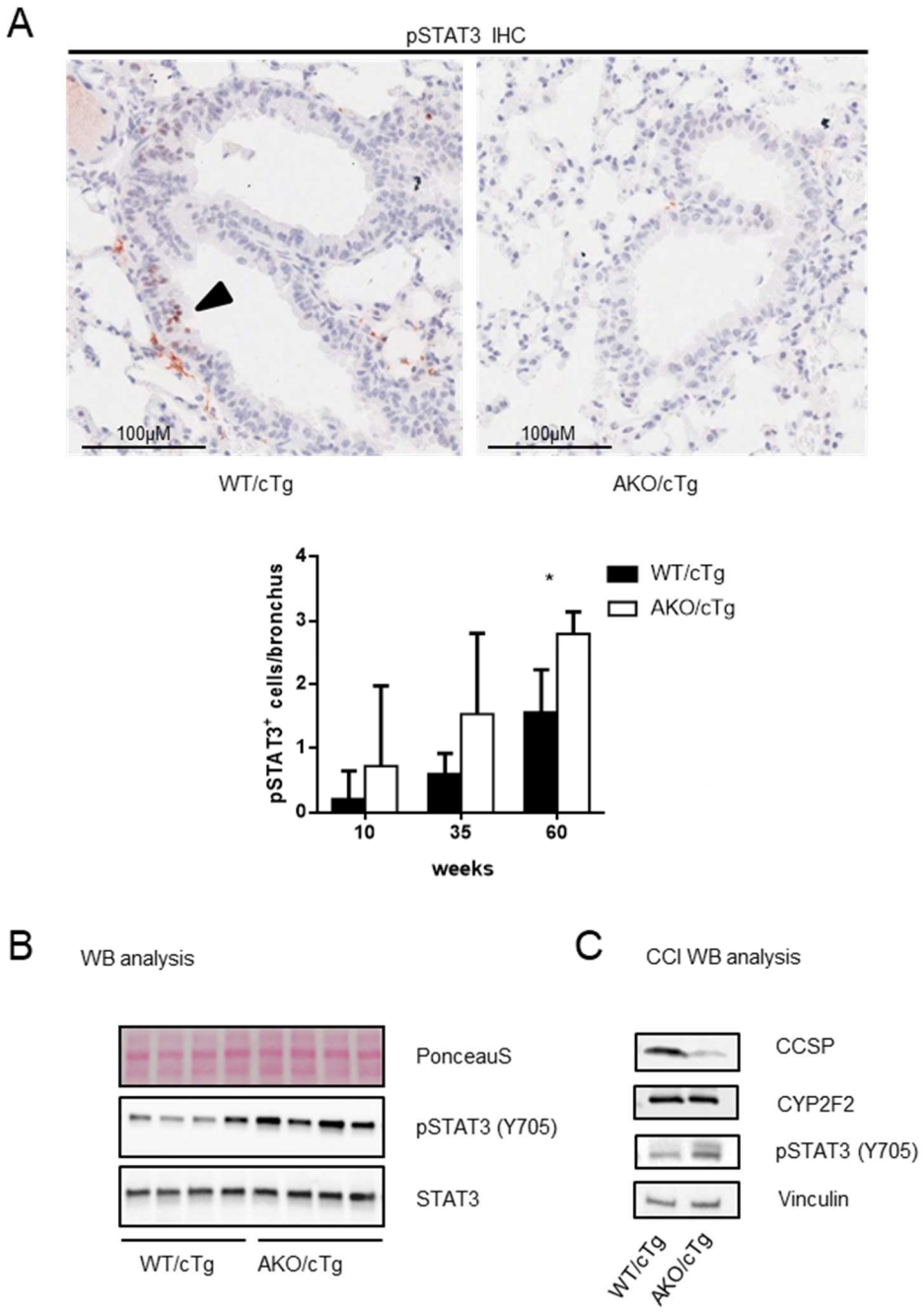

Figure 24: Increased pSTAT3 in lung bronchial epithelial cells and club cells isolates. (A) pSTAT3 IHC images of 60 weeks old mice. Bars represent quantification of pSTAT3 (Y705) IHC images and show pSTAT3$^+$ cells in the bronchiolar epithelium of WT/cTg and AKO/cTg mice as they age. Each data set represents mean and SD of the quantification of at least 3 independent biological replicates. At least 10 bronchioles per replicate were analysed. **(B)** Western blot analysis of lung tissue samples from 60 weeks old mice. 4 independent biological replicates have been analysed using the indicated antibodies. PonceauS was used as a loading control. **(C)** Western blot analysis of club cell isolates from 40 weeks old mice. 4 independent biological replicates were pooled per

genotype and analysed using the indicated antibodies. Vinculin was used as a loading control. Statistically significant differences were determined by Student's unpaired t-test (two tailed; *, $p < 0.05$ between genotypes).

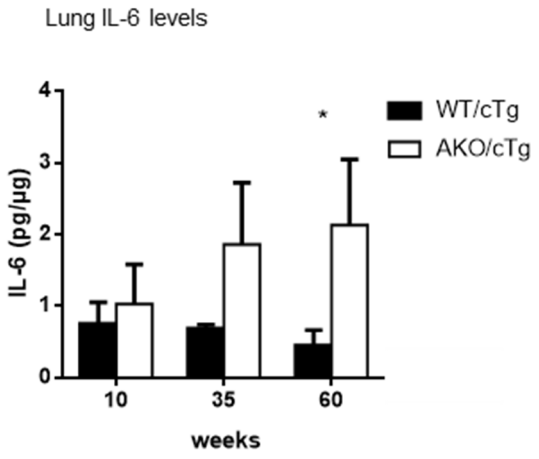

Figure 25: IL-6 levels increase with age. Lung IL-6 levels. Whole lung homogenates were analysed using an IL-6 ELISA. Shown are lung IL-6 levels of WT/cTg and AKO/cTg mice as they age. Each data set represents mean and SD at least 4 independent biological replicates. Statistically significant differences were determined by Student's unpaired t-test (two tailed; *, $p < 0.05$ between genotypes).

We excluded that increased IL-6/pSTAT3 levels derived from immune cell infiltrates, as immuno-FACS analysis of BALF and lung parenchyma of WT/cTg and AKO/cTg mice was comparable (data not shown). In addition, pathohistological analysis of HE stained lung cross sections from WT/cTg and AKO/cTg mice did not show different numbers of immune cells.

Therefore, it can be hypothesized that bronchial epithelial insults, which happen as mice age, trigger bronchial epithelial repair signaling in AKO/cTg mice. Inefficient regeneration, as seen also after acute NA and mNA treatment, might lead to chronic activation of STAT3 signaling and subsequent neoplasia development of BECs.

3.6 ATRA rescues bronchial epithelial regeneration

One of the important factors for lung cell proliferation and differentiation is the active signaling molecule of vitamin A, retinoic acid. Since we noticed that vitamin A metabolism is disturbed in AKO/cTg animals, we hypothesized that retinoic acid supplementation in the form of all-trans retinoic acid (ATRA) might rescue club cell differentiation and regeneration. Therefore, we treated mice with a similar mNA protocol, but in addition, supplemented mice with ATRA and compared them to vehicle treated controls. Strikingly, ATRA supplementation could indeed rescue CYP2F2^{+} club cell number in the bronchiolar epithelium of mNA treated AKO/cTg mice (Figure 26A). Moreover, CYP2F2 protein expression in AKO/cTg lungs was restored to WT/cTg levels as seen by Western blot analysis (Figure 26B). Interestingly, pSTAT3 a well as pS6 signaling remained quite diverse between genotypes.

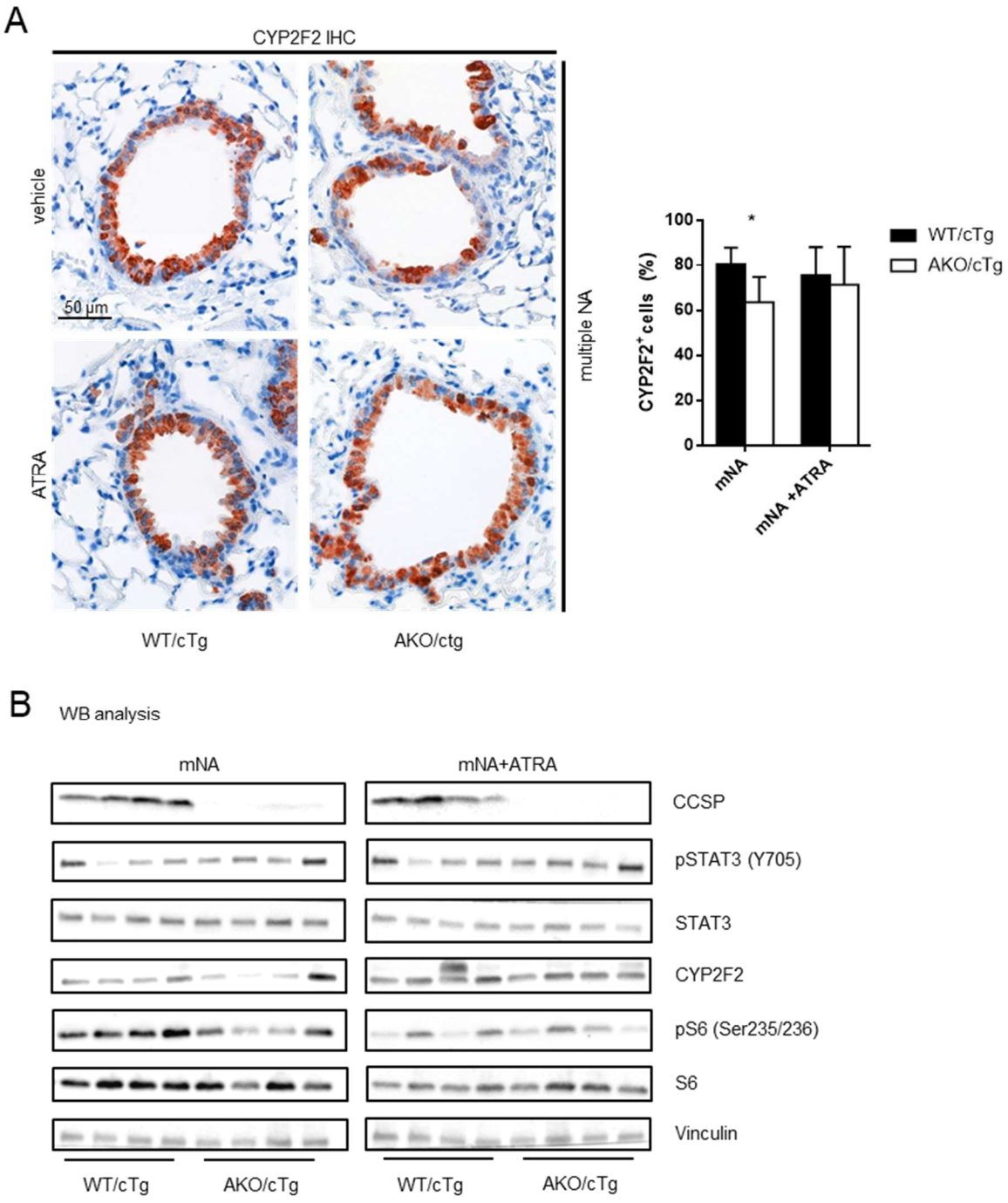

Figure 26: ATRA supplementation rescues club cell regeneration. (A) CYP2F2 IHC of mNA treated mice, with or without ATRA supplementation. All 22-40 weeks old mice were treated with 4 doses of NA (mNA) and had a subsequent regeneration period of 8 weeks. During this time mice received either ATRA supplementation (mNA+ATRA) or vehicle (mNA). Bars represent quantification of CYP2F2 cells by immunohistochemistry. Percentage of $CYP2F2^{+}$ cells in the bronchiolar epithelium after NA treatment is shown. Each data set represents the mean and SD of the quantification of at least 4 independent biological replicates. At least 10 bronchioles per replicate were analysed. **(B)** Western blot

analysis of lung tissue samples from mice treated with mNA, with and without ATRA supplementation. Shown are 4 independent biological samples analysed using the antibodies indicated. Vinculin was used as a loading control. Statistically significant differences were determined by Student's unpaired t-test (two-tailed; *, $p < 0.05$ between genotypes).

This result suggests, that retinoic acid is an important molecule, needed for bronchial epithelial repair, especially for club cell differentiation and regeneration. It implies, that AKO/cTg club cells are dependent on functional vitamin A signaling in order to fulfil their metabolic and regenerative functions.

3.7 Characterization of a club cell specific ATGL knockout mouse

Analysis of the AKO/cTg mouse model, pointed towards an important function of ATGL in bronchial epithelial club cells. Therefore, we decided to establish a club cell specific ATGL KO mouse model to investigate ATGL's specific role in this particular cell type. For that reason, we bred CCSP-driven Cre expressing mice with ATGL floxed mice, to exclusively knockout ATGL in club cells. We checked if the knockout was functional by examining lipid accumulation by ORO staining and TG analysis. Club cell specific ATGL KO mice (CC-AKO) have increased neutral lipid content (Figure 27AB), specifically in bronchial epithelial cells, confirming ATGL knockout. Next, we determined mitochondria and lipid droplet numbers in club cells by analyzing electron microscopy images, similar to the analysis of AKO/cTg mice. However, we could not detect any significant changes in this mouse model. Additionally, when we checked CCSP expression by WB analysis we could not observe the CCSP reduction as seen in AKO/cTg mice. Neoplasia development as well as functional NA studies have not been finalized at this stage of the thesis, but initial observations seem to not fully coincide with results of AKO/cTg mice.

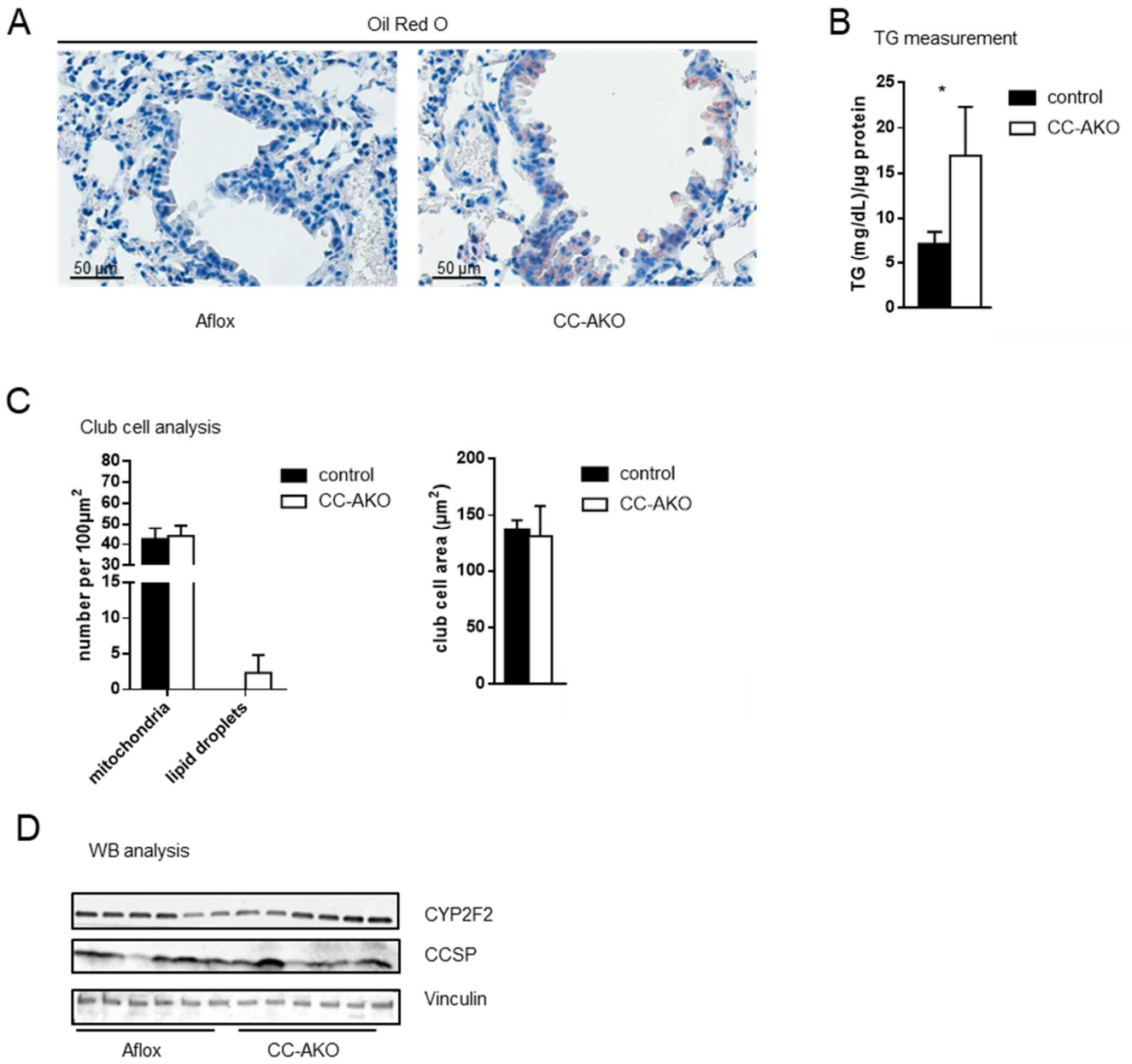

Figure 27: Characterization of CC-AKO mice. (A) Oil Red O staining of 30-40 weeks old control and CC-AKO mice. **(B)** Targeted biochemical measurement of TG. Each data set represents mean and SD of at least 4 independent biological replicates. **(C)** Club cell analysis. Bars represent quantification of electron microscopy images and each data set represents the mean and SD of at least 4 independent biological replicates. Number of mitochondria and lipid droplets per size of club cell and the average size of club cells in control and CC-AKO mice are shown. **(D)** Western blot analysis of lung samples of 30-40 weeks old mice. Six independent biological replicates per genotype analysed with the antibodies indicated are shown. Vinculin was used as a loading control. Statistically significant differences were determined by Student's unpaired t-test (two-tailed; *, $p < 0.05$ between genotypes).

3.8 $KRAS^{G12D}$ activation and concomitant ATGL, CGI-58 or G0S2 loss did not promote lung tumor development

One important, highly mutated oncogene in several tumor types, and also especially prominent in lung cancer, is KRAS. Specifically, the $KRAS^{G12D}$ mutation is often found in tumors of lung cancer patients. Therefore, the lab of Tyler Jacks established a mouse model for lung cancer initiation using an adenovirus based Cre/loxP system (74). A mouse heterozygous for the lox-stop-lox containing $KRAS^{G12D}$ gene and homozygous for a floxed gene of interest is infected with Ad5-Cre by inhalation. This will activate $KRAS^{G12D}$ expression by removing the preceding stop codon and inactivate the gene of interest by removing floxed regions in the same cell of the mouse lung.

We used this system to evaluate concomitant activation of $KRAS^{G12D}$ and loss of several lipolytic keyplayers, namely ATGL, CGI-58 and G0S2. We hypothesized, that defective lipolysis might worsen the tumor burden caused by $KRAS^{G12D}$ action.

Therefore, we inhaled 8-10 weeks old A-flox/$KRAS^{G12D}$ (ATGL-flox/$KRAS^{G12D}$, C-flox/$KRAS^{G12D}$ (CGI-58-flox/$KRAS^{G12D}$) and G0S2 (G-flox/$KRAS^{G12D}$) mice and analyzed their lungs 11 weeks post Ad5-Cre inhalation. Strikingly, we could not detect any differences between the $KRAS^{G12D}$ control group and the groups deficient in either ATGL, CGI-58 or G0S2 with additional $KRAS^{G12D}$ activation. Tumor area as well as the number of proliferating cells indicated by Ki67 staining was comparable between the groups (Figure 28AB).

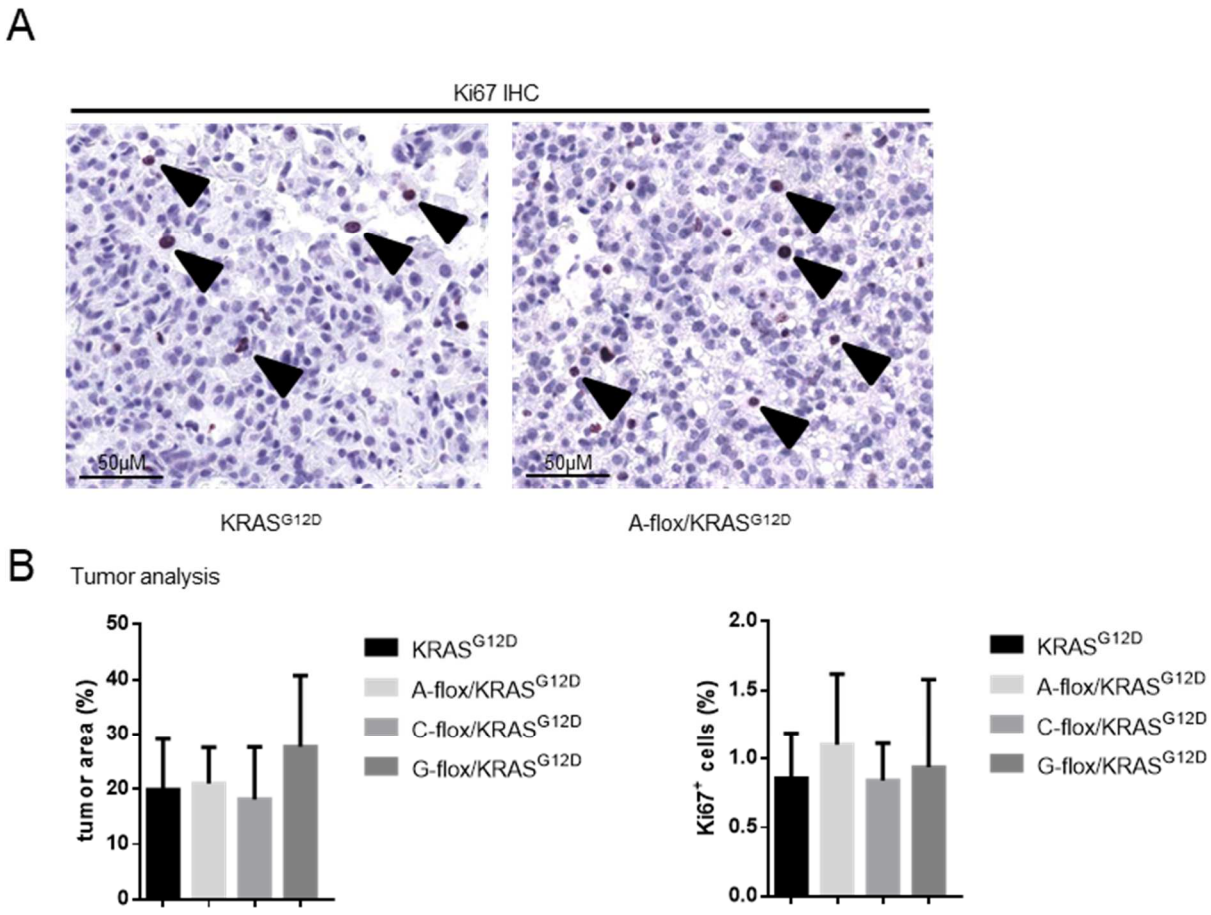

Figure 28: KRAS^{G12D} activation and concomitant ATGL, CGI-58 or G0S2 loss by Ad-Cre inhalation did not promote tumor development. (A) H&E images of KRAS^{G12D} and A-flox/KRAS^{G12D} mice 13 weeks post Ad-Cre inhalation. **(B)** Tumor analysis. Percentage of tumor area was determined by measuring the tumor area in the H&E sections. Percentage of Ki67^{+} cells was determined by counting positive cells in a Ki67 IHC. Each data set represents mean and SD of at least 5 independent biological replicates.

Figure 29 also shows an overview of cancer development in this mouse model. Due to the unspecific targeting and action of the Ad5-Cre virus, cancer foci originate from bronchial epithelial as well as alveolar cells, which might explain the lack of significant differences. We have learned from the analysis of AKO/cTg mice that neoplastic lesions probably arise from bronchial epithelial cells and that specifically ATGL deficient club cells are impaired in their metabolic and regenerative capacity. Moreover, KRAS^{G12D} is a very strong oncogenic driver, which might obscure any ATGL related differences.

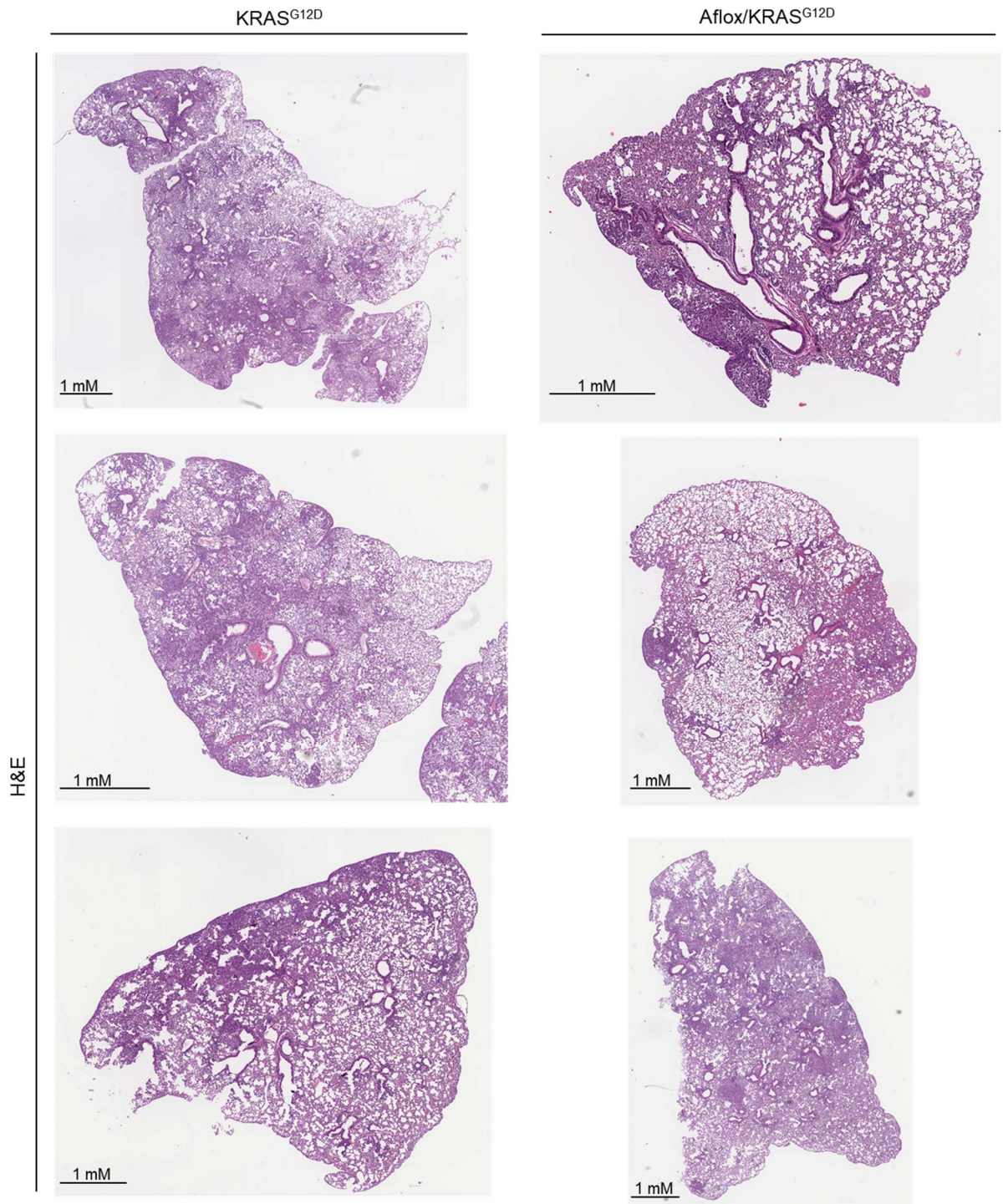

Figure 29: Overview of KRAS^{G12D} and A-flox KRAS^{G12D} lung sections. Representative H&E images of mice inhaled with Ad-Cre to induce tumor development in the lung.

4. Conclusion and Discussion

Lung cancer is the world's third leading cause of cancer-associated deaths. It is commonly known that smoking is one of the main risk factors for lung cancer development. Not much is known, however, how metabolic perturbations influence lung cancer initiation.

We have previously reported that AKO/cTg mice spontaneously develop bronchial epithelial neoplasia and adenocarcinomas as they age. Here, we show that neoplastic lesions in AKO/cTg mice most likely originate from bronchial epithelial club cells. Club cells as wells as ATII cells strongly depend on ATGL-mediated lipolysis, as they accumulate massive amounts of TG when ATGL is missing. Moreover, we determined that ATGL is not only an important TG hydrolase in the lung, but has also prominent retinylester hydrolase activity as metabolites of the vitamin A signaling pathway are deregulated in the lungs of AKO/cTg mice.

Bronchial epithelial club cells, in particular, are significantly impaired in their function. AKO/cTg club cells are incapable of producing the most abundant secreted protein in the lung, CCSP. Besides having less secretory vesicles, the main sites for CCSP storage, they have also reduced amounts of mitochondria, implying an energetic imbalance. Moreover, mRNA expression analysis pointed to impaired PPAR-γ signaling, and oxygen measurements confirmed reduced mitochondrial respiration in AKO/cTg club cells.

Assessment of club cell functionality *in vivo* using the club cell toxin NA, revealed that AKO/cTg club cells have defective regeneration and are not able to fully repair NA induced bronchial epithelial damage. In addition, we observe increased pro-oncogenic, inflammatory STAT3 signaling, which might promote bronchial epithelial proliferation.

Interestingly, ATRA supplementation intended to rescue defective vitamin A signaling, was able to restore bronchial epithelial regeneration after NA challenge.

Taken together these results indicate that lipid accumulation and/or energetic imbalance impair broncho-protective club cell functions. This could trigger enhanced repair/inflammatory processes in the bronchiolar epithelium leading to neoplasia development.

Besides ATGL's crucial function in mouse lung cancer initiation, we also noted that ATGL is frequently downregulated in human smooth muscle sarcoma as well as in

pancreas and lung adenocarcinoma (39). Moreover, we have seen that ATGL is very low expressed in many different cancer cell lines in culture (data not shown), which might explain why further knockdown or knockout of ATGL did not influence their malignant behavior. Possibly, the downregulation of ATGL among cancer cell lines and human cancers is due to the action of insulin, which was shown by Chakrabati *et al*. to be a conserved pathway via the action of mTORC1 and Egr1 to reduce ATGL expression (82). As many cancers have increased insulin/mTOR signaling, it might explain the fact that ATGL is often downregulated in tumors. However, it is also known that oncogenes direct nutrient uptake (e.g. glucose) and, thereby, induce reprogramming of the cellular metabolism (e.g. increased glycolysis). Therefore, a remaining question and still under current investigation is, if and what oncogenes influence ATGL expression *in vivo* and *in vitro*.

Not much is known about the role of lipolysis on cancer development and progression. It is well established that lipogenesis is highly upregulated in many different cancer types (83). Moreover, the excess of lipids/ obesity is considered a common risk factor not only for cardiovascular disease but also for cancer development. Therefore, the AKO/cTg mouse model is a valuable tool to investigate spontaneous development of malignant tumors caused by metabolic perturbations. AKO/cTg mice accumulate lipids in all tissues including the lung. Surprisingly, not much is known about the importance of lipolysis in lung metabolism as glycolysis seems to be the main energetic pathway exploited by lung cells (84). In this work we show, that at least two cell populations in the mouse lung strongly rely on lipolysis. Club as well as ATII cells accumulate massive amounts of lipids when faced with ATGL-deficiency. Hence, not all lung cell types might solely depend on glucose as their main energy source.

Although club as well as ATII cells are affected by ATGL KO, we propose that club cells play an important role in adenocarcinoma development of AKO/cTg mice. This is based on the observation that neoplastic lesions always appear in the bronchiolar epithelium and grow into the alveolar space. Moreover, bronchial epithelial cells as well as adenocarcinomas are both CK-19 positive. However, further investigations using the already established club cell specific ATGL KO (CC-AKO) mouse model as well as an ATII cell specific AKO mouse model will be needed to study this in more detail.

In the bronchiolar epithelium, only club cells seem to be affected by ATGL KO, as lipid droplets visualized by transmission electron microscopy (TEM) are only apparent in this specific cell type. Moreover, CCSP, the most abundant secreted protein in the mouse lung, is drastically reduced in AKO/cTg mice. As CCSP is reported to be highly anti-inflammatory and also cyto-protective, we investigated a possible connection of CCSP loss and neoplasia development (51, 85, 54). However, CCSP knockout mice did not show lung neoplasia development, which might exclude CCSP loss as the sole reason for lung cancer formation in AKO/cTg mice.

Interestingly, TEM images also showed that bronchial epithelial club cells harbor a lot of mitochondria, further strengthening the observation that club cells rely on oxidative metabolism and fatty acid oxidation. Similarly, to what has been reported on ATGL-deficiency in the heart, we observed reduced mitochondrial content and respiration as well as reduced PPAR(γ) signaling in AKO/cTg club cells (18). Therefore, we decided to treat AKO/cTg mice with fenofibrate, which reduced lipid levels in the hearts of AKO mice and restored mitochondrial function. However, treatment with fenofibrate was not able to improve the severe lipid accumulation and/or affect cancer development in the lung of AKO/cTg mice. Preliminary results also showed that treatment with the PPAR-γ agonist rosiglitazone did not reduce lipid droplet numbers, nor rescue mitochondria and secretory vesicles counts (data not shown).
Notably, another PPAR-α agonist, WY 14643, was more successful. Kanti and colleagues could show that WY 14643 was able to correct the mitochondrial defect of AKO/ctg club cells by normalizing mitochondrial number and oxygen consumption rates as well as significantly reducing lipid droplet numbers (1). A possible explanation for the increased effectivity of WY 14643 compared to fenofibrate could be the differing mode of administration. Whereas fenofibrate was administered via the food, WY 14643 was given by gavage. It is conceivable that drug delivery by gavage (exact amount, time of the day,…) is more efficient than by diet. Furthermore, WY 14643 might be pharmacologically different (e.g. pleiotropic effects). In addition, Kanti and colleagues showed that treatment with WY 14643, followed by acute injury of NA, could restore the regenerative capacity of bronchiolar epithelia from mice lacking ATGL (1). Moreover, they observed induction of PPAR-α signaling in the bronchiolar epithelium when challenged with NA. Specifically, the PPAR-α target genes *Pdk4*, *Hmgcs2* and *Angptl4* were significantly upregulated during bronchiolar regeneration in control mice,

but not in AKO/cTg mice. These data point towards a very important role for PPAR signaling in the mouse lung, especially under injury conditions.

NA studies using AKO/cTg mice revealed that ATGL-deficient club cells are not able to fully repair and regenerate the bronchiolar epithelium. Interestingly, injury severity also influences which cells and to what extent proliferation occurs. Mild injury is repaired by surviving club cells. Severe injury, leading to death of most club cells, stimulates proliferation of variant club cells located at NEBs and BASCs. Therefore, severe injury leads to clonal expansion, resulting in a “patchy” epithelium (63). Especially, mNA treatment resulted in the occurrence of ciliated cell patches to compensate for the lack of CYP2F2 expressing club cells in the bronchiolar epithelium of AKO/cTg mice. This suggests, that AKO/cTg mice are more affected by NA treatment, suffering from more severe bronchial epithelial injury.
Unfortunately, we were not able to determine the number of variant club cells in AKO/cTg mice due to their very low number in the murine lung. However, as NECs and BASCs tend to be upregulated in AKO/cTg mice, future efforts should be directed towards identifying these cells and their involvement in the regenerative phenotype.

Intriguingly, we found that AKO/cTg mice have impaired vitamin A signaling in the lung due to ATGL’s retinylester hydrolase activity. Moreover, ATRA supplementation in order to rescue retinoic acid signaling was able to restore regeneration after mNA treatment, arguing for an essential role of RA in cellular differentiation and repair of the bronchiolar epithelium. In the literature it has been reported that RA is essential for several organs during their development. In a study by Hind and Maden, it was also shown that RA induces alveolar regeneration in the adult mouse lung by reactivating developmental gene programs (81). Therefore, it is possible that RA is also crucial for not only the development but also the regeneration of bronchial epithelial cells. Unfortunately, we were not able to identify any genes induced by ATRA treatment, which might be responsible for the rescue, due to the fact that ATRA target gene induction is short lived. Therefore, future studies are needed to identify which genes are responsible for rescue of bronchial epithelial regeneration after mNA and ATRA treatment.

Interestingly, we observed concomitant with the decreased regeneration capacity, increased pro-oncogenic, inflammatory pSTAT3 signaling. As shown in the literature, pSTAT3 is essential for regeneration of the bronchiolar epithelium (66). Therefore, activation of pSTAT3 might indicate an ongoing repair process in AKO/cTg mice. This is also supported by the fact that AKO/cTg mice are not able to fully regenerate CYP2F2 expressing club cells after mNA treatment. In my analysis, a trend towards increased proliferation (assessed by EdU+ cells after acute NA injury) of BECs of AKO/cTg mice was observed. Reassessment of the staining by Kanti was able to depict significant differences between the genotypes, suggesting increased proliferation in the bronchiolar epithelium of AKO/cTg mice.
In addition to slightly increased proliferation, we observed an increase in IL6-STAT3 signaling as the mice age. The JAK/STAT pathway is very often hyper-activated in human lung cancer. STAT3 is upregulated in over 50% of primary human NSCLCs, and one of the activators of the JAK/STAT pathway, namely IL-6 is also up in 40% of lung cancer patients (86). Enhanced pSTAT3 signaling is known to promote proliferation, angiogenesis, cell survival and metastasis. Therefore, it is possible that activation of pSTAT3 in order to repair chronic damage in the bronchiolar epithelium is leading to neoplasia development.

Another question was if AKO/cTg mice solely develop neoplastic lesions in the lung or if also other organs are affected by ATGL-deficiency in a similar manner. We analyzed several other tissues (among others pancreas, muscle, WAT) regarding neoplasia occurrence but observed neoplasia development specifically in the lungs of AKO/cTg mice. This might be due to the fact that lung cells are in contact with airborne. Club cells are characterized by the P450 enzyme system, needed for detoxification of xenobiotics entering the lung. Therefore, these cells might rely on functional ATGL-mediated lipid catabolism in order to detoxify and fulfil their normal functions. This is supported by the fact that club cells of AKO/cTg mice are more susceptible to NA induced injury, which is commonly found in cigarette smoke.
Of note, ATGL downregulation is associated with not only lung but also smooth muscle and pancreas cancer in human patients (39). Although, we did not observe any malignant development in other tissues of AKO/cTg mice, this could be due to a combination of low tumor incidence and the number of mice analyzed. Therefore,

future efforts should be directed to find out if tumor development due to lack of ATGL is exclusive to the lung.

In order to find out if ATGL deficiency specifically in club cells is leading to neoplasia initiation we developed the CC-AKO mouse. Initial characterization of this mouse model showed that ATGL-deficient club cells do accumulate lipid but still express normal levels of CCSP. However, more time and effort are needed to assess knockout efficiency, neoplasia incidence and regenerative potential in this mouse model.

Another important key player in lung cancer development is KRAS, which is frequently mutated in human lung cancer. 29.61% of lung adenocarcinomas harbor a KRAS mutation, and 4.26% are $KRAS^{G12D}$ (according to https://www.mycancergenome.org/content/disease/lung-cancer/kras/34/ (Updated December 27, 2021). Therefore, we decided to combine ATGL knockout with $KRAS^{G12D}$ activation by using the LSL-KRAS lung cancer mouse model. However, ATGL loss did not promote or ameliorate lung cancer progression driven by $KRAS^{G12D}$. One reason could be that KRAS is a very strong cancer driver and that its activation is conceiling any effects of ATGL loss. Another explanation could be the fact that cancer initiation is not limited to a specific lung cell type in the model we applied and that a more selective approach is needed to analyze a combined effect of ATGL loss and KRAS activation.

In conclusion, we could show that ATGL is crucial for mouse lung and club cell function. Furthermore, we could show that club cells rely on ATGL for energy production and mitochondrial function. ATGL loss leads to impaired regeneration, low-grade inflammation and neoplasia development. Therefore, we propose that ATGL has tumor suppressive functions and might be a marker for lung tissue fitness. Moreover, we report that RA is an essential molecule for regeneration of the bronchiolar epithelium and ATRA supplementation might be a potential therapeutic avenue to improve regenerative processes in the human lung.

5. References

1. Kanti MM, Striessnig-Bina I, Wieser BI, Schauer S, Leitinger G, Eichmann TO et al. Adipose triglyceride lipase mediated lipid catabolism is essential for bronchiolar regeneration. JCI Insight 2022; in press.

2. Xie H, Heier C, Kien B, Vesely PW, Tang Z, Sexl V et al. Adipose triglyceride lipase activity regulates cancer cell proliferation via AMP-kinase and mTOR signaling. Biochim Biophys Acta Mol Cell Biol Lipids 2020; 1865(9):158737.

3. Hanahan D, Weinberg RA. Hallmarks of cancer: the next generation. Cell 2011; 144(5):646–74.

4. WARBURG O. On the origin of cancer cells. Science 1956; 123(3191):309–14.

5. Cantor JR, Sabatini DM. Cancer Cell Metabolism: One Hallmark, Many Faces. Cancer Discov 2012; 2(10):881–98.

6. Desai TJ, Brownfield DG, Krasnow MA. Alveolar progenitor and stem cells in lung development, renewal and cancer. Nature 2014; 507(7491):190–4.

7. Zaidi N, Lupien L, Kuemmerle NB, Kinlaw WB, Swinnen JV, Smans K. Lipogenesis and lipolysis: the pathways exploited by the cancer cells to acquire fatty acids. Prog Lipid Res 2013; 52(4):585–9.

8. Zechner R, Zimmermann R, Eichmann TO, Kohlwein SD, Haemmerle G, Lass A et al. FAT SIGNALS--lipases and lipolysis in lipid metabolism and signaling. Cell Metab 2012; 15(3):279–91.

9. Eichmann TO, Kumari M, Haas JT, Farese RV, Zimmermann R, Lass A et al. Studies on the substrate and stereo/regioselectivity of adipose triglyceride lipase, hormone-sensitive lipase, and diacylglycerol-O-acyltransferases. J Biol Chem 2012; 287(49):41446–57.

10. Rodriguez JA, Ben Ali Y, Abdelkafi S, Mendoza LD, Leclaire J, Fotiadu F et al. In vitro stereoselective hydrolysis of diacylglycerols by hormone-sensitive lipase. Biochim Biophys Acta 2010; 1801(1):77–83.

11. Tornqvist H, Belfrage P. Purification and some properties of a monoacylglycerol-hydrolyzing enzyme of rat adipose tissue. J Biol Chem 1976; 251(3):813–9.

12. Zimmermann R, Strauss JG, Haemmerle G, Schoiswohl G, Birner-Gruenberger R, Riederer M et al. Fat mobilization in adipose tissue is promoted by adipose triglyceride lipase. Science 2004; 306(5700):1383–6.

13. Jenkins CM, Mancuso DJ, Yan W, Sims HF, Gibson B, Gross RW. Identification, cloning, expression, and purification of three novel human calcium-independent phospholipase A2 family members possessing triacylglycerol lipase and acylglycerol transacylase activities. J Biol Chem 2004; 279(47):48968–75.

14. Villena JA, Roy S, Sarkadi-Nagy E, Kim K-H, Sul HS. Desnutrin, an adipocyte gene encoding a novel patatin domain-containing protein, is induced by fasting and glucocorticoids: ectopic expression of desnutrin increases triglyceride hydrolysis. J Biol Chem 2004; 279(45):47066–75.

15. Lass A, Zimmermann R, Haemmerle G, Riederer M, Schoiswohl G, Schweiger M et al. Adipose triglyceride lipase-mediated lipolysis of cellular fat stores is activated by CGI-58 and defective in Chanarin-Dorfman Syndrome. Cell Metab 2006; 3(5):309–19.

16. Miyoshi H, Perfield JW, Souza SC, Shen W-J, Zhang H-H, Stancheva ZS et al. Control of adipose triglyceride lipase action by serine 517 of perilipin A globally regulates protein kinase A-stimulated lipolysis in adipocytes. J Biol Chem 2007; 282(2):996–1002.

17. Nielsen TS, Vendelbo MH, Jessen N, Pedersen SB, Jørgensen JO, Lund S et al. Fasting, but not exercise, increases adipose triglyceride lipase (ATGL) protein and reduces G(0)/G(1) switch gene 2 (G0S2) protein and mRNA content in human adipose tissue. J Clin Endocrinol Metab 2011; 96(8):E1293-7.

18. Haemmerle G, Moustafa T, Woelkart G, Büttner S, Schmidt A, van de Weijer T et al. ATGL-mediated fat catabolism regulates cardiac mitochondrial function via PPAR-α and PGC-1. Nat Med 2011; 17(9):1076–85.

19. Zechner R, Kienesberger PC, Haemmerle G, Zimmermann R, Lass A. Adipose triglyceride lipase and the lipolytic catabolism of cellular fat stores. J Lipid Res 2009; 50(1):3–21.

20. Taschler U, Schreiber R, Chitraju C, Grabner GF, Romauch M, Wolinski H et al. Adipose triglyceride lipase is involved in the mobilization of triglyceride and

retinoid stores of hepatic stellate cells. Biochim Biophys Acta 2015; 1851(7):937–45.

21. Zechner R, Langin D. Hormone-sensitive lipase deficiency in humans. Cell Metab 2014; 20(2):199–201.

22. Fowler CJ. Monoacylglycerol lipase - a target for drug development? Br J Pharmacol 2012; 166(5):1568–85.

23. Nomura DK, Long JZ, Niessen S, Hoover HS, Ng S-W, Cravatt BF. Monoacylglycerol lipase regulates a fatty acid network that promotes cancer pathogenesis. Cell 2010; 140(1):49–61.

24. Sun H, Jiang L, Luo X, Jin W, He Q, An J et al. Potential tumor-suppressive role of monoglyceride lipase in human colorectal cancer. Oncogene 2013; 32(2):234–41.

25. Liu R. Monoglyceride lipase gene knockout in mice leads to increased incidence of lung adenocarcinoma.

26. Xu M, Chang H-H, Jung X, Moro A, Chou CEN, King J et al. Deficiency in hormone-sensitive lipase accelerates the development of pancreatic cancer in conditional KrasG12D mice. BMC Cancer 2018; 18(1):797.

27. Wu JW, Preuss C, Wang SP, Yang H, Ji B, Carter GW et al. Epistatic interaction between the lipase-encoding genes Pnpla2 and Lipe causes liposarcoma in mice. PLoS Genet 2017; 13(5):e1006716.

28. Russell L, Forsdyke DR. A human putative lymphocyte G0/G1 switch gene containing a CpG-rich island encodes a small basic protein with the potential to be phosphorylated. DNA Cell Biol 1991; 10(8):581–91.

29. Yamada T, Park CS, Burns A, Nakada D, Lacorazza HD. The cytosolic protein G0S2 maintains quiescence in hematopoietic stem cells. PLoS ONE 2012; 7(5):e38280.

30. Kitareewan S, Blumen S, Sekula D, Bissonnette RP, Lamph WW, Cui Q et al. G0S2 is an all-trans-retinoic acid target gene. Int J Oncol 2008; 33(2):397–404.

31. Zagani R, El-Assaad W, Gamache I, Teodoro JG. Inhibition of adipose triglyceride lipase (ATGL) by the putative tumor suppressor G0S2 or a small

molecule inhibitor attenuates the growth of cancer cells. Oncotarget 2015; 6(29):28282–95.

32. Welch C, Santra MK, El-Assaad W, Zhu X, Huber WE, Keys RA et al. Identification of a protein, G0S2, that lacks Bcl-2 homology domains and interacts with and antagonizes Bcl-2. Cancer Res 2009; 69(17):6782–9.

33. Yim CY, Sekula DJ, Hever-Jardine MP, Liu X, Warzecha JM, Tam J et al. G0S2 Suppresses Oncogenic Transformation by Repressing a MYC-Regulated Transcriptional Program. Cancer Res 2016; 76(5):1204–13.

34. Kusakabe M, Kutomi T, Watanabe K, Emoto N, Aki N, Kage H et al. Identification of G0S2 as a gene frequently methylated in squamous lung cancer by combination of in silico and experimental approaches. Int J Cancer 2010; 126(8):1895–902.

35. Kusakabe M, Watanabe K, Emoto N, Aki N, Kage H, Nagase T et al. Impact of DNA demethylation of the G0S2 gene on the transcription of G0S2 in squamous lung cancer cell lines with or without nuclear receptor agonists. Biochem Biophys Res Commun 2009; 390(4):1283–7.

36. Tokumaru Y, Yamashita K, Osada M, Nomoto S, Sun D-I, Xiao Y et al. Inverse correlation between cyclin A1 hypermethylation and p53 mutation in head and neck cancer identified by reversal of epigenetic silencing. Cancer Res 2004; 64(17):5982–7.

37. Ou J, Miao H, Ma Y, Guo F, Deng J, Wei X et al. Loss of abhd5 promotes colorectal tumor development and progression by inducing aerobic glycolysis and epithelial-mesenchymal transition. Cell Rep 2014; 9(5):1798–811.

38. Tomin T, Fritz K, Gindlhuber J, Waldherr L, Pucher B, Thallinger GG et al. Deletion of Adipose Triglyceride Lipase Links Triacylglycerol Accumulation to a More-Aggressive Phenotype in A549 Lung Carcinoma Cells. J Proteome Res 2018; 17(4):1415–25.

39. Al-Zoughbi W, Pichler M, Gorkiewicz G, Guertl-Lackner B, Haybaeck J, Jahn SW et al. Loss of adipose triglyceride lipase is associated with human cancer and induces mouse pulmonary neoplasia. Oncotarget 2016; 7(23):33832–40.

40. Zorn AM, Wells JM. Vertebrate endoderm development and organ formation. Annu Rev Cell Dev Biol 2009; 25:221–51.

41. Kimura S, Hara Y, Pineau T, Fernandez-Salguero P, Fox CH, Ward JM et al. The T/ebp null mouse: thyroid-specific enhancer-binding protein is essential for the organogenesis of the thyroid, lung, ventral forebrain, and pituitary. Genes Dev 1996; 10(1):60–9.

42. Herriges M, Morrisey EE. Lung development: orchestrating the generation and regeneration of a complex organ. Development 2014; 141(3):502–13.

43. Goss AM, Tian Y, Tsukiyama T, Cohen ED, Zhou D, Lu MM et al. Wnt2/2b and beta-catenin signaling are necessary and sufficient to specify lung progenitors in the foregut. Dev Cell 2009; 17(2):290–8.

44. Domyan ET, Ferretti E, Throckmorton K, Mishina Y, Nicolis SK, Sun X. Signaling through BMP receptors promotes respiratory identity in the foregut via repression of Sox2. Development 2011; 138(5):971–81.

45. Bellusci S, Furuta Y, Rush MG, Henderson R, Winnier G, Hogan BL. Involvement of Sonic hedgehog (Shh) in mouse embryonic lung growth and morphogenesis. Development 1997; 124(1):53–63.

46. Weaver M, Dunn NR, Hogan BL. Bmp4 and Fgf10 play opposing roles during lung bud morphogenesis. Development 2000; 127(12):2695–704.

47. Sakai T, Larsen M, Yamada KM. Fibronectin requirement in branching morphogenesis. Nature 2003; 423(6942):876–81.

48. Rawlins EL, Clark CP, Xue Y, Hogan BLM. The Id2+ distal tip lung epithelium contains individual multipotent embryonic progenitor cells. Development 2009; 136(22):3741–5.

49. Rock JR, Onaitis MW, Rawlins EL, Lu Y, Clark CP, Xue Y et al. Basal cells as stem cells of the mouse trachea and human airway epithelium. Proc Natl Acad Sci U S A 2009; 106(31):12771–5.

50. Wang Y, Tian Y, Morley MP, Lu MM, DeMayo FJ, Olson EN et al. Development and regeneration of Sox2+ endoderm progenitors is regulated by a HDAC1/2-Bmp4/Rb1 regulatory pathway. Dev Cell 2013; 24(4):345–58.

51. Stripp BR, Reynolds SD, Plopper CG, Bøe IM, Lund J. Pulmonary phenotype of CCSP/UG deficient mice: a consequence of CCSP deficiency or altered Clara cell function? Ann N Y Acad Sci 2000; 923:202–9.

52. Barnes PJ. Club cells, their secretory protein, and COPD. Chest 2015; 147(6):1447–8.

53. Snyder JC, Reynolds SD, Hollingsworth JW, Li Z, Kaminski N, Stripp BR. Clara cells attenuate the inflammatory response through regulation of macrophage behavior. Am J Respir Cell Mol Biol 2010; 42(2):161–71.

54. Wang S-Z, Rosenberger CL, Bao Y-X, Stark JM, Harrod KS. Clara cell secretory protein modulates lung inflammatory and immune responses to respiratory syncytial virus infection. J Immunol 2003; 171(2):1051–60.

55. Zhu L, Di PYP, Wu R, Pinkerton KE, Chen Y. Repression of CC16 by cigarette smoke (CS) exposure. PLoS ONE 2015; 10(1):e0116159.

56. Plopper CG, Mango GW, Hatch GE, Wong VJ, Toskala E, Reynolds SD et al. Elevation of susceptibility to ozone-induced acute tracheobronchial injury in transgenic mice deficient in Clara cell secretory protein. Toxicol Appl Pharmacol 2006; 213(1):74–85.

57. Song H, Yao E, Lin C, Gacayan R, Chen M-H, Chuang P-T. Functional characterization of pulmonary neuroendocrine cells in lung development, injury, and tumorigenesis. Proc Natl Acad Sci U S A 2012; 109(43):17531–6.

58. Ling T-Y, Kuo M-D, Li C-L, Yu AL, Huang Y-H, Wu T-J et al. Identification of pulmonary Oct-4+ stem/progenitor cells and demonstration of their susceptibility to SARS coronavirus (SARS-CoV) infection in vitro. Proc Natl Acad Sci U S A 2006; 103(25):9530–5.

59. Guha A, Deshpande A, Jain A, Sebastiani P, Cardoso WV. Uroplakin 3a+ Cells Are a Distinctive Population of Epithelial Progenitors that Contribute to Airway Maintenance and Post-injury Repair. Cell Rep 2017; 19(2):246–54.

60. Rawlins EL, Okubo T, Xue Y, Brass DM, Auten RL, Hasegawa H et al. The role of Scgb1a1+ Clara cells in the long-term maintenance and repair of lung airway, but not alveolar, epithelium. Cell Stem Cell 2009; 4(6):525–34.

61. Noh MS, Jun B-H, Kim S, Kang H, Woo M-A, Minai-Tehrani A et al. Magnetic surface-enhanced Raman spectroscopic (M-SERS) dots for the identification of bronchioalveolar stem cells in normal and lung cancer mice. Biomaterials 2009; 30(23-24):3915–25.

62. Barkauskas CE, Cronce MJ, Rackley CR, Bowie EJ, Keene DR, Stripp BR et al. Type 2 alveolar cells are stem cells in adult lung. J Clin Invest 2013; 123(7):3025–36.

63. Giangreco A, Arwert EN, Rosewell IR, Snyder J, Watt FM, Stripp BR. Stem cells are dispensable for lung homeostasis but restore airways after injury. Proc Natl Acad Sci U S A 2009; 106(23):9286–91.

64. Volckaert T, Dill E, Campbell A, Tiozzo C, Majka S, Bellusci S et al. Parabronchial smooth muscle constitutes an airway epithelial stem cell niche in the mouse lung after injury. J Clin Invest 2011; 121(11):4409–19.

65. Raggioli A. Beta-catenin is required for maintenance of chromosomal stability in mouse embryonic stem cells [@Freiburg i. Br., Univ., Diss., 2013]. Available from: URL: http://nbn-resolving.de/urn:nbn:de:bsz:25-opus-89987.

66. Kida H, Mucenski ML, Thitoff AR, Le Cras TD, Park K-S, Ikegami M et al. GP130-STAT3 regulates epithelial cell migration and is required for repair of the bronchiolar epithelium. Am J Pathol 2008; 172(6):1542–54.

67. Park K-S, Wells JM, Zorn AM, Wert SE, Laubach VE, Fernandez LG et al. Transdifferentiation of ciliated cells during repair of the respiratory epithelium. Am J Respir Cell Mol Biol 2006; 34(2):151–7.

68. Ng-Blichfeldt J-P, Schrik A, Kortekaas RK, Noordhoek JA, Heijink IH, Hiemstra PS et al. Retinoic acid signaling balances adult distal lung epithelial progenitor cell growth and differentiation. EBioMedicine 2018; 36:461–74.

69. Weber E, Ravi RK, Knudsen ES, Williams JR, Dillehay LE, Nelkin BD et al. Retinoic acid-mediated growth inhibition of small cell lung cancer cells is associated with reduced myc and increased p27Kip1 expression. Int J Cancer 1999; 80(6):935–43.

70. Huntly BJP, Gilliland DG. Leukaemia stem cells and the evolution of cancer-stem-cell research. Nat Rev Cancer 2005; 5(4):311–21.

71. Rowbotham SP, Kim CF. Diverse cells at the origin of lung adenocarcinoma. Proc Natl Acad Sci U S A 2014; 111(13):4745–6.

72. Haemmerle G, Moustafa T, Woelkart G, Büttner S, Schmidt A, van de Weijer T et al. ATGL-mediated fat catabolism regulates cardiac mitochondrial function via PPAR-α and PGC-1. Nat Med 2011; 17(9):1076–85.

73. Ma T, Lopez-Aguiar AGN, Li A, Lu Y, Sekula D, Nattie EE et al. Mice lacking G0S2 are lean and cold-tolerant. Cancer Biol Ther 2014; 15(5):643–50.

74. DuPage M, Dooley AL, Jacks T. Conditional mouse lung cancer models using adenoviral or lentiviral delivery of Cre recombinase. Nat Protoc 2009; 4(7):1064–72.

75. Nagaraj C, Haitchi HM, Heinemann A, Howarth PH, Olschewski A, Marsh LM. Increased Expression of p22phox Mediates Airway Hyperresponsiveness in an Experimental Model of Asthma. Antioxid Redox Signal 2017; 27(18):1460–72.

76. Cook HC. Origins of … tinctorial methods in histology. J Clin Pathol 1997; 50(9):716–20.

77. Oreffo VI, Morgan A, Richards RJ. Isolation of Clara cells from the mouse lung. Environ Health Perspect 1990; 85:51–64.

78. FOLCH J, LEES M, SLOANE STANLEY GH. A simple method for the isolation and purification of total lipides from animal tissues. J Biol Chem 1957; 226(1):497–509.

79. Knittelfelder OL, Weberhofer BP, Eichmann TO, Kohlwein SD, Rechberger GN. A versatile ultra-high performance LC-MS method for lipid profiling. J Chromatogr B Analyt Technol Biomed Life Sci 2014; 951-952:119–28.

80. Hartler J, Tharakan R, Köfeler HC, Graham DR, Thallinger GG. Bioinformatics tools and challenges in structural analysis of lipidomics MS/MS data. Brief Bioinformatics 2013; 14(3):375–90.

81. Hind M, Maden M. Retinoic acid induces alveolar regeneration in the adult mouse lung. Eur Respir J 2004; 23(1):20–7.

82. Chakrabarti P, Kim JY, Singh M, Shin Y-K, Kim J, Kumbrink J et al. Insulin inhibits lipolysis in adipocytes via the evolutionarily conserved mTORC1-Egr1-ATGL-mediated pathway. Mol Cell Biol 2013; 33(18):3659–66.

83. Zaidi N, Lupien L, Kuemmerle NB, Kinlaw WB, Swinnen JV, Smans K. Lipogenesis and lipolysis: the pathways exploited by the cancer cells to acquire fatty acids. Prog Lipid Res 2013; 52(4):585–9.

84. Fisher AB. Intermediary metabolism of the lung. Environ Health Perspect 1984; 55:149–58.

85. Watson TM, Reynolds SD, Mango GW, Boe IM, Lund J, Stripp BR. Altered lung gene expression in CCSP-null mice suggests immunoregulatory roles for Clara cells. Am J Physiol Lung Cell Mol Physiol 2001; 281(6):L1523-30.

86. Dutta P, Sabri N, Li J, Li WX. Role of STAT3 in lung cancer. JAKSTAT 2015; 3(4).

6. Appendix

Table 4: Significantly deregulated genes of AKO/cTg and WT/cTg enriched club cell preparations. Club cells were prepped from 40 weeks old mice. Afterwards RNA was isolated and amplified for subsequent microarray analysis. Genes were filtered for 1.3 fold change, a p-value of 0.05 and microarray expression RMA of 5.

Transcript ID	Gene Symbol	p-value(A0C vs. A2C)	Fold-Change(A0C vs. A2C)
17549150		1,62E-02	7,16936
17549062		1,50E-02	6,46696
17459318	Igkv17-121	3,08E-02	3,77919
17306104	Rnase2a	1,62E-02	2,92814
17284482	Ighv9-4	1,85E-02	2,55795
17438955	Cxcl5	8,51E-03	2,42615
17367652	Il1f9	2,59E-02	2,41235
17467513	Igkv7-33	1,93E-02	2,40404
17284463	Ighv7-3	1,83E-02	2,37655
17284376	Igh-VX24	3,01E-02	2,36957
17284515	Ighv1-12	3,90E-02	2,36639
17459350	Igkv14-100	4,34E-02	2,28165
17467407	Igkv1-88	3,99E-02	2,2403
17459327	Igkv2-116	4,49E-02	2,20658
17240303	G630090E17Rik	1,52E-02	2,1586
17471394	BC048546	1,96E-02	2,14472
17487759	Cd177	2,22E-02	2,09394
17284426	Ighv2-9	2,99E-02	2,06343
17549170		3,91E-02	2,04039
17508848	Gm23128	3,02E-02	1,985
17254300	Wfdc21	8,05E-04	1,9702
17239630	4930405J17Rik	1,52E-02	1,87463
17445689	Speer4c	3,35E-02	1,87026
17405082	Slc7a11	1,43E-02	1,84982
17459355	Igkv1-99	2,32E-03	1,83915
17514553	Mmp8	3,39E-02	1,83073
17514495	Mmp12	1,18E-02	1,78856
17299965	Trav16n	2,59E-02	1,78129
17442282	Gm23458	1,40E-03	1,75019
17400994	Gm12474	7,88E-03	1,73494
17400365	Ctsk	1,63E-02	1,73299
17532694	Pisd-ps3	3,17E-02	1,69884
17472443	Slco1a5	2,91E-02	1,69681
17290072	Gm25985	3,08E-02	1,693
17299589	Rnase2b	1,13E-02	1,69036

17224251	Cxcr1	6,02E-03	1,6715
17329020	Iglv3	1,35E-02	1,67092
17289237	Gm25109	4,77E-02	1,65153
17462788	Clec4n	3,20E-03	1,64842
17373996	BC048594	2,96E-02	1,64693
17266581	AU040972	7,83E-03	1,62075
17535707	Gm14817	3,43E-02	1,61526
17446580	Shh	3,60E-03	1,60144
17249962	Gm12246	3,56E-02	1,58244
17360440	Adra2a	4,81E-02	1,57331
17433656	5930403L14Rik	3,77E-03	1,57323
17218060	Ptgs2	6,45E-04	1,56946
17364111	Ch25h	1,52E-02	1,56684
17213478	Ctla4	3,34E-02	1,56324
17445667	Gm21149	3,47E-02	1,55276
17510492		2,66E-02	1,54385
17339501	Gm22858	2,67E-02	1,53724
17284390	Ighv2-4	2,20E-03	1,53557
17238822	Gm25694	1,97E-02	1,52933
17512628	Dpep2	1,52E-03	1,52233
17282021	AI463170	2,32E-02	1,51856
17220721	A430027H14Rik	3,60E-02	1,51207
17382363	Noxa1	4,11E-02	1,51093
17526982	Gm684	7,34E-03	1,5108
17524211	Ccdc67	3,38E-03	1,50678
17265496	Nlrp1b	2,94E-02	1,50076
17512732	Nqo1	2,08E-02	1,49398
17403509	Lpar3	3,44E-02	1,48191
17240467	Ccdc162	3,90E-02	1,47968
17451195	Cryba4	2,68E-02	1,47845
17473720		2,92E-02	1,47769
17215629	Mlph	3,07E-02	1,47423
17285223		1,67E-02	1,47399
17418934	Tmem54	3,73E-02	1,47341
17263058	2010001A14Rik	2,97E-02	1,47
17328550	Spag6	1,35E-02	1,468
17532811	Foxp3	2,43E-02	1,45839
17548115		2,15E-02	1,45801
17495958	Ern2	3,20E-02	1,45507
17463617	n-R5s167	1,15E-02	1,45371
17271776	Cd300lf	6,08E-03	1,45342
17241810	Rsph14	1,32E-03	1,45287
17405005	Pgrmc2	1,17E-02	1,44723
17475809	Rps16	4,74E-02	1,44616
17280138	2410004P03Rik	2,19E-02	1,44345
17507532	Gm15351	4,73E-02	1,44282
17333707	Mirlet7e	1,87E-02	1,4376

17517215	Gm32819	2,71E-02	1,43494
17353599	Slc23a1	3,31E-05	1,43087
17536600	Gdpd2	1,26E-02	1,43004
17488151	Mia	4,04E-02	1,42754
17467554	Igkv6-13	4,02E-02	1,42678
17216926	Gm15674	1,13E-02	1,42642
17400521	Sv2a	4,16E-03	1,42304
17520394	Gm24178	3,91E-02	1,42181
17410729	Bmpr1b	4,58E-02	1,41972
17453634	Styxl1	3,99E-02	1,41891
17435636	Gm26894	8,05E-03	1,41874
17546232	Zf12	1,57E-02	1,41682
17356216	Pcx	1,40E-02	1,41459
17336788	Slc44a4	3,76E-02	1,4129
17511550	Tox3	5,78E-03	1,41206
17281332	LOC102642272	5,72E-03	1,41066
17299663	Slc39a2	3,36E-02	1,40953
17343153	1700097N02Rik	1,71E-03	1,40673
17226618	Cd55	4,47E-02	1,40068
17212548	Dnah7b	5,31E-04	1,39839
17269266	Krtap17-1	1,28E-02	1,39839
17482079	Sox6os	2,95E-02	1,39612
17389836	Ppp1r14d	4,53E-02	1,3953
17469941	Efcab12	4,60E-03	1,39502
17501317	BC030500	2,39E-02	1,39475
17467458	Igkv4-57-1	3,41E-02	1,38877
17245085	Kcnmb4	1,13E-02	1,38874
17488845	Sipa1l3	4,88E-02	1,38644
17255511	Ttll6	3,97E-02	1,38582
17547929	A930007A09Rik	3,11E-02	1,38458
17319734	Tbrg3	2,90E-02	1,38456
17340774	Pacrg	1,49E-02	1,38447
17330544	Sidt1	8,69E-03	1,38328
17400998	Vtcn1	1,59E-02	1,37948
17405469	F630111L10Rik	2,68E-02	1,37618
17511731	Ces1f	4,82E-02	1,37585
17285242		2,26E-02	1,37569
17419418		3,56E-02	1,37547
17241598	Gm7075	3,37E-02	1,37539
17238558	Mmp19	1,98E-03	1,37493
17224397	Ccdc108	3,93E-02	1,36819
17343263	Sik1	1,87E-02	1,36777
17339388	Gm26561	3,58E-02	1,36703
17403806	Erich3	1,09E-02	1,36684
17288548	Slc12a7	1,60E-02	1,36567
17520198	Rasgrf1	3,95E-03	1,36365
17260869	Slc1a4	4,57E-02	1,36285

17217174	Klhdc8a	2,01E-02	1,36126
17474974	Plaur	1,01E-02	1,35942
17461648	Ttll3	8,14E-03	1,35673
17352862	Aqp4	4,66E-02	1,35632
17469814	Atp2b2	2,35E-03	1,3547
17370499	Wdr38	2,34E-02	1,35354
17437996	Gm24368	3,69E-02	1,35243
17332583	Ripk4	4,65E-02	1,35188
17331585	E330011O21Rik	4,88E-02	1,35179
17485320	Kcnq1	3,33E-02	1,35111
17226701	LOC102640771	1,03E-02	1,34934
17338371	Trem3	4,89E-02	1,34875
17540402	Efhc2	1,74E-02	1,34797
17525240	St14	1,97E-02	1,34782
17550520		4,44E-02	1,34662
17467700	4933431G14Rik	2,58E-02	1,34411
17420557	Rnf186	1,19E-02	1,34374
17508779	Cldn23	3,24E-02	1,34263
17360177	Gm19557	4,73E-02	1,33788
17252253	Gm19967	4,50E-03	1,33782
17297006	Gm16741	4,97E-02	1,33594
17368523	Gm20071	3,49E-02	1,33449
17524930	Acp5	3,80E-02	1,33431
17293489	Gm3604	2,70E-02	1,33318
17478001	Fam83e	2,67E-02	1,33051
17240022	Cenpw	4,06E-02	1,32939
17428589	Tspan1	2,06E-02	1,32875
17355607	Setbp1	3,52E-02	1,3278
17379949	Gm14321	1,50E-02	1,32778
17391259	Fahd2a	4,35E-03	1,32629
17518777	Gm15563	2,36E-02	1,3262
17461408		7,25E-03	1,326
17448135	Cckar	2,57E-02	1,32512
17345712	Prickle4	3,74E-02	1,32487
17285240	Gm25804	2,22E-02	1,3241
17319806	Arfgap3	1,76E-02	1,32376
17335966	Cyp4f16	4,77E-02	1,32296
17536264	Pcyt1b	6,87E-04	1,32066
17322578	4930562C15Rik	4,56E-02	1,32062
17507128	Fcor	2,82E-02	1,32001
17340427	Gm20939	1,05E-02	1,31979
17545712	Cnksr2	2,78E-02	1,31703
17488117	Gm15883	1,72E-02	1,31609
17398095	Lekr1	4,07E-02	1,3152
17492016	Gm23233	5,40E-03	1,3143
17256632	Wnk4	5,56E-03	1,31263
17500535	Dusp4	2,62E-02	1,31209

17374880	Tyro3	4,13E-02	1,31202
17214663	Gm25974	4,21E-02	1,30969
17533535	Chst7	6,57E-03	1,30936
17500996	Acsl1	2,54E-02	1,30917
17367910	Tmem210	1,39E-02	1,30837
17216949	Fcamr	3,51E-03	1,30351
17482699	Scnn1b	2,14E-02	1,30328
17310250	Capsl	3,59E-02	1,30213
17462987	Pianp	4,30E-03	1,30129
17230902	Kcnk2	9,22E-03	1,30026
17516074	Esam	2,84E-02	-1,30099
17480324	Kctd21	2,09E-02	-1,30167
17298262	Mustn1	4,57E-02	-1,30173
17502816	Inpp4b	2,66E-03	-1,3028
17299867	Trav3d-3	4,31E-02	-1,30468
17299944	Trav3d-3	4,31E-02	-1,30468
17516960	Cadm1	1,34E-02	-1,30496
17380466	Gm14296	4,17E-02	-1,30595
17383104	Agpat2	1,53E-02	-1,30683
17325592	Popdc2	1,89E-02	-1,30787
17220439	Aida	2,13E-03	-1,30888
17234066	Ank3	2,15E-02	-1,30938
17430430	Fam167b	4,74E-03	-1,31356
17468573	Antxr1	4,35E-02	-1,31587
17370807	Fmnl2	1,31E-02	-1,31631
17289551	Gm16416	4,92E-02	-1,31637
17463542	Tmem52b	5,75E-06	-1,31674
17533282	Mid1ip1	9,17E-03	-1,3174
17293362	Ctla2a	4,80E-02	-1,31751
17334062	Gm26695	3,16E-02	-1,31774
17239546	Arfgef3	3,35E-02	-1,31856
17370598	Acvr2a	4,40E-02	-1,32069
17480528		2,84E-02	-1,32087
17310339	C1qtnf3	2,76E-02	-1,32098
17303147	Gm8356	3,16E-02	-1,32223
17308388	Sftpc	3,55E-04	-1,32529
17397511	Lhfp	3,62E-02	-1,3258
17545488	Kctd12b	3,11E-02	-1,32613
17442185	Gm6444	2,91E-02	-1,32739
17520602	Rpl7a-ps10	3,12E-02	-1,32807
17464539	Hepacam2	3,44E-02	-1,32869
17333521	Ermard	6,50E-03	-1,32971
17386210	Lrp2	1,89E-02	-1,32993
17254244	1700020L24Rik	9,21E-03	-1,33176
17482000	Spon1	3,24E-02	-1,33634
17411918	Runx1t1	1,58E-02	-1,33861
17234136	Slc16a9	1,12E-02	-1,33889

17287175	Ogn	4,40E-02	-1,33902
17411892	Rbm12b1	3,26E-02	-1,33909
17523531	Tmem42	4,49E-02	-1,33995
17230087	Ifi203	1,00E-02	-1,34039
17243868	Dram1	2,34E-02	-1,34063
17248754	Adam19	1,23E-02	-1,34073
17330499	Zdhhc23	5,01E-03	-1,34161
17213666	Gm26649	3,71E-02	-1,34347
17471757	Klra9	4,88E-02	-1,34387
17230067	Mndal	2,64E-02	-1,34497
17501208		1,81E-02	-1,34502
17405510	9330121J05Rik	1,38E-02	-1,34819
17511450	Siah1a	3,35E-02	-1,3494
17288294	Zfp759	2,61E-02	-1,34973
17549530		7,73E-03	-1,35078
17549682		7,73E-03	-1,35078
17337208	Sfta2	2,21E-02	-1,35226
17541713	Gm14586	1,87E-02	-1,35275
17230225	Hmga2-ps1	2,70E-02	-1,35276
17451746	1110006O24Rik	4,23E-02	-1,353
17371195	Gm13561	3,18E-02	-1,35305
17333999	Zfp758	1,72E-02	-1,35345
17544687	Mir1970	4,61E-02	-1,35927
17517300	Kdelc2	4,83E-02	-1,36182
17350856	Slc27a6	2,40E-02	-1,36239
17245751	Arhgef25	4,72E-02	-1,3624
17491415		4,15E-02	-1,36245
17236182	Timp3	4,41E-02	-1,36389
17546790	n-R5s1	4,93E-02	-1,36393
17413107	Gm3893	1,99E-02	-1,36574
17412296	Epha7	2,97E-02	-1,36586
17473637	Peg3os	6,12E-03	-1,36653
17355844	Gm25005	1,92E-02	-1,36725
17405482	P2ry12	2,66E-02	-1,3673
17468571	2610306M01Rik	1,04E-03	-1,36783
17354810	Afap1l1	4,83E-02	-1,37007
17417767	Elovl1	1,10E-02	-1,37091
17299820	Trav11d	7,86E-03	-1,37184
17300012	Trav11d	7,86E-03	-1,37184
17442940	Gm23245	4,86E-02	-1,37225
17272509	Mxra7	6,00E-03	-1,37339
17409826	Snx7	3,55E-04	-1,37574
17315975		6,23E-03	-1,37862
17279858	Fkbp1b	3,29E-02	-1,37865
17540378	Maob	2,49E-02	-1,38019
17373937		2,69E-02	-1,3824
17471528	Clec1a	3,89E-02	-1,38523

17506206	Crispld2	4,34E-02	-1,38696
17479974	Nox4	3,04E-02	-1,39017
17235826	Zfp433	3,20E-02	-1,39283
17434290	Gm9615	1,42E-02	-1,3939
17549490		1,97E-03	-1,39559
17549638		1,97E-03	-1,39559
17337770	Adgrf5	4,08E-02	-1,39598
17462756	Clec4b1	2,42E-03	-1,39698
17370141	Gm13449	1,49E-02	-1,40051
17251959	Mgl2	3,86E-02	-1,40102
17466861	Mira	2,93E-03	-1,40125
17426117	Zfp37	3,15E-02	-1,40613
17349956	LOC105246409	1,01E-02	-1,40751
17533446	Gpr34	2,83E-02	-1,40879
17227797	Rgs18	2,06E-02	-1,41254
17376908	Ism1	3,80E-02	-1,41313
17468461	Cml1	3,14E-02	-1,41318
17238054	Ndufa4l2	4,20E-02	-1,41457
17535420	Gabrq	2,35E-03	-1,41795
17285513	Tcrg-V4	4,47E-02	-1,4192
17341975	Npw	1,85E-02	-1,42159
17214753	Irs1	3,41E-02	-1,42163
17257221	Myl4	3,37E-04	-1,423
17547610		7,96E-03	-1,42388
17494322	Gm15135	2,18E-02	-1,42442
17365098	Scd1	2,94E-02	-1,42687
17534746	Cxx1c	2,66E-02	-1,42732
17379922	Snai1	1,52E-02	-1,43062
17378168	Bpifb5	3,21E-02	-1,43301
17509146	Snx25	1,05E-02	-1,4332
17220944	Lamb3	2,69E-02	-1,43342
17412952	Gm29804	3,00E-02	-1,43356
17213687	Ccnyl1	1,10E-02	-1,43627
17364208	Ppp1r3c	1,66E-02	-1,43985
17232593	Lama4	4,22E-02	-1,44093
17403571	Ttll7	1,86E-02	-1,44456
17489214	Upk1a	3,61E-02	-1,44491
17379482	Wfdc10	3,79E-02	-1,44567
17387131	Ccdc141	3,16E-02	-1,44765
17532564	Xcr1	3,84E-02	-1,44908
17424407	Gm13303	2,05E-02	-1,45081
17464654	Pdk4	4,86E-02	-1,4517
17333966	Zfp760	2,88E-02	-1,45531
17293933	Zfp595	2,70E-03	-1,45949
17523555	Exosc7	1,53E-03	-1,46232
17221432	Gm10566	2,50E-02	-1,46252
17232417	9330159F19Rik	2,08E-02	-1,46525

17434095	LOC100041536	3,96E-02	-1,46542
17265524	Gm23266	2,00E-02	-1,46807
17231100	Traf5	1,35E-02	-1,4682
17507209	Cd209c	3,17E-02	-1,47123
17542047	Slitrk4	2,78E-02	-1,473
17427181	Gm12669	2,61E-02	-1,47928
17503650	Nkd1	4,58E-03	-1,47966
17539536	Figf	3,58E-02	-1,48415
17301823	Gfra2	3,36E-02	-1,48575
17448821	Ociad2	3,40E-02	-1,49397
17520425	Pcolce2	3,69E-02	-1,49547
17290139	4833420G17Rik	1,15E-04	-1,49667
17506991	Nrp1	1,11E-02	-1,5001
17415338	Gm13275	3,25E-02	-1,50183
17424279	Cntfr	4,25E-02	-1,50384
17424656	Tpm2	2,24E-02	-1,50501
17507799	Angpt2	2,31E-03	-1,50649
17361090	BC021614	8,67E-03	-1,50673
17293945	Zfp953	3,03E-02	-1,50777
17465080	Aass	1,33E-02	-1,50942
17512299	Cdh16	7,45E-03	-1,51387
17227864	Gm4322	1,54E-02	-1,51406
17500453	Tex15	1,84E-02	-1,51554
17413000	Gm3893	3,08E-02	-1,51768
17217058	Slc26a9	2,19E-02	-1,52288
17325671	Lsamp	6,42E-04	-1,52322
17484892	Gm4535	2,16E-02	-1,52364
17338353	n-R5s28	3,13E-02	-1,52865
17396162	Car2	2,53E-02	-1,53199
17400862	Hmgcs2	9,63E-03	-1,53855
17491368	Csrp3	5,31E-03	-1,54624
17278398	Bdkrb2	6,77E-03	-1,54632
17213189	Gm20257	2,99E-02	-1,54796
17260236	Myl7	3,83E-03	-1,55353
17424405		1,15E-02	-1,55908
17272468	St6galnac2	1,16E-02	-1,56248
17468183	Actg2	2,88E-03	-1,56824
17507161	Cd209a	4,00E-03	-1,57057
17273348	Fasn	2,19E-03	-1,57117
17511310	Zfp791	1,40E-02	-1,57167
17358422	Vldlr	5,45E-03	-1,57401
17350203	Spink5	1,95E-02	-1,57477
17239638	Pde7b	1,52E-02	-1,57535
17237547	Cpm	2,65E-02	-1,57971
17496857	Cox6a2	3,28E-02	-1,57997
17379401	Rbpjl	3,22E-02	-1,58237
17211305	Pi15	4,73E-02	-1,58279

17323192	Snai2	2,37E-02	-1,58845
17231423	Akap12	4,18E-02	-1,60095
17437887	Limch1	5,00E-02	-1,60366
17388886	Gm22761	2,99E-02	-1,60584
17456339	Cped1	4,44E-02	-1,60883
17285532	Tcrg-C3	3,93E-02	-1,60912
17448099	5033403H07Rik	2,20E-02	-1,62059
17358591	Mlana	1,55E-02	-1,62315
17241704	Gm7097	2,09E-02	-1,63403
17435114		2,09E-02	-1,64015
17438530	Adgrl3	2,68E-02	-1,64144
17327218	Kcne2	2,67E-02	-1,64485
17491896	Gm23042	2,62E-02	-1,64716
17476119	Ppp1r14a	4,56E-02	-1,6475
17412998		1,31E-02	-1,65874
17424410		1,31E-02	-1,65874
17434127		1,31E-02	-1,65874
17523921	Arhgap42	4,65E-02	-1,66948
17468959	Gm8724	1,78E-02	-1,67995
17471231	Prmt8	2,25E-02	-1,68559
17468425	Gm11128	1,68E-02	-1,68832
17477508	Napsa	3,58E-03	-1,69428
17343628	Angptl4	3,93E-02	-1,70583
17290205	BC147527	2,39E-02	-1,71003
17428276		1,85E-02	-1,72592
17275062	Meox2	1,31E-02	-1,73057
17287160	Aspn	1,59E-02	-1,73932
17393764	Gm23134	2,24E-02	-1,7407
17394160	Matn4	3,76E-03	-1,7459
17515402	Cnn1	1,70E-02	-1,75265
17219662	Pyhin1	2,92E-02	-1,75631
17333642	Zfp960	3,76E-03	-1,75693
17358098	E030003E18Rik	1,14E-02	-1,77693
17377395	Cst8	2,20E-02	-1,77851
17246755	Mir3060	8,34E-03	-1,78043
17545899	S100g	6,91E-03	-1,78847
17530094	Cldn18	1,52E-02	-1,7954
17459207	Ndnf	1,45E-02	-1,79793
17410251	Enpep	2,78E-03	-1,85748
17288467	Lpcat1	2,46E-03	-1,86187
17217651	Tnnt2	1,37E-03	-1,86909
17323040	Mir365-1	2,82E-02	-1,87828
17286830	Edn1	2,40E-02	-1,90715
17389510	Actc1	1,19E-03	-1,90738
17517360	Sln	5,80E-03	-1,9602
17231349	Ppp1r14c	4,27E-03	-1,99392
17239714	Tcf21	1,30E-02	-2,00047

17500639	Gm6213	1,05E-02	-2,01272
17547943		7,62E-04	-2,0128
17437459	Slc34a2	2,45E-03	-2,01661
17214665	Sgpp2	1,13E-02	-2,06205
17397990	Mme	1,70E-03	-2,10845
17320225	Mlc1	1,34E-02	-2,22177
17298267	Itih4	1,93E-03	-2,2234
17329298	Etv5	2,16E-03	-2,33794
17375935	Acoxl	9,21E-03	-2,35203
17301746	Lgi3	7,03E-03	-2,38043
17546055	Egfl6	1,51E-03	-2,54499
17284484	Ighg	4,94E-02	-2,61584
17548979	Gm4322	4,48E-03	-2,65423
17544691	Bex2	4,16E-03	-2,71035
17384374	Hc	6,12E-04	-2,77128
17291874	Nrn1	5,09E-03	-2,83576
17329046	Lamp3	1,18E-03	-2,87812
17484909	Pnpla2	5,75E-06	-3,2912
17537878	Bex4	1,90E-03	-3,46786
17528934	Tinag	5,85E-04	-3,68405